Master's thesis

NTNU
Norwegian University of Science and Technology
Faculty of Engineering
Department of Geoscience and Petroleum

Oluwatosin Triumphant Nana

Diagenesis and reservoir quality preserving mechanism in the deeply buried Lower to Middle Jurassic Formation in the Halten Terrace, offshore Mid-Norway.

A mineralogical, petrographic and petrophysical perspective.

Master's thesis in Petroleum Geoscience
Supervisor: Professor Mai Britt E. Mørk
January 2022

NTNU
Norwegian University of
Science and Technology

Oluwatosin Triumphant Nana

Diagenesis and reservoir quality preserving mechanism in the deeply buried Lower to Middle Jurassic Formation in the Halten Terrace, offshore Mid-Norway.

A mineralogical, petrographic and petrophysical perspective.

Master's thesis in Petroleum Geoscience
Supervisor: Professor Mai Britt E. Mørk
January 2022

Norwegian University of Science and Technology
Faculty of Engineering
Department of Geoscience and Petroleum

NTNU
Norwegian University of
Science and Technology

Dedication

This work is dedicated to my almighty God for being my source of inspiration, strength, and provision during the course of my master’s degree program.

Acknowledgement

My appreciation goes to God almighty my maker and my sustainer, for his grace and compassion over me and also the strength he granted me all through this work.

Special appreciation goes to my project supervisor Professor Mai Britt E. Mørk for devoting countless hours to review and advise me. And also, for her guidance, correction, and constructive criticism which has brought out the best in me in the course of my project work. I would also like to thank her for providing the thin sections used for this study.

I would like to express my appreciation to Gwenn Peron-Pinvidic for providing the well log data used in this study. Also, my special thanks go to Kjetil Eriksen for his time and technical support during the course of SEM analysis and point counting analysis.

My profound and unreserved heart-felt gratitude goes to my parents Pastor and Deaconess A.M. Nana and my siblings for their moral, spiritual, and financial support. I say a big thank you for standing by me thus far.

Oluwatosin Triumphant Nana.

January 2022, Trondheim.

Abstract

Deeply buried heterolithic sandstone reservoirs in the Halten Terrace, offshore mid-Norway, have been investigated for diagenetic impact on reservoir quality. A total of twenty-seven (27) polished and blue epoxy impregnated thin sections from six wells (6406/2-1,6406/2-2, 6506/12-1, 6506/12-10, 6506/12-10A, and 6506/11-5S) in the Tilje, Tofte, and Ile Formations (16 from the Tilje Formation, 8 from the Tofte Formation, and 3 from the Ile Formation) were analyzed under a petrographic microscope, out of which seven (7) were selected for analysis under a scanning electron microscope. Five petrophysical well logs (6406/2-1, 6406/2-2, 6506/12-1, 6506/12-10, and 6506/12-10A) were correlated and interpreted to determine the lithology and identify areas of high and low porosity.

The result of the analysis reveals sublithic arenite to subarkosic sandstone compositions which has been affected by diagenetic processes including quartz and carbonate cementation, grain coatings, mineral replacements, and dissolution. Chlorite and illite are the clay minerals found in all three studied formations, these authigenic clay minerals also form the coatings observed on grains. The illite is interpreted to have originated from smectite and kaolinite precursors, and chlorite from a berthierine precursor where it is found to be associated with clay rims. The shale volume of the studied sandstone interval has been described as high to low based on the combination of Gamma-ray log, Neutron log, and Bulk density log data.

The reservoir quality in the Tilje Formation is described to be good to moderate, this is due to the effectiveness of chlorite and illite coatings in the preservation of primary porosity through the inhibition of quartz cement growth on detrital grains, and presence of secondary porosity resulting from dissolution and fracture pores. Tofte and Ile Formation equally show a moderate quality. In some of the samples the permeability of the reservoir is affected due to the presence of fibrous pore-bridging authigenic illites and carbonate cement precipitated in pore spaces. In some samples, where chlorite coatings are absent, quartz cementation is extensive, with secondary porosity due to the dissolution of less stable minerals serving as the only form of porosity.

Table of Contents

List of Figures

List of Tables

Chapter One: Introduction

1.1 Background Knowledge

Quartz cementation is considered as the most dominant mechanism that reduces porosity and permeability in many reservoir sandstones at a depth greater than 2.5-3km (90-100^{o}C) (Bjørlykke et al. 1992; Molenaar et al. 2007). Quartz overgrowth may be prevented or reduced by different types of grain coatings, including micro-quartz, chlorites, illite, and asphalt (Storvoll et al. 2002). This study partly focuses on the effect of chlorite coating on the porosity of sandstone reservoirs. Different previously published studies have shown that high porosity in deeply buried sandstones may be a result of grain-coating authigenic chlorite formed during the early diagenetic stage, enhancing compaction resistance and inhibiting quartz cementation by reducing the nucleation area for overgrowths (Ehrenberg 1993; Yu et al. 2016). Chlorites that occur as pore-filling can also reduce porosity and permeability (Islam 2009; Nadeau 2000; Dowey et al. 2012). Hillier (1994) stated that chlorite formation must have taken place within the first few hundred meters of burial during the early diagenetic stage. However, occurrences of these chlorites have not been documented yet from such shallow depths. It is not necessarily the amount of grain-coating chlorite that matters, but the distribution of the grain-coating chlorite in the sample, as relatively thin coatings can be very effective if they are continuous and cover most of the grains in the sample. Continuous grain-coating chlorites are often the cause of high porosity values in deeply buried sandstone reservoirs; this is important for hydrocarbon exploration because it can provide good reservoir quality at depths far below the economic basement (Ehrenberg 1993). Some criteria needed for grain-coating minerals to be effective in preserving porosity at great depth will be discussed in a later chapter of this report. According to Ehrenberg (1993), designing production strategies for reservoirs with chlorite coating requires knowledge and understanding of the geometry and petrophysical characteristics of chlorite-coated high porosity zones.

1.2 Purpose of the study

In the Halten Terrace, hydrocarbon production is mainly from heterolithic siliciclastic successions and diagenetically altered sandstones (Martinius et al. 2011). As part of the diagenetic process in the Halten Terrace, this study focuses on improving and adding to the pre-existing knowledge on the different factors controlling porosity, grain coating, and other diagenetic process in the deeply buried early to middle Jurassic sandstones of the Halten Terrace, offshore Mid-Norway. An understanding of these factors will aid in predicting the reservoir quality in Lower to Middle Jurassic formations of the Halten Terrace, offshore Mid-Norway.

1.3 Study Area

The study area is located in the Haltenbanken area of offshore mid-Norway in exploration wells situated in block 6406/2, 6506/12, and 6506/11. The information of these wells was retrieved from NPD fact page (NPD). Well 6406/2-1 and 6406/2-2 are exploration wells drilled on the northern and southern segment of the B-prospect (Lavrans discovery), respectively, in the eastern part of block 6406/2. Well 6506/12-1 was drilled on the Alpha structure in the northwest part of the block 6506/12 while well 6506/12-10 and 6506/12-10A were drilled to appraise the down flanks hydrocarbons in the Garn, Ile, Tilje, and the Åre Formation, on the Smørbukk Field. Well 6506/11-5S was drilled to appraise hydrocarbons in the Smørbrukk Field and collect reservoir quality and fluid distribution data. (Figure 1.1).

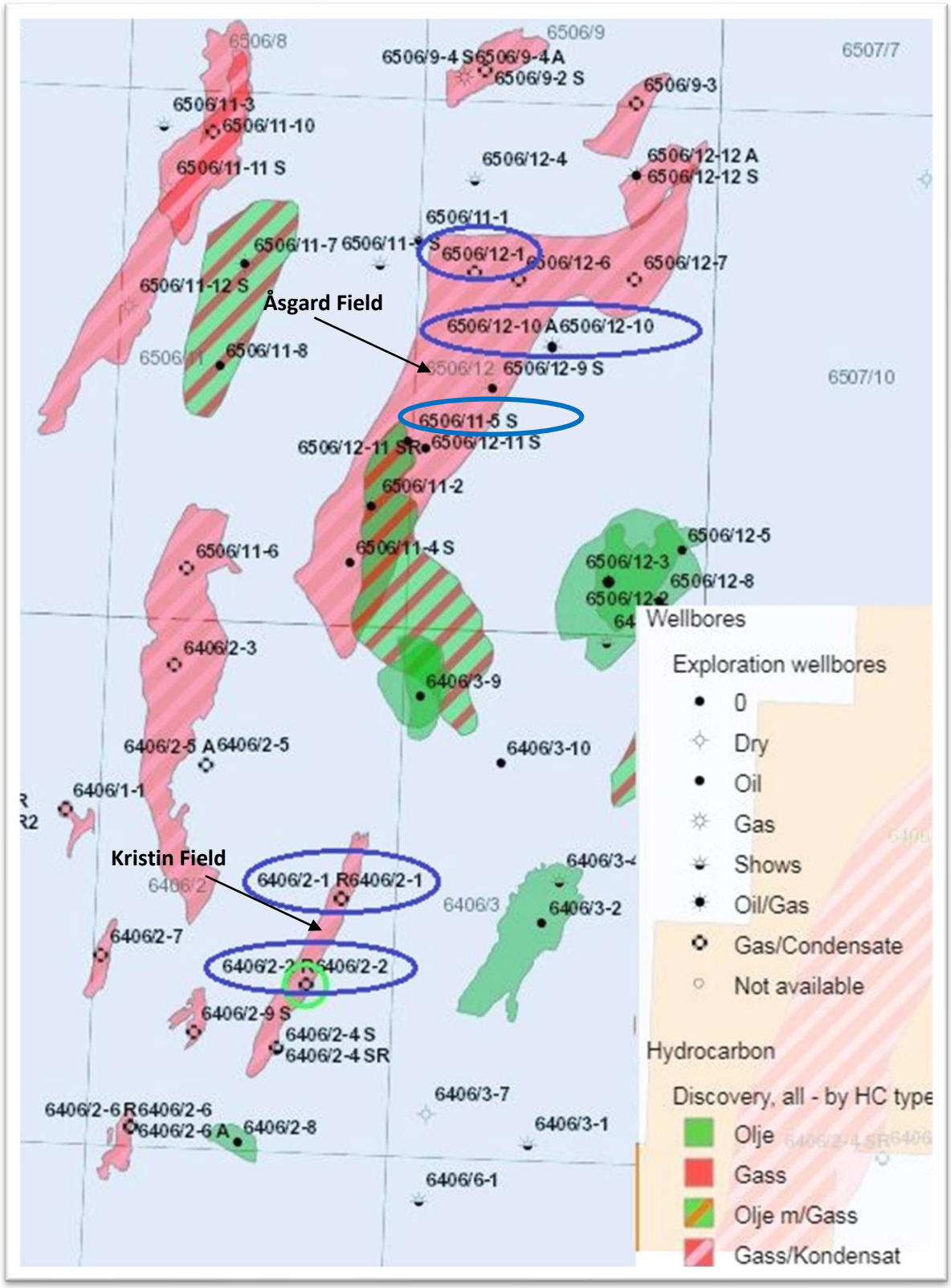

Figure 1.1. Study area. Selected wells are cycled in blue (modified from NPD)

1.4 Review of previous work

Exploration of hydrocarbon in the Haltenbanken area, offshore mid-Norway, started in the early 1980s with the first discovery of the Midgard Field in 1981, after which several major discoveries have been made. Today, the area is known as a fairly mature hydrocarbon province (Martinius et al. 2001). The major hydrocarbon discoveries are located on the Halten Terrace and in the western margin of the Trøndelag Platform (Heum and Larsen 1990). The most important reservoir rocks in this area include the alternating sandstones and shales from the Åre, Tilje, Tofte, Ile, and Garn formations of the Early to Middle Jurassic age (Faleide et al. 2010). The Normal porosity depth-trend in the Haltenbanken area is between 8-10% (Bjørlykke et al. 1989; Ehrenberg 1990; Rønnevik 2000). Porosity values above this depth trend are most likely due to clay coating in this area. The Smørbrukk Field lies at 4km depth where quartz cementation is prevalent (Faleide et al 2010). Ehrenberg et al. (1993) studied the porosity of Tilje and Tofte formation in relation to grain coating chlorite, and his study showed that samples from the Tilje Formation studied from block 6506/12 and 6507/3 is characterised by high porosity (>20%) in areas with thick chlorite coating. And the least porous samples tend to have much higher quartz cementation and either lack chlorite coatings or have relatively thin, discontinuous coatings that allow direct contact between quartz grains and the optically continuous quartz overgrowths. He further stated that porosity is not a simple function of quartz cementation but also a function of the percentage of intergranular volume (IGV) because many low-porosity samples from these wells have low to moderate quartz cement. Tofte Formation samples studied from well 6506/12-1 and 6506/12-6 show poor chlorite content and extensive quartz cementation, resulting in low porosity, while in well 6506/11-1, the Tofte Formation has anomalously high porosity due to abundant continuous chlorite coatings.

In the Lavrans and Kristin fields which lie at more than 5 km, the temperature can reach 170-180^{o}C. In this situation, it is the degree of quartz cementation which essentially determines whether there is sufficient porosity to produce petroleum (Faleide et al. 2010). Storvoll et al. (2002) illustrate the effect of continuity of grain-coating minerals on porosity. Their study is based on the comparison of Garn Formation from Kristin field (6406/2-3T3 and 6406/2-5) and Lavrans field (6406/2-1 and 6406/2-2). The study shows a low porosity sandstone in the Lavrans wells, and this is because the Garn Formation sandstone in this well does not contain a continuous or well-developed clay coating. As a result, they are thoroughly quartz cemented. However, in the Kristin wells, the sandstones of the Garn Formation are coated with continuous

illite and illite/chlorite coatings with less quartz cement, resulting in high porosity ranging between 15-20%.

Chapter Two: Geological Background

2.1 Introduction

This chapter describes the geological setting of Offshore Mid-Norway with emphasis on the tectonic framework, the stratigraphic framework of early to middle Jurassic, and major structural elements in relation to the Halten Terrace.

2.2 Tectonic

Blytstad et al. (1995) divided the tectonic history of the Norwegian Sea region of the Norwegian continental shelf into three episodes: the pre-Late Devonian (closure of the Iapetus Ocean during the Caledonian Orogeny in Late Silurian and Early Devonian time), the Late Devonian to Palaeocene (dominated by episodic extensional deformation culminating with the continental separation between Eurasia and Greenland at the Palaeocene-Eocene boundary), the Earliest Eocene to present, characterized by active seafloor spreading between Eurasia and Greenland.

The second episode dominated by episodic extension is the episode of interest since this study is based on the Jurassic sandstones in Halten Terrace. A summary of the tectonic evolution in this area is shown in Figure 2.1.

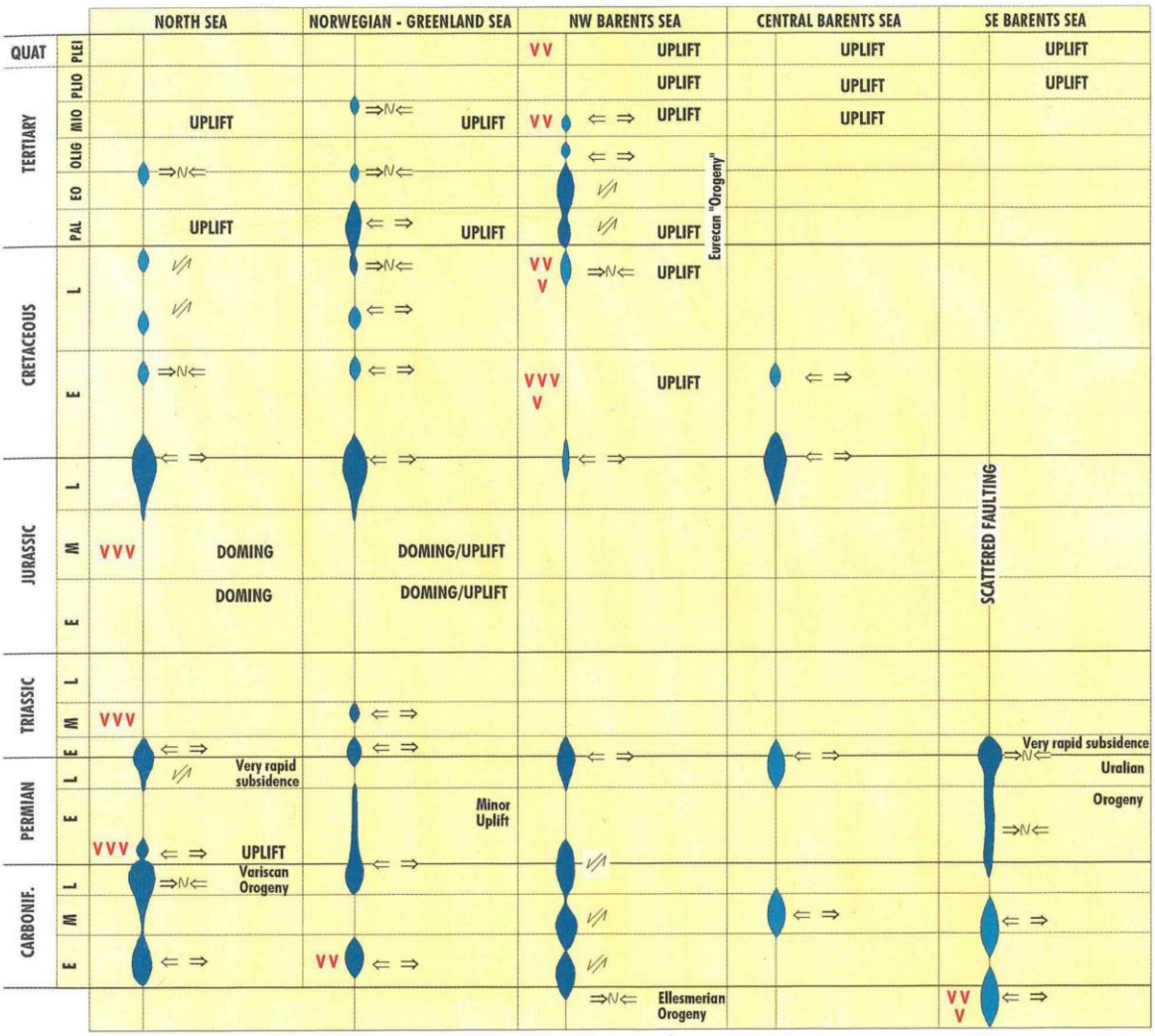

Figure 2.1. Summary of the tectonic evolution Norwegian Sea. Blue patches indicate the timing and duration of tectonic events, red 'v's indicate the timing of significant magmatic events. Arrows indicate sense of tectonic movements: diverging arrows - extension, converging arrows - compression, lateral arrows - strike-slip movement (Brekke et al. 2001).

2.2.1 Pre-Break Up Stage

Three major rift episodes have contributed to the development of Offshore Mid-Norway:

1. The Late Palaeozoic-Early Mesozoic rift episode
2. Late Middle Jurassic–Early Cretaceous rift episode
3. Late Cretaceous – Paleocene rift episode

2.2.1.1 Late Palaeozoic–Early Mesozoic rift episodes

The Late Palaeozoic–Early Mesozoic rift episodes occurred in mid-Carboniferous, Carboniferous–Permian, and Permian–Early Triassic times (Dore 1991). During these periods

(Late Carboniferous to Early Permian), active tectonism is recorded over large parts of the proto-North Atlantic area (Blystand 1995). Part of the active tectonism includes the southward movement of the Arctic North Atlantic rift system, which occurred in the Early Permian (Gabrielsen et al. 1999). Sediment packages associated with these movements are poorly resolved, mainly because of overprint by younger tectonism and burial by thick sedimentary strata (Faleide 2008). Only a little information is available on the Carboniferous in this area (Gabrielsen et al. 1999). The Late Permian to Early Triassic rifting and formation of N-S to NE-SW trending rotated fault blocks occurred on the Halten Terrace and parts of the Trøndelag Platform. The Froan Basin and Vestfjorden Basin were formed during this period (Blystad et al. 1995; Osmundsen et al. 2002; Faleide et al. 2008). A period of relative tectonic quiescence interpreted to represent a period of thermal cooling is recorded in the Mid – Late Triassic times (Gabrielsen et al. 1999). However, some block fault along the Permo-Triassic master faults, occurred in the Mid – Late Triassic period. The Late Triassic and Early Jurassic seemed to have been a quiet tectonic period and thermal relaxation except during the Sinemurian/Pliensbachian time, when NNE trending growth faults may be observed to have detached Triassic sediments (Blystad et al. 1995). During the Middle to Late Jurassic, intermittent tectonic activity is seen again in this area (Brekke et al. 2001).

2.2.1.2 Late Middle Jurassic–Early Cretaceous rift episode

A shift in the extensional stress field vector to NW-SE is recorded by the prominent NE Atlantic-Arctic late Middle Jurassic– earliest Cretaceous rift episode, an event associated with northward propagation of Atlantic rifting. These episodes of events led to the development of major Cretaceous basins; the basins have undergone rapid differential subsidence and segmentation into sub-basins and highs (Faleide et al. 1993; Faleide et al. 2008). Blystad et al. (1995) subdivided the late Middle Jurassic – Early Cretaceous rifting episode into three phases according to the time of occurrence:

1. Bathonian/Callovian time
2. Kimmeridgian
3. Neocomian

During the first two phases (Bathonian/Callovian and Kimmeridgian), the Halten Terrace, which is the main study area, and Dønna Terrace made up the western and tectonically most active parts of the Trøndelag Platform, with the Halten and Dønna Terrace downfaulted in relation to the Trøndelag Platform. Pronounced flexuring and faulting took place along the eastern flanks of the Møre and Træna Basins, and the Vøring Basin subsided in relation to the

Terrace areas to the west (Blystad et al. 1995; Brekke et al. 2001). During the Neocomian phase, the basin margins developed further, and the separation between the platform and Terraces became more accentuated. Deep erosion of the western edges of the Halten Terrace (Sklinna Ridge) and the Trøndelag Platform (Frøya High and Nordland Ridge) occurred during this second rifting phase. The Vøring and Møre Basin experienced subsidence between the Neocomian rifting phase and the end of the Cenomanian (Blystad et al. 1995; NPD).

2.2.1.3 Late Cretaceous – Palaeocene rift episode

Following the subsidence at the end of Cenomanian, evidence for the onset of an episode of tectonic activity is observed in the Jan Mayen Lineament (Blystad et al. 1995). Ren et al. (2003) indicated that the main period of brittle faulting occurred in Campanian time, followed by smaller-scale activity towards breakup. The Campanian rifting resulted in low-angle detachment structures that updome thick Cretaceous sequences and sole out at medium-to deep intra-crustal levels on the Vøring and Lofoten-Vesterålen margins (Tsikalas et al. 2001; Gernigon et al. 2003; Ren et al. 2003). The Cretaceous-Cenozoic development in the Møre Basin was tectonically quiet and generally dominated by subsidence (Blystad et al. 1995; Gabrielsen et al. 1999). Most of the structure of Late Cretaceous – Palaeocene tectonics is covered by a wide area of lava along the outer Møre and Lofoten-Vesterålen margins; these structures, however, appear to continue seawards underneath the breakup lavas (Blystad et al. 1995; Faleide et al. 2008). The final intra-continental rifting episode between Eurasia and Greenland probably lasted from Campanian/Maastrichtian times until continental separation at the Palaeocene-Eocene boundary (Blystad et al. 1995).

2.3 Structural Elements

Sedimentation and tectonic development in this area are controlled by the Magnus-Fosen Fault Zone (MFFZ), the Jan Mayen Fracture Zone Trend (JMFZT), and the Senja Fracture Zone Trend (SFZT). The lineaments allow a division of the area into three main provinces with different geological histories (Figure 2.2); the Southern Province south of the JMFZT, the Middle Province between the JMFZT and the SFZT, and the Northern Province east of the SFZT (Brekke & Riis 1987). Two deep Cretaceous basins, namely Vøring and Møre Basins dominate the central area of the offshore Norway continental margin (between 62 and 69^0N). These two basins are flanked to the east by platforms (dominated by shallow water Late Jurassic to Early Cretaceous Trøndelag Platform) and Terraces (dominated by deep Dønna Terrace and intermediate Halten Terrace) (Marsh et al. 2009) (Figure 2.3). Where the Vøring

basin is separated from the Møre Basin by Jan Mayen Fracture Zone Trend (JMFZT) and Bivrost Lineament/Transfer Zone (Brekke & Riis 1987; Blystad et al. 1995; Faleide et al. 2010).

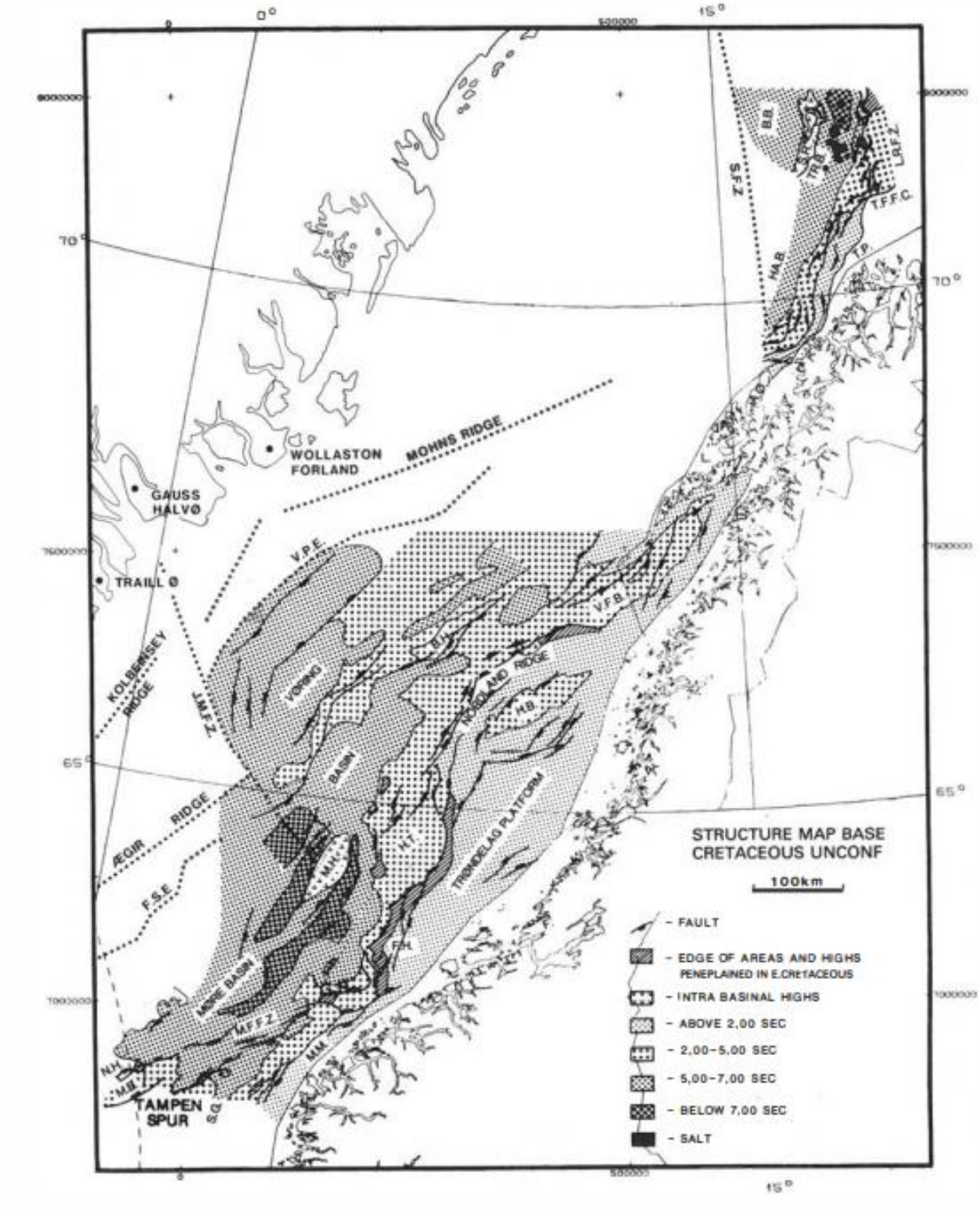

Figure 2.2. Map showing the fault and fracture zones J.M.F.F.Z. - Jan Mayen Fracture Zone. S.F.Z. - Senja Fracture Zone. and M.F.F.Z. - Magnus-Fosen Fault Zone. (Brekke and Riis 1987).

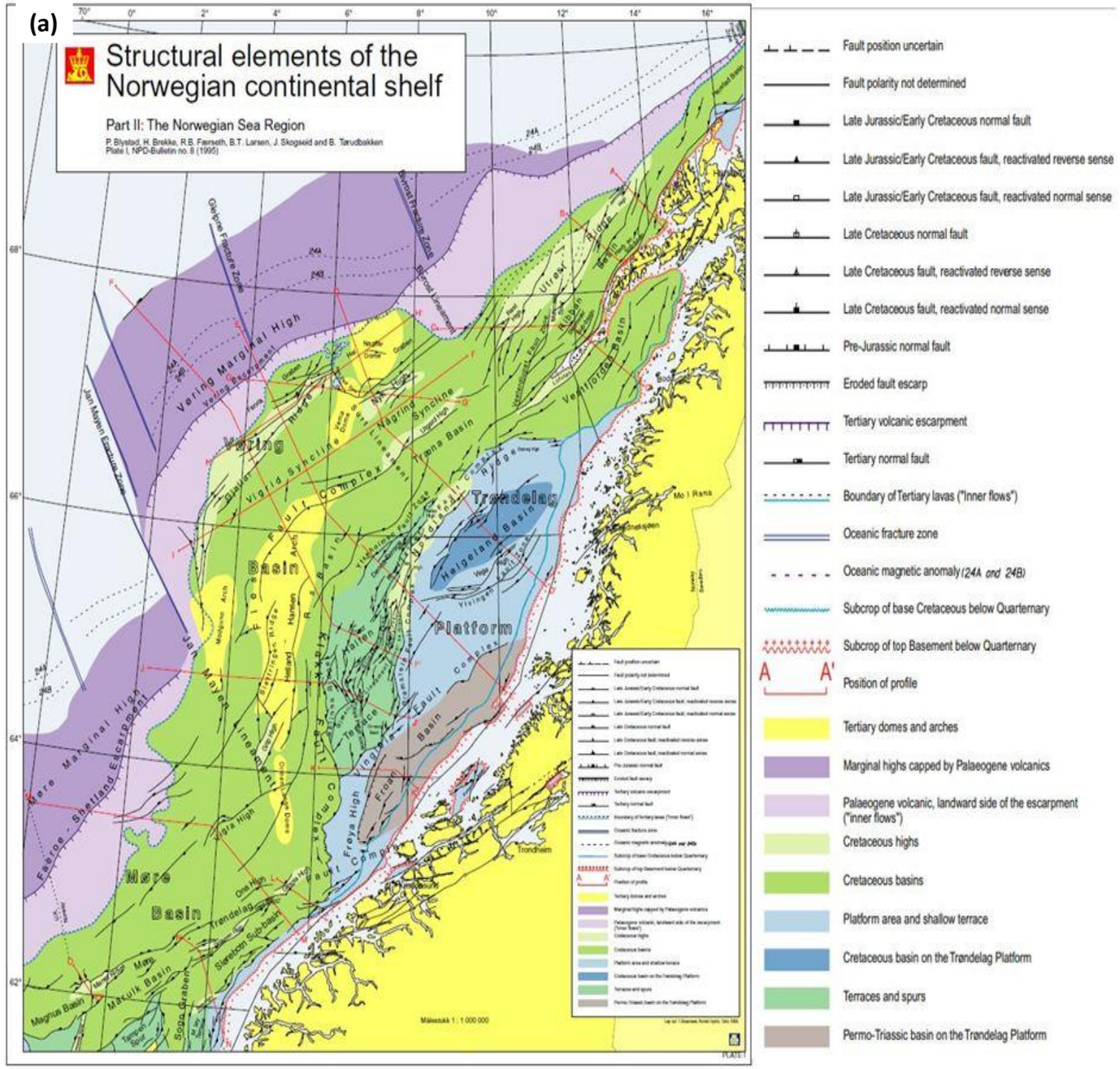

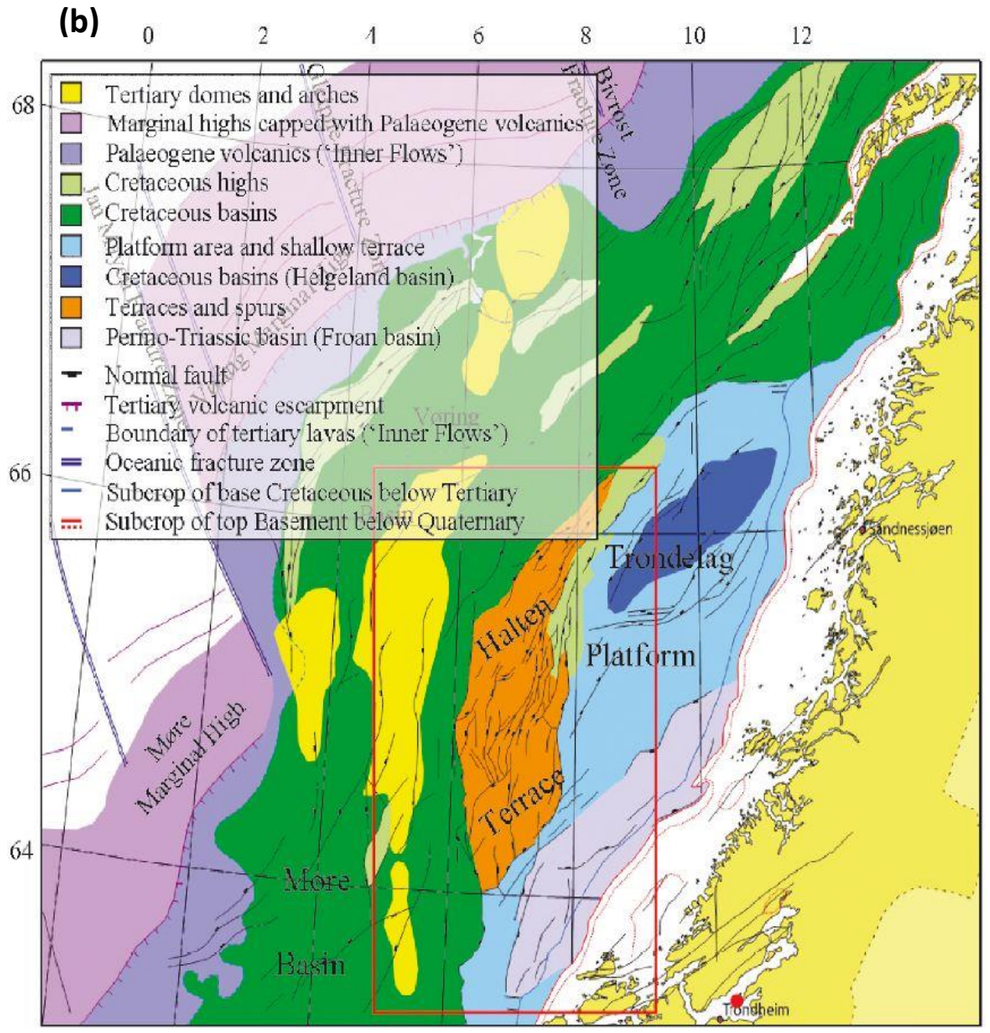

Figure 2.3.(a) Structural elements of the Norwegian continental shelf (Blystad et al. 1995) (b) Structural map offshore mid-Norway showing the Location of Halten Terrace in relation to other structural elements (Marsh et al. 2009).(Marsh et al. 2009)

According to Brekke and Riis (1987), the Southern Province south of the JMFZT is characterized by the Møre Basin and the Møre Marginal High. At the same time, the Middle Province (JMFZT - 68°30'N) comprises (from southeast to northwest) the Trøndelag Platform, the Halten and Dønna Terraces, the Vøring Basin, and the Vøring Marginal High (Figure 2.4).

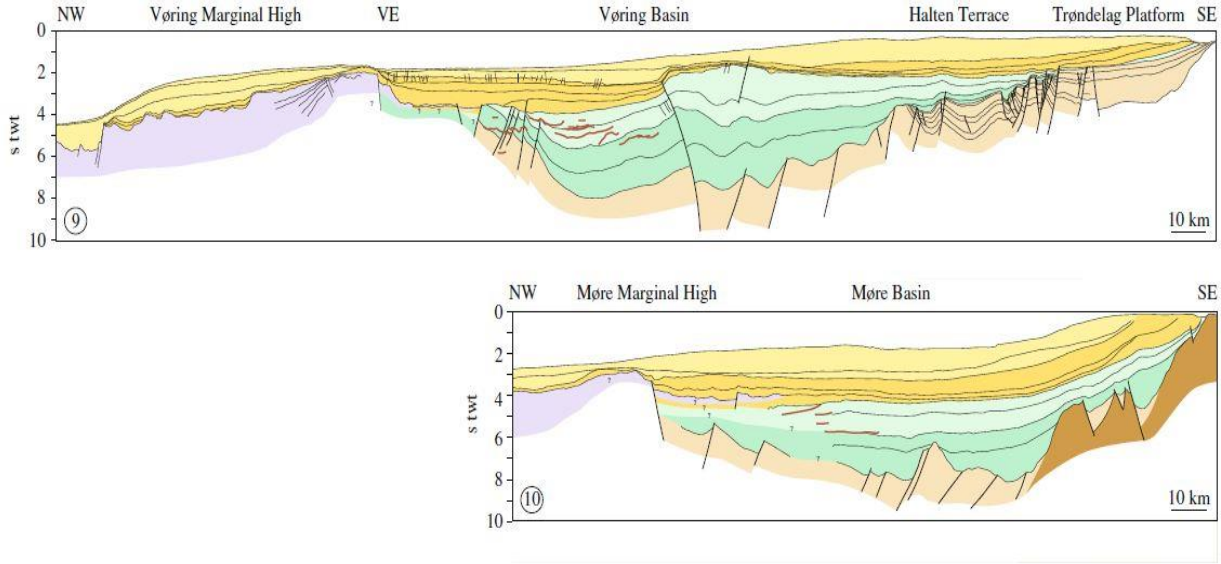

Figure 2.4. Regional profiles across the Mid-Norwegian Margin (Faliede et al. 2010). VE- Vøring Escarpment.

2.3.1 Møre Basin and Møre Marginal High

The Møre Basin situated between 62^0N – 65^0N and 0^0E – 6^0E is bounded by northern termination of the Tampen Spur to the south and to the north by JMFZT which separates it from the Vøring Basin, it is bounded by the southern termination of Frøya High and the Faeroe-Shetland Escarpment along the Møre Marginal High to the east and west respectively (Blystad et al. 1995). The Late Jurassic-Early Cretaceous crustal stretching and thinning, faulting and subsequent thermal cooling, and subsidence created the Møre Basin (Blystad et al. 1995). These Late Jurassic-Early Cretaceous events also formed sub-basins within the Møre Basin and are separated by intrabasinal highs (Faleide et al. 2010). In the axial parts of the Basin, Cretaceous and younger strata may exceed 5000m in thickness (Grunnaleite and Gabreilsen, 1995). The upper Cretaceous sequence is probably somewhat thicker than the lower Cretaceous sequence (Brekke & Riis 1987). Lavas of Cretaceous within the Møre Basin have been identified, and the Cretaceous-Tertiary basin fill is reported to be folded and affected by reverse faults (Hamar et al. 1980; Hamar and Hjelle, 1984; Grunnaleite and Gabreilsen, 1995).

Møre Marginal High, previously known as the Møre Platform (Hamar and Hjelle 1984), is located from 62^0N – 65^0N and 5^0W – 3^0E between the Faeroe Plateau and the JMFZT. It is

bounded to the east and west by the Faeroe-Shetland Escarpment and the transition to oceanic crust, respectively. The Møre Marginal High formed as part of the volcanic passive margin developed through the Maastrichtian-Palaeocene continental extension. This event led to the uplift and magmatic activity experienced by the outer parts of the Møre Basin and the marginal high (Blystad et al. 1995).

2.3.2 The Vøring Basin

The Vøring Basin is described as a Cretaceous sedimentary basin formed by the late Middle Jurassic-early Cretaceous extensional event. It is bounded to the east by the fault complexes along the edge of the Trøndelag Platform and to the west by the Vøring Escarpment along Vøring Marginl High (Brekke 2000). The Vøring Plateau represents a distinct bathymetric feature, including the Vøring Marginal High and the Vøring Escarpment (Figure 2.4) (Faleide et al. 2010). The north boundary is not yet clearly defined (Brekke & Riis 1987). However, (Blystad et al. 1995) stated that the Vøring Basin is bounded to the north by Bivrost Lineament and to the south by Jan Mayen Lineament. The Surt Lineament represents an important structural divide within this basin parallel to the lineaments bounding both north and south of the Vøring Basin. South of the Surt Lineament, the Vøring Basin comprises of two synclines: the Vigrid Syncline to the west and the Rås Basin to the east. The Vøring Basin, north of the Surt Lineament, is characterized by three synclines: the Træna Basin due east, and the Någrind Syncline and Hel Graben due west and separated by the Utgard and Nyk Highs (Blystad et al. 1995). As in the Møre Basin, the Late Jurassic – Early Cretaceous basin evolution created a series of subbasins and highs within the Vøring Basin (Faleide et al. 2010). The description of Cretaceous basin-fill thickness varies with different authors as a result of the inability to determine the precise location of the base due to the presence of sills and dikes with strong seismic reflectors inhibiting the seismic resolution of deeper levels (Blystad et al. 1995; Brekke 2000).

2.3.3 The Halten Terrace

The Halten Terrace was developed during the Late Jurassic/Early Cretaceous tectonic phase due to faulting along its boundary faults, forming a rhomboidal structural feature between 64 and $65^0$30'N, and 6 and 8^0E. The Terrace is separated from the Trøndelag Platform by the Bremstein Fault Zone to the east, from the Frøya High in the southeast by the Vingleia Fault Complex and from the Møre and Rås Basins by the Klakk Fault Zone to the west. The Terrace

merges with the Dønna Terrace towards the north. It is approximately 80 km wide and 130 km in length, totaling an area of 10 400 km^2 (Blystad et al. 1995; Bukovics et al. 1984; Marsh et al. 2009). Triassic salt-related extension has impacted the structure in the north-western part of the Halten Terrace resulting in the development of low-angle detachment faults and steeper-dipping structures (Jackson and Hastings, 1986; Pascoe et al. 1999). The Terrace is made up of Cretaceous strata with thickness of about 1200m, the Upper and Lower Cretaceous have almost equal thickness. Tertiary and Jurassic strata also occur on the Terrace, with the Tertiary being characterized by 2000m thick strata, and the Jurassic strata is well represented in all parts of the Terrace except in the western part of the Sklinna Ridge along the Klakk Fault Zone where the Jurassic is eroded, and older strata dip steeply to the east (Blystad et al. 1995). According to Osmundsen et al. (2002) and Osmundsen and Ebbing (2008), the relationship between the pre- Middle Triassic basins in the Trøndelag Platform area and the Jurassic basins on the Halten Terrace involves the successive development of two generations of extensional detachments and their interaction with a deep-seated, antiformal culmination (metamorphic-core-complex).

2.3.4 The Trøndelag Platform

The Trøndelag Platform is located between 63ºN – 65ºN and 6º20'E – 12ºE, covering an area of more than 50,000km^2. The platform is bounded by the Møre-Trøndelag Fault Complex in the south-eastern part, in the north and west by Revfallet Fault Complex, which runs along the Nordland Ridge separating it from the Vestfjorden and Træna Basins in the north and the Dønna Terrace in the south, to the west, Bremstein Fault Complex separates the Halten Terrace from the platform (Blystad et al. 1995). The platform area has been the site of active rifting and major basin development in pre-Cretaceous times, and during the Early Cretaceous, the Trøndelag Platform became a stable platform area (Brekke and Riis, 1987). However, Blystad et al. (1995) stated that the Trøndelag Platform has been largely stable since Jurassic time and includes deep basins filled by flat-lying and mostly parallel-bedded Triassic and Upper Palaeozoic sediments usually dipping gently in the northwest direction. Cretaceous sediments are thin and partly absent, except for the thick accumulations in local half graben subbasins. The Trøndelag platform includes sub-elements like Nordland Ridge, Helgeland Basin, Frøya High, Froan Basin, Ylvingen Fault one and Vega High (Blystad et al. 1995). Cretaceous sediments are thin and partly absent, except for the thick accumulations in local half graben subbasins.

2.3.5 Vøring Marginal High

The Vøring Marginal High, which occurs as a northwest – southwest trending structure between 66ºN – 69º15'N and 0º15'E – 13ºE has been described by Hinz (1981), Talwani et al. (1983), and other authors as part of the volcanic margin developed in response to regional Maastrichtian – Palaeocene continental extension. It is bounded by Vøring Escarpment to the east and by the transition to oceanic crust in the west and north (Blystad et al. 1995). In addition, two oceanic fracture zones, the Vøring, and Lofoten fracture zones, now renamed Gleipne and Bivrost Fracture Zones, respectively, subdivided the Vøring Marginal High (Hagevang et al. 1983).

2.4 Stratigraphy

This work focuses on the Lower and Middle Jurassic samples of the Halten Terrace, Offshore Mid Norway. The Sedimentation in the Lower and Middle Jurassic in the study area represents a period of the sand-prone sedimentary environment (Figure 2.5).

2.4.1 Lower Jurassic

Following the Transgression that started in the Late Triassic, a shallow marine environment characterized the early Jurassic time (Brekke et al. 2001), representing a transition from continental environment in the Triassic time to the shallow marine environment in the early Jurassic time (Faleide et al. 2010). The lower Jurassic is made up of a sequence of basal coal-coaly-shale-sandstone overlying Triassic red beds (Karlsson 1984). The rapid change from red to grey beds as a result of increasing humid climate (due to a northward drift of Mid-Norway in late Triassic time) marks the initiation of a trend that ended in the deposition of paralic, coal-bearing sediments of the Early Jurassic Åre Formation (Swiecicki et al. 1998). The coal sequence ranges in age from the Middle Rhaetian to well into the Sinemurian, where individual coals can be up to 8m thick (Karlsson 1984; Dalland et al. 1988). The Åre Formation represents a delta plain deposit (swamps and channels) passing upward into marginal marine facies (Dalland et al. 1988). Overlying the Åre Formation is a Sinemuria - Toarcian shallow marine sandstone/siltstone unit of the Tilje Formation with a simultaneous deposition of the Neil Klinter Group sediments and a corresponding age as the upper part of the Amundsen and Cook Formations in the North Sea (Karlsson 1984; Martinius et al. 2001). An overall sea-level rise is inferred for the late Pliensbachian to early Toarcian led to the diachronous deposition of the

transgressive, tidally influenced sandstones of the Tilje Formation (Haq et al. 1987; Hallam, 1988; Surlyk 1990; Swiecicki et al. 1998). Martinius et al. (2001) pointed out that the thickness and depositional facies of the Tilje Formation over the Halten Terrace area differ considerably from the type section due to local variations in subsidence rate and depositional patterns. The stratigraphic subdivision of the Tilje Formation differs slightly from field to field; the Tilje Formation is divided into three units in the Smørbrukk Field and divided into four in the Heidrun Field (Martinius et al. 2001). After the deposition of Tilje Formation, Marine transgression continued leading to the deposition of an upward-coarsening sequence of marine shale of the Ror Formation with storm-deposited sandstone beds in its upper portion. Around the Smørbrukk field, Ror deposition was interrupted by the localized deposition of a fan delta of coarse-grained, very poorly sorted sand of the Tofte Formation (Dalland et al. 1988; Ehrenberg 1993; Swiecicki et al. 1998). In the Halten Terrace, the Tofte Formation is only recognized in the western part and wedging out with the Ror Formation towards the east (Dalland et al. 1988).

2.4.2 Middle Jurassic

The Fangst and Viking Groups of the Middle Jurassic comprises of the tidal to increasingly open-marine facies of the Ile, Not, Garn, and Melke Formations (Dalland et al. 1988).

In the Middle Jurassic time, two major cycles of regression and transgression can be recognized. The first cycles (Aalenian to early Bajocian age) started with a regressive tidally influenced, shallow marine and shoreface sandstones of the Ile Formation passing on into transgressive, shelfal mudstones of the lower Not Formation at the top (Dalland et al. 1988; Swiecicki et al. 1998). The second cycle (late Bajocian to mid Callovian age) is made up of the easterly progradational deltaic and shoreface sandstones of the middle Not and Garn formations, the shallow marine mudstones of the upper Not Formation, and the succeeding open marine claystones of the lowest Melke Formation (Swiecicki et al. 1998). In northern Haltenbanken, and in all of the structurally high areas, at least the upper member of the Fangst Group has been partly or totally eroded. This is evident also in areas where thin Upper Jurassic shales are present (Fagerland, 1990). In the Smørbrukk region, the contact between Garn Formation and the underlying Not Formation is often sharp and erosive, this contact is marked by coarse pebble lag, and it is assumed to represent a regionally significant regressive erosion surface of intra -early Bajocian age as mentioned above by Dalland et al. 1988 and Swiecicki et al. 1998. However, the contact between Not and Garn Formation is more gradational,

associated with a genetically related progradational association of facies from offshore/shelf to upper shoreface/shelf in other nearby Halten wells (Corfield et al. 2001).

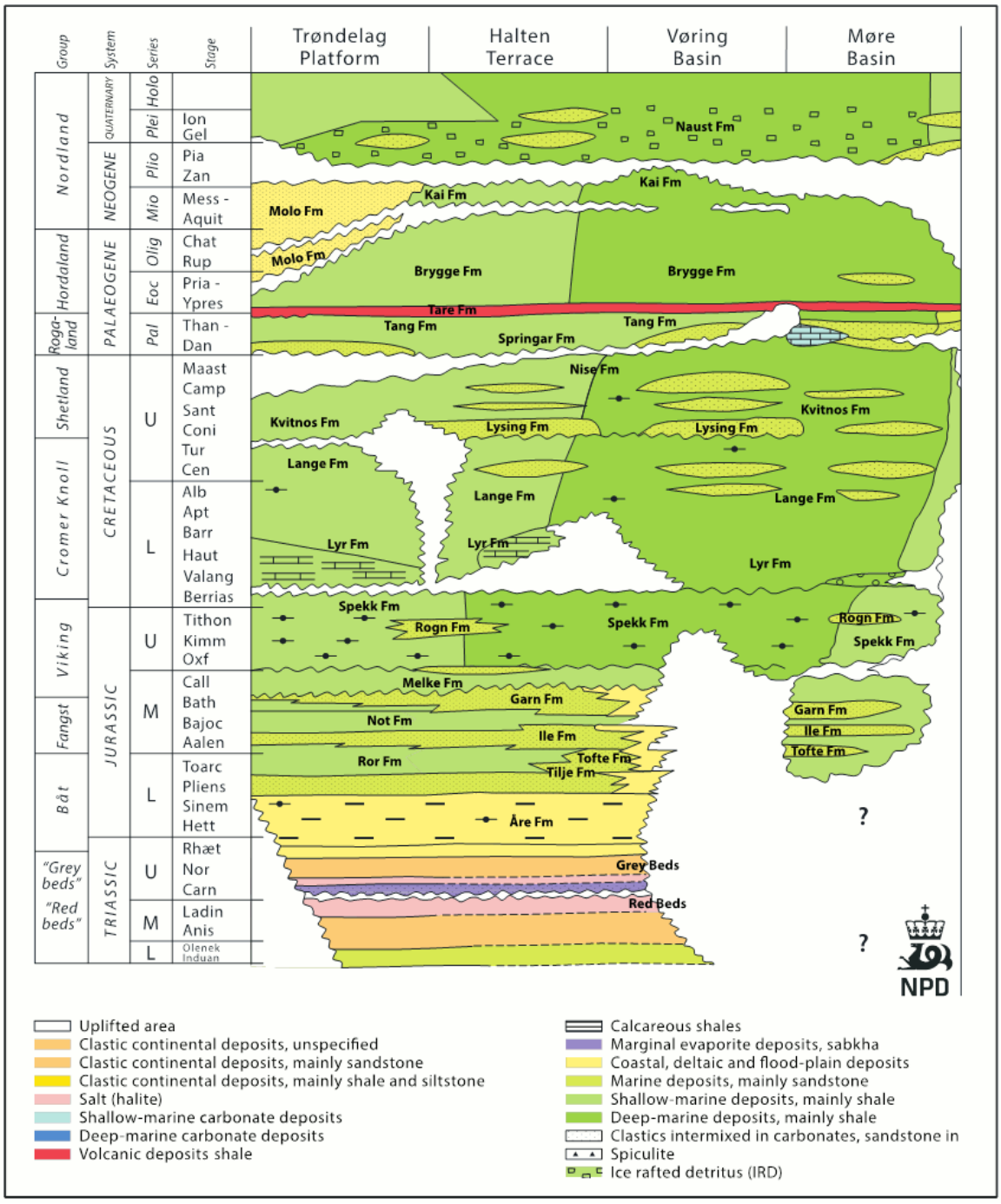

Figure 2.5. Lithostratigraphy chart of the Norwegian Sea (NPD).

Chapter Three: Theoretical Background

3.1 Introduction

According to Bjørlykke and Jahren (2010), sandstone reservoir properties depend on the primary composition of the sandstone, and this primary composition is controlled by the textural and mineralogical composition (provenance) of the depositional environment and the diagenetic processes near the surface and during burial.

Porosity and permeability are two basic parameters used to appraise the superiority and inferiority of a reservoir's physical properties (Shang and Li 2018). According to Society of Petroleum Engineers Glossary, the fundamental property of a reservoir rock is porosity. However, for explorationists, in the effective reservoir rock, the most fundamental reservoir rock property is its permeability. These physical properties of a reservoir rock are continuously changing, from the time the sediments are deposited through to their burial at great depth and during any subsequent uplift. This is a combined function of mechanical compaction and of chemical processes involving the dissolution and the precipitation of minerals (Bjørlykke and Jahren 2010).

In the mechanical regime, compaction is controlled by the vertical effective stress, which results in reorienting, breaking, and consequently a denser and more stable packing of sand grains with increasing stress. In the chemical regime, compaction involves the dissolution of minerals or amorphous material and the precipitation of mineral cement. Here, time and temperature play a major role in controlling quartz cementation together with factors such as detrital mineralogy and texture. As burial temperatures reach about 60-80°C the precipitation rate of quartz will become sufficient for quartz cementation to strengthen the rock and mark the transition from mechanical to chemical compaction (Figure 3.1) (Bjørlykke, 2003; Bjørlykke and Egeberg, 1993; Walderhaug, 1994b).

Different studies have shown that grain-coating reduces the effect of quartz cementation at depth. The process can improve the reservoir quality of a sandstone reservoir at depth by decreasing the surface area available for precipitation of quartz cement (Ehrenberg 1993).

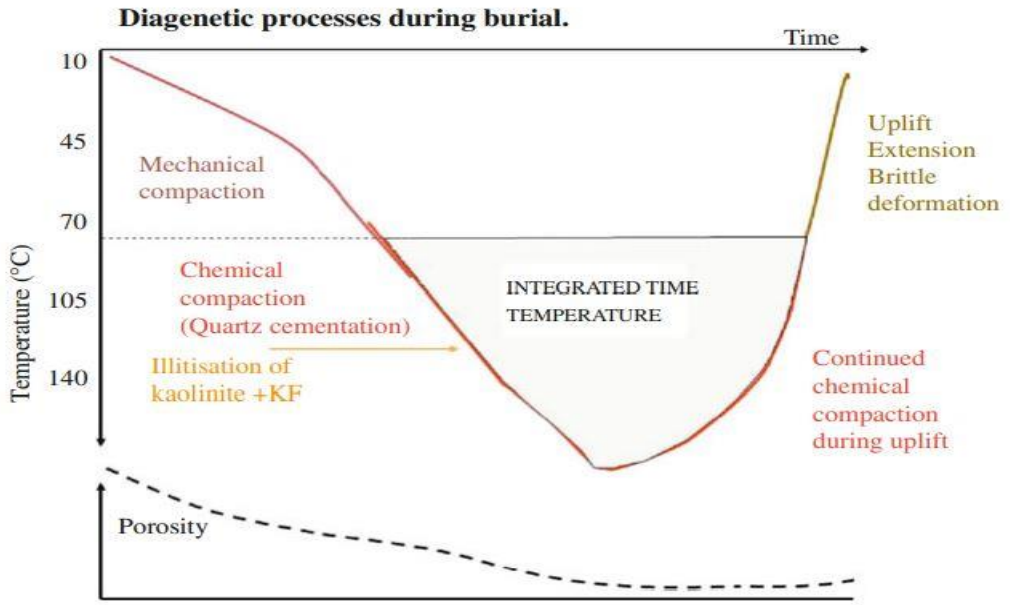

Figure 3.1. Overview of important diagenetic processes in clastic sandstone reservoirs (Bjørlykke and Jahren 2010)

3.2 Mechanical Compaction

During mechanical compaction, well-sorted sand with initial intragranular porosity of 40%-42% can be reduced to 35-25% when subjected to the stress of 20–30 MPa corresponding to 2–3 km depending on the grain strength and grain size. This process involves rearrangement, repacking, deformation and fracturing of grain (Bjørlykke and Jahren 2010; Houseknecht, 1987).

Grain rearrangement has been regarded as the primary control on compaction of well-sorted sandstones that are poor in matrix and ductile grains. Various authors have described the effect of grain rearrangement on the intergranular volume (IGV) of sandstone. Intergranular Volume (IGV) represents the total volume of the intergranular void space, matrix, and cement at the base of mechanical compaction (Paxton et al. 2002). Lander and Walderhaug, in their 1999, paper showed this effect as described by different workers; Exxon workers reported that a stable packing configuration represented by an intergranular volume (IGV) of 26% is reached (Figure 3.2) through grain rearrangement by approximately 2km burial depth for well-sorted samples (Paxton et al. 1990; Ajdukiewicz et al. 1991; Szabo and Paxton, 1991). Other workers have suggested that such a stable packing configuration cannot be achieved without some minor dissolution at grain contacts sufficient for grains to slip past each other (Füchtbauer, 1967). Palmer and Barton (1987) contended that rearrangement reduces IGV to a minimum of

34% and that further compaction requires some grain dissolution. Siever and Stone (1994) asserted that grain rearrangement accounts for an IGV decline to approximately 31% and that a stable packing configuration of 24% IGV requires a minor pressure solution. The degree of porosity loss by mechanical compaction determines the intergranular volume (IGV) at the onset of chemical compaction (quartz cementation).

Chuhan et al. (2002), in their experimental result, shows the effect of grain size on porosity in response to vertical effective stress of 25MPa. The result shows that coarse-grained quartz-rich sand loses more porosity than fine- and medium-grained quartz-rich sand. But after the effective stress of 20-25MPa, the porosity loss in both coarse, medium, and fine sandstone becomes rather similar regardless of the composition (Figure 3.3).

Overpressure reduces the effective stress and preserves porosity due to reduced mechanical compaction (Bjørlykke and Jahren 2010). This is, however, not the case in the Kristin field, where the porosity shows significant variations even though the sandstone units have been subjected to high overpressure (900 bar) and low effective stresses (Storvoll et al. 2002).

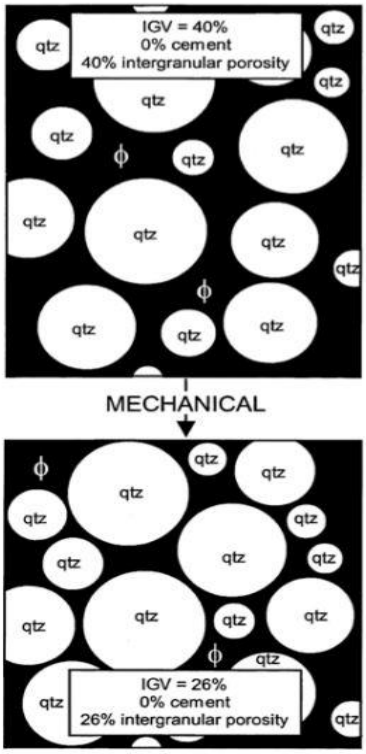

Figure 3.2. Illustration of compaction and decreasing IGV with increased depth down to chemical compaction starts. (Paxton et al. 2002).

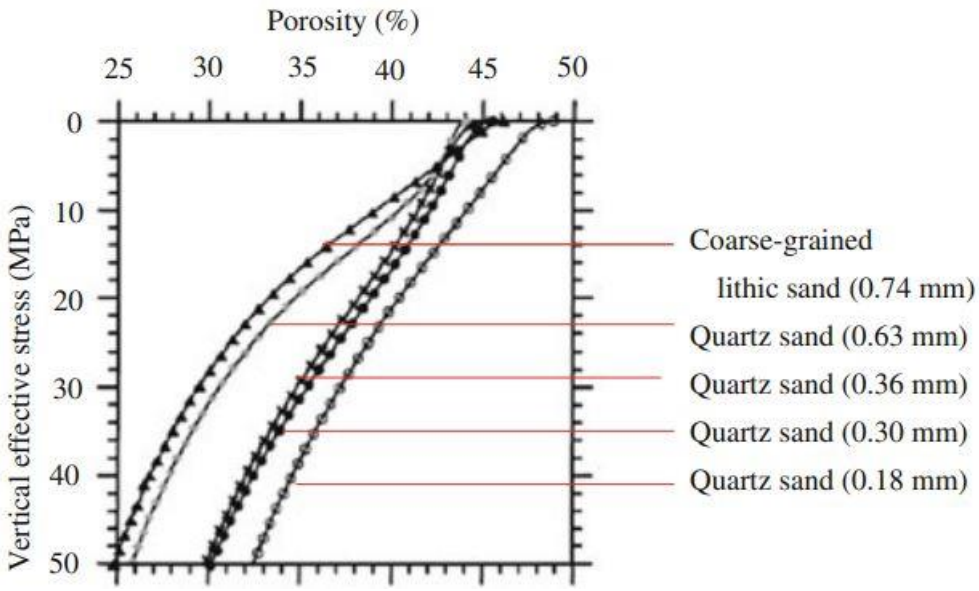

Figure 3.3. Illustration of compaction and decreasing IGV with increased depth down to chemical compaction starts. (Paxton et al. 2002).

3.3 Quartz Cementation

At a normal geothermal gradient, about 2.5km burial depth and 70-80^{o}C temperature, chemical compaction takes over while mechanical compaction ceases to be the prevailing porosity reducing factor since at this depth, quartz cementation which stabilises the grain framework dominates. The rocks are strengthened at a much faster rate by quartz cementation than the increase in vertical stress from the overburden. Further mechanical compaction in sandstone will, in most cases, be effectively stopped by only 2-4% quartz cement. The quartz cementation does not stop until nearly all the porosity is lost unless the temperature drops below 70-80^{o}C. In some cases, mechanical compaction prevails to deeper depth than 2.5km before quartz cementation takes over. For example, in areas with low geothermal gradient, quartz cementation may not start before 4–6 km burial depth. Porosity loss will then occur by mechanical compaction and severe grain crushing up to about 50 MPa effective stress (Bjørlykke and Jahren 2010).

The rate of quartz cement precipitation is a function of the surface area available. Walderhaug (1996) estimates the rate of quartz cementation by a factor of 1.7 for every 10^{o}C temperature increase. Some sources of quartz cement in sandstone reservoirs include dissolution of quartz associated with siltstones, dissolution/conversion of volcanic fragments, smectite to illite reaction, pressure solution at micro stylolites, K-feldspars dissolution, and kaolinite to illite conversion (Fuchtbauer 1983; Xi et al. 2015). Bulk of the quartz cement in Jurassic quartzose

sandstones from the North Sea and mid-Norwegian continental shelf is sourced from quartz dissolution at mica or illitic clay/quartz interfaces in adjoining stylolites (Oelkers et al. 1996). Dissolution at grain contacts requires stress, but the degree of stress needed is only relatively moderate (Bjørlykke and Jahren 2010). However, Oelkers et al. (1996) and Bjørkum (1996) claim that the magnitude of stress (overburden load) is unnecessary for quartz dissolution since there is no physical deformation on the mica grain surfaces facing the pores where quartz overgrowth forms.

The silica dissolved at grain contacts or along stylolites is transported by diffusion to the grain surfaces where the quartz overgrowth forms (Figure 3.4). Porosity depends strongly on the distance of stylolites from each other. If the interstylolite distance is large, the amount of quartz cement decreases away from the stylolite therefore the porosity is high, compared to small interstylolite with low porosity (Figure 3.5) (Bjørlykke and Jahren 2010; Oelkers et al. 1996)

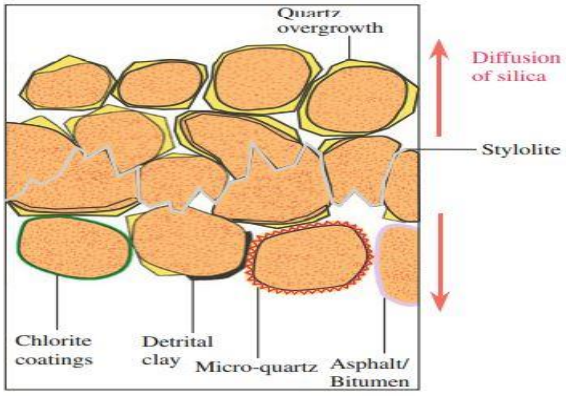

Figure 3.4. Schematic illustration of a stylolite. The dissolved silica is transported away from the clay-rich stylolite by diffusion. Grain coatings such as chlorite, micro-quartz and bitumen prevent or retard quartz cementation (Bjørlykke and Jahren 2010)

.

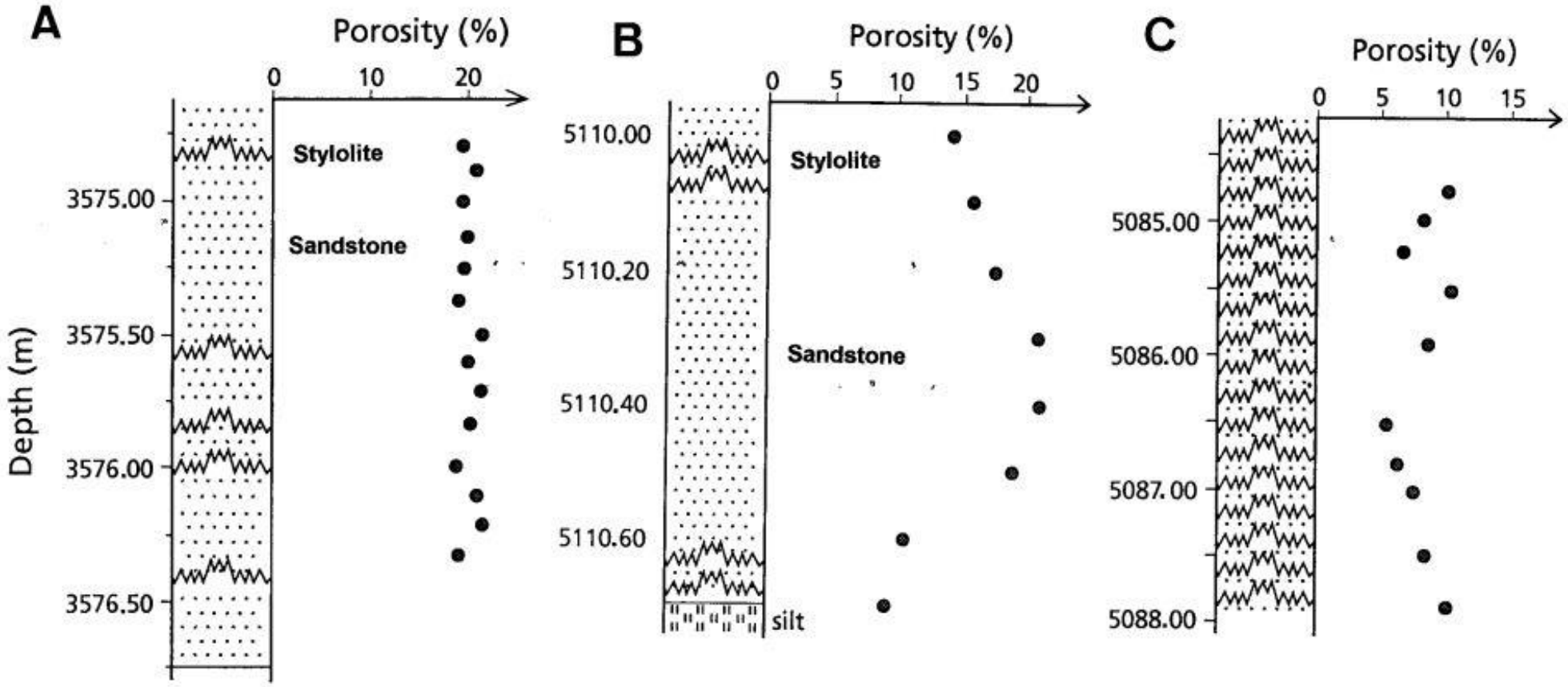

Figure 3.5. Variation of porosity with depth in three sections of sandstones cores obtained from (A) Hugin Formation at a depth of ~3.6 km; and (B) and (C) Bryne Formations at a depth of ~5.1*km. Jagged solid lines denote locations of stylolites (Oelkers et al. 1996)*

3.4 Porosity preservation in deeply buried sandstone

Since quartz cementation is the main process responsible for the reduction of porosity at depth, preservation of porosity at depth will depend on the factors capable of inhibiting quartz cementation. Bloch et al. (2002) outlined three factors capable of inhibiting quartz cementation and causing anomalously high porosity in deeply buried sandstone, they include:

1. grain coats and grain rims (effective only in detrital-quartz–rich sandstones)
2. early emplacement of hydrocarbons
3. shallow development of fluid overpressure

Quartz cementation is inhibited or stopped for some time, if the surfaces of sand grains are coated with minerals like chlorite, illite, haematite, micro-quartz, detrital clay or with substances like petroleum or bitumen. To avoid confusing clay mineral (chlorite and illite) coating with a detrital clay coating, Wilson (1992) proposed the term "inherited clay rims" to describe detrital clay coating on framework grains.

Several authors have studied the effect of oil emplacement in inhibiting quartz cementation. Some authors have argued that oil emplacement does not inhibit quartz cementation (Walderhaug, 1990; Ramm and Bjørlykke, 1994; Marcussen et al. 2010). Walderhaug (1990) showed that quartz cement produced by pressure solution might continue after oil emplacement since quartz produced by pressure solution at stylolites or at grain contacts would only have to diffuse a short distance through water films to sites of precipitation. He further mentioned that in a water wet system, the rate of quartz cementation might decrease and as oil saturation increases because the transport of silica by advection as well as by diffusion becomes much less efficient. However, oil or bitumen may form effective coatings on quartz surface in an oil wet reservoir, thereby preventing precipitation on the grain surface (Bjørlykke and Jahren 2010). The extent of retardation depends on the sandstone fabric and oil saturation (Worden et al. 1995).

Numerous published studies have shown that inhibition of quartz cementation by grain coating minerals like chlorite, micro-quartz and illite can preserve high primary porosity in deeply buried sandstone (Figure 3.6). Examples of such studies relevant to this project include the abundant chlorite coatings and illite and illite/chlorite coatings in the Jurassic Tilje and Garn formations at Haltenbanken, offshore mid-Norway (Ehrenberg 1993; Storvoll et al. 2002).

Sandstones with grain coatings may remain uncemented down to 4–5 km burial depth and be subjected to 40–50 MPa effective stress, causing pervasive grain crushing (Chuhan et al. 2002). For grain-coating to be effective, the clay minerals must cover the grains before significant quartz cementation starts (>2–3 km), the coating must be continuous and cover the entire grain surface, the coating must be present on most of the grains in the sample (Storvoll et al. 2002).

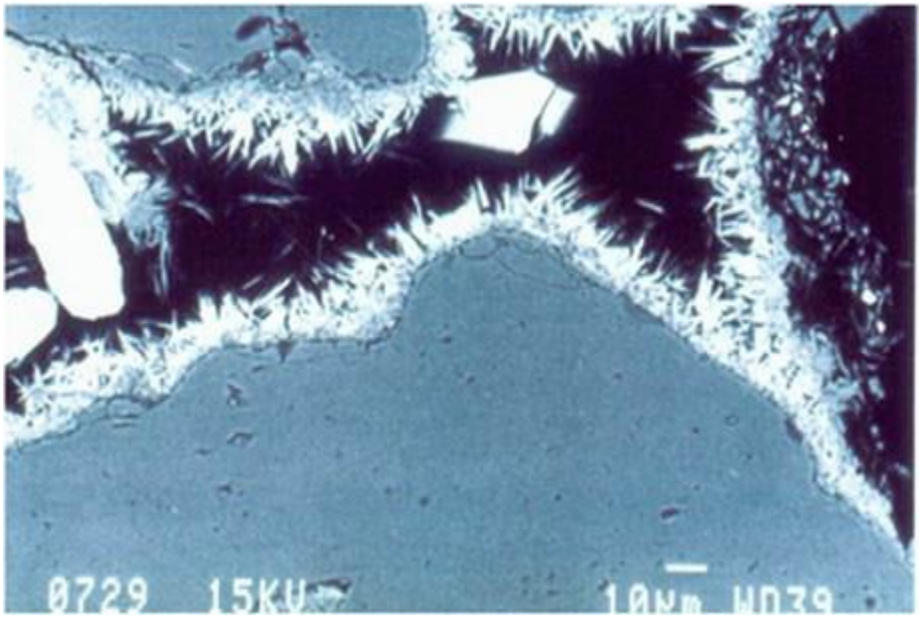

Figure 3.6. Needle like structure is chlorite coating over quartz grains (Bjørlykke and Jahren, 2010).

3.4.1 Chlorite coating

Authigenic chlorite (Figure 3.6) is the most reported effective coat occurring in hydrocarbon reservoirs (Pittman et al. 1992). Chlorites have variable chemistry, but the two most important types are Fe-rich (e.g. chamosite) and Mg-rich (e.g. clinochlore) chlorite. The Fe-rich chlorite occurs in near-shore marine sandstones (frequently deltaic) while Mg-rich chlorite occurs in arid and semi-arid sabkha environments or any facies with close contact with evaporite basins (Hillier, 1994; Bloch et al. 2002; Ehrenberg 1993).

In order to predict the high porosity in deeply buried sandstone reservoir caused by chlorite coating, it is important to understand what controls the development of authigenic chlorite. The dominant control on the occurrence and type of chlorite is the initial mineralogy. The composition of the precursor mineral controls the development of chlorite coating (Dowey et al. 2012). The chlorite found in marine sandstones is most probably an alteration product of an earlier iron silicate phase (precursor) formed on the seafloor and which may be linked to facies (Bjørlykke and Jahren 2010).

A summary of chlorite-coats precursor clay minerals and diagenetic chlorite-coats formed from the dissolution of detrital grain described by different authors in Dowey et al. (2012) is shown in Table 3.1 and Table 3.2 below.

Table 3.1. Chlorite-coats precursor clay minerals

Precursor clay mineral	*References*
Berthierine	*Ehrenberg, (1993)*
Odinite	*Ryan and Reynolds, (1997)*
Kaolinite	*Boles and Frank, (1997); Hillier and Velde (1992)*
Smectite	*Chang et al. (1986); Humphreys et al. (1989); Anjos et al. (2003); Bloch et al. (2002); Ajdukiewicz et al. (2010); Kugler and McHugh (1990); Gaupp et al. (1993); Hillier et al. (1996); Platt, (1994); Pay et al. (2000)*

Table 3.2. chlorite-coats formed from the dissolution of detrital grain

Dissolution of detrital grain	*References*
Dissolution of iron- and magnesium-rich detrital grains and volcanic rock fragment	*AlDahan and Morad, (1986); Anjos et al. (2000); Blackbourn and Thomson, (2000); Burns and Ethridge, (1979); De Ros et al. (1994); Remy, (1994); Thomson, (1979); Valloni et al. (1991); Worden and Morad, (2003)*
Dissolution of mud intraclasts	*Worden and Morad, (2003)*
Dissolution of volcanic ash	*Storvoll et al. (2002); Humphreys et al. (1994)*

3.4.2 Illite Coating

Illites, just like chlorites, form continuous grain coatings on grains, and they can be very effective in resisting quartz cementation and preserving porosity in deeply buried sandstone (Storvoll et al. 2002). Due to its fibrous and flaky appearance, illite coatings appear to be thick (6 to 8µm). Ramm and Ryseth (1996) made a conclusion that late-stage illite and precipitation of quartz in pore throat control reservoir permeability at depths greater than 3.5km. Illite formation generally requires pore fluid and pore space rich in potassium, silica, and aluminium (Chima et al. 2018). However, the dissolution of K-feldspar which serves as a potassium source to convert kaolinite to illite results in the formation of this late stage illite (Bjørlykke and Aagaard, 1992).

Chapter Four: Methodology and Dataset

4.1 Introduction

The focus of this thesis has been to understand the diagenetic processes and the factors that help preserve the reservoir quality of deeply buried sandstone. Different techniques have been used to achieve this objective; they include quantification and identification of minerals in thin sections under an optical microscope and scanning electron microscope, and petrophysical evaluation using available well logs to identify lithology/distribution of shale, correlate zones, and estimate porosity. However, these techniques have various levels of resolution in acquiring data and result needed for this study. As a result, the techniques are susceptible to errors.

4.2 Petrophysical analysis

For this study, six (6) petrophysical well log data from wells drilled in offshore Mid-Norway were provided. The wells are: 6406/2-1, 6406/2-2, 6506/12-1, 6506/12-10, 6506/12-10A, and 6506/11-5S. However, well log data from well 6506/11-5S was not included in this project's petrophysical analysis mainly because the neutron log data was erroneous. Information on the wells was collected from the Norwegian Petroleum Directorate (NPD) webpage. They are presented in Table 4.1 below.

Table 4.1. Information on the wells from Norwegian Petroleum Directorate (NPD) webpage

Attribute/well name	6406/2-1	6406/2-2	6506/12-1	6506/12-10	6506/12-10A	6506/11-5S
Purpose	Wildcat	Appraisal	Wildcat	Appraisal	Appraisal	Appraisal
Water Depth (m)	278.0	272.0	250.0	285.0	285.0	288.0
Total depth (MD) [m RKB]	5292.0	5367.0	4924.0	5097.0	6260.0	4790.0
True vertical depth (TVD) [m RKB]	5283.0	5351.0	-	5096.0	5361.0	4729.0
Maximum inclination (°C)	15.3	15.3	-	2.6	57.7	16.7
Bottom hole temperature (°C)	172	183	168	160	189	156
Kelly bush elevation (m)	24.0	24.0	22.0	24.0	24.0	22.0
Oldest penetrated age	Early Jurassic	Early Jurassic	Early Jurassic	Early Jurassic	Early Jurassic	Early Jurassic
UTM Zone	32	32	32	32	32	32
Content	Gas/Condensate	Gas/Condensate	Gas/Condensate	Shows	Oil/Gas	Oil/Gas
Temperature (°C)	163 (@4525m)	176 (@4898m)	143.6 (@4225m)	165.2 (@4713m)	165.2 (@4713m)	Limited reading

4.2.1 Well Correlation and Interpretation

In petrophysical analysis, well log interpretation is an analysis of well logs interpreted to determine vertical stratigraphic sections based on the characteristics of the log (Homewood et al. 1992*).* For this study, well logs were interpreted to determine the lithology and identify areas of high and low porosity. The wells were also divided into formations for correlation purposes. To effectively describe lithology and porosity. A combination of Gamma-ray log, Neutron log, and Bulk density log was used to make a good description.

The following wells: 6406/2-1, 6406/2-2, 6506/12-1, 6506/12-10, and 6506/12-10A were correlated to understand the vertical and lateral relationship and continuation of the sand bodies.

All these interpretations were made on a log and core interpretation software called “techlog”.

4.2.2 Cross plotting

Cross plotting is a useful petrophysical tool for understanding the relationship between two or more petrophysical variables. In this study, different cross plots, including porosity/depth, neutron/density, gamma-ray/density, and gamma-ray/neutron cross plots, were used to describe the porosity distribution with depth and define depth lithology, respectively. Techlog software was also used to compute the petrophysical cross plots used in this study.

4.3 Petrographic analysis

The methods used for the petrographic study of the data for this project include:

1. Thin section analysis
2. Point counting and grain size analysis
3. Scanning Electron Microscope (SEM) analysis

4.3.1 Thin section analysis

Thin sections analysis for this study incorporates mineral identification, cementation, grain coating, porosity, textural analysis, and point counting. These analyses were performed to understand the depositional environment, estimate the bulk mineralogical composition, classify the sandstone, and determine the influence of mineralogy and cementation on reservoir quality.

A total of twenty-seven (27) polished and blue epoxy impregnated thin sections from six wells in Tilje, Tofte, and Ile Formations (16 from the Tilje Formation, 8 from the Tofte Formation, and 3 from the Ile Formation) in the Halten Terrace, offshore Mid-Norway were analyzed under a polarizing petrographic microscope for this purpose (Table 4.2). Photomicrographs of selected samples were taken using a camera (Jenoptik ProgRes CT3) mounted on the petrographic microscope and linked to the computer using ProgRes CapturePro software.

Table 4.2. Thin section sample depths used for this study from six wells in Ile, Tofte, and Tilje Formations

6406/2-1	6406/2-2	6506/12-1	6506/12-10	6506/12-10A	6506/11-5S
4844.75	4706.25	4255.00	4943.25	5686.85	4554.54
4847.50	4716.25	4271.66	5012.85	5694.70	4703.28
4850.25	4726.25	4273.66			
5101.50	4884.50				
5104.00	4897.00				
	4897.75				
	4910.25		KEY:	Formation	
	4919.75			Ile	
	4984.25			Tofte	
	4986.75			Tilje	
	5119.55				
	5126.50				

4.3.2 Point counting and grain size analysis

A total of 300 points per thin section were counted under an optical microscope. This was achieved with the aid of pelcon automatic point counter mounted on the turning disc stage of the optical microscope. The purpose of this point counting is to determine the percentage of the sandstone framework grain compositions (quartz, feldspar, and rock fragments) cements (carbonate and quartz), clays, matrix, and pore space (primary and secondary porosity). A ternary plot was made from the point count data with the aid of the Tri-Plot program. Intergranular volume (IGV) was also calculated from this point count data.

Grain size analysis was performed with the help of ImageJ software. This analysis was carried out on representative photomicrographs of each sample by measuring the area of 20 to 60 grains from each thin section using ImageJ software. The mean of the measured area is calculated and converted to diameter to determine the grain size using the Udden-Wentworth grain size scale (Wentworth, 1992). The results of these point counts were cross plotted using Microsoft excel program to see the relationship of the different parameters.

4.3.3 Scanning Electron Microscope (SEM) analysis

Seven (7) carbon-coated thin sections were selected from the 27 thin sections based on similarities in lithology (Table 4.3). These samples were examined using JEOL JSM-6460LV Scanning Electron Microscope (backscattered electrons) with a LINK INCA Energy 300 Energy Dispersive X-ray (EDS) system primarily for identification and confirmation of minerals that seemed difficult to identify under the petrographic microscope. In addition, SEM was also used to analyze the effects and distribution of pore-filling clay minerals and clay coatings.

The Energy-dispersive X-ray spectroscopy (EDS), which relies on the interaction between the X-ray excitation source and the sample, gives an elemental analysis of the sample. This makes it possible to determine the mineral under probe (Goldstein et al. 2018).

Table 4.3. Selected carbon-coated thin section sample depths selected for SEM analysis

6406/2-1	6406/2-2	6506/12-1	6506/12-10	6506/11-5S
5101.50	4884.50	4255.00	4943.25	4554.54
5104.00				4703.28

4.4 Uncertainties of Petrographic analysis

When analyzing minerals in thin sections under a petrographic microscope, misinterpretation of minerals is possible. Some misinterpretations encountered in this study include difficulty differentiating untwined albite grain and quartz grain, as both grains exhibit similar optical features. The consequence of this is the underestimation of albite content which in return will affect the feldspar quantity.

Some of the thin sections have been poorly preserved, as they contain a lot of dark material, which masks some minerals leading to difficulty in identifying these minerals.

The method used for grain size analysis is subject to some level of error since the interpreter chooses the measured grains, and some of the grains are not rounded. This can affect the grain size accuracy. In addition, an overestimation of grain size due to quartz overgrowth with weakly developed dust-rim is possible.

The use of a cathodoluminescence detector was unfortunately not available. This resulted in the use of point counting to quantify quartz cement and overgrowths. As a result, inaccuracy

in quantifying quartz overgrowths and cement is possible since some of the samples exhibit weak to no dust rims.

Chapter Five: Petrophysical Analysis Results

5.1 Introduction

A typical petrophysical evaluation includes well log analysis and core analysis. However, due to the unavailability of core samples, well correlation and the determination of reservoir quality through the evaluation of porosity and lithology distribution in the studied well was limited to only well log analysis. Well log analysis was performed on all wells except well 6506/11-5S.

5.2 Cross Plots

Petrophysical analysis software (Techlog 2020.1.1) was used to determine/describe lithology and porosity and their distribution in five of the wells provided. Lithology description is based on cross plots between neutron and density log (Figure 5.1), gamma-ray and neutron log (Figure 5.2), and gamma-ray and density log (Figure 5.3). Each of these logs responds to shales, sandy shales, and sands differently.

Neutron-density cross-plot is an essential petrophysical tool that can be used to differentiate lithology with the help of a pure lithology line (quartz sandstone, calcite, and dolomite) overlay. This cross plot is also useful in identifying shales. Clean sand to shaly sand and the shale composition of the wells are shown in the neutron-density cross plots below (Figure 5.1).

While gamma-ray log considers the natural radioactivity of the formation, and it is not affected by porosity, neutron logs measure the hydrogen content of a formation. This measurement shows an increase in shale content and gives a nearly constant response when measured through sand (Figure 5.2) (Heslop and Heslop, 2003). The gamma-ray and density log cross plots show a trend indicated by the nearly constant response of shale to bulk density and an increase in bulk density of sand as the gamma-ray increases, this pattern shows the sand becomes shalier as it approaches the sand/shale boundary (Figure 5.3). Carbonate cement shows an increase in bulk density and constant gamma-ray response. Following these data trends on both gamma-ray/neutron and gamma-ray/density cross-plot, we can identify sand/shale boundary in the different wells to be 75API units. The data trending to the right represents carbonate cement in the sand.

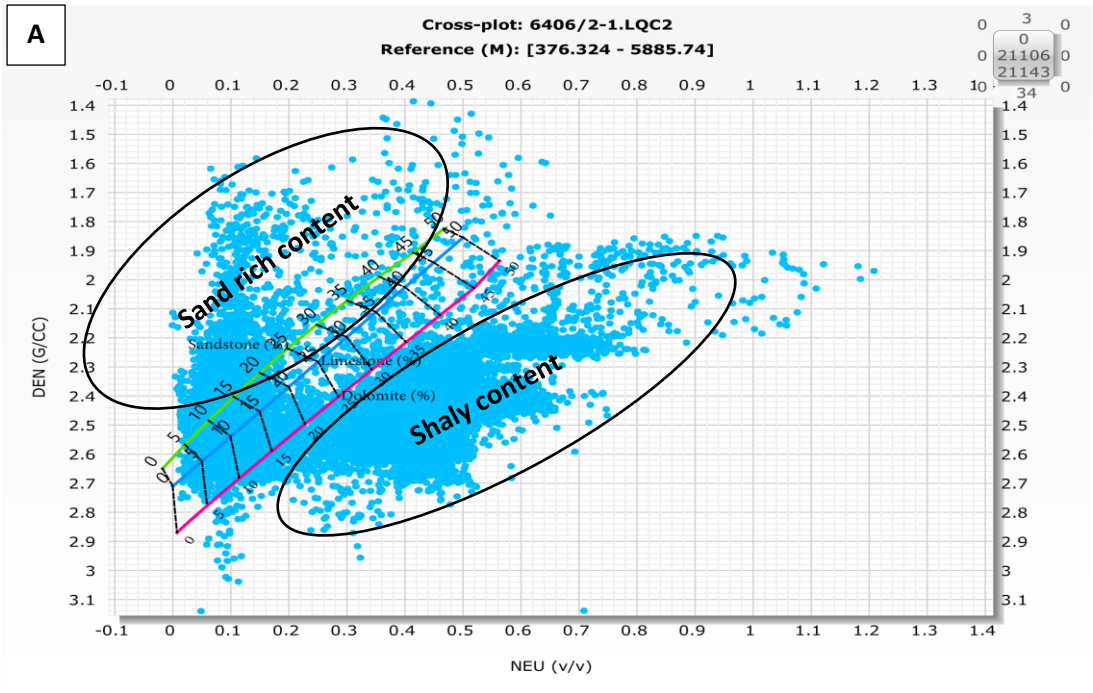

Charts:

Schlumberger, Por-11 & Por-12, Neutron Porosity vs Bulk Density, TNPH (rhof = 1 g/cm3, NaCl = 0 kppm)

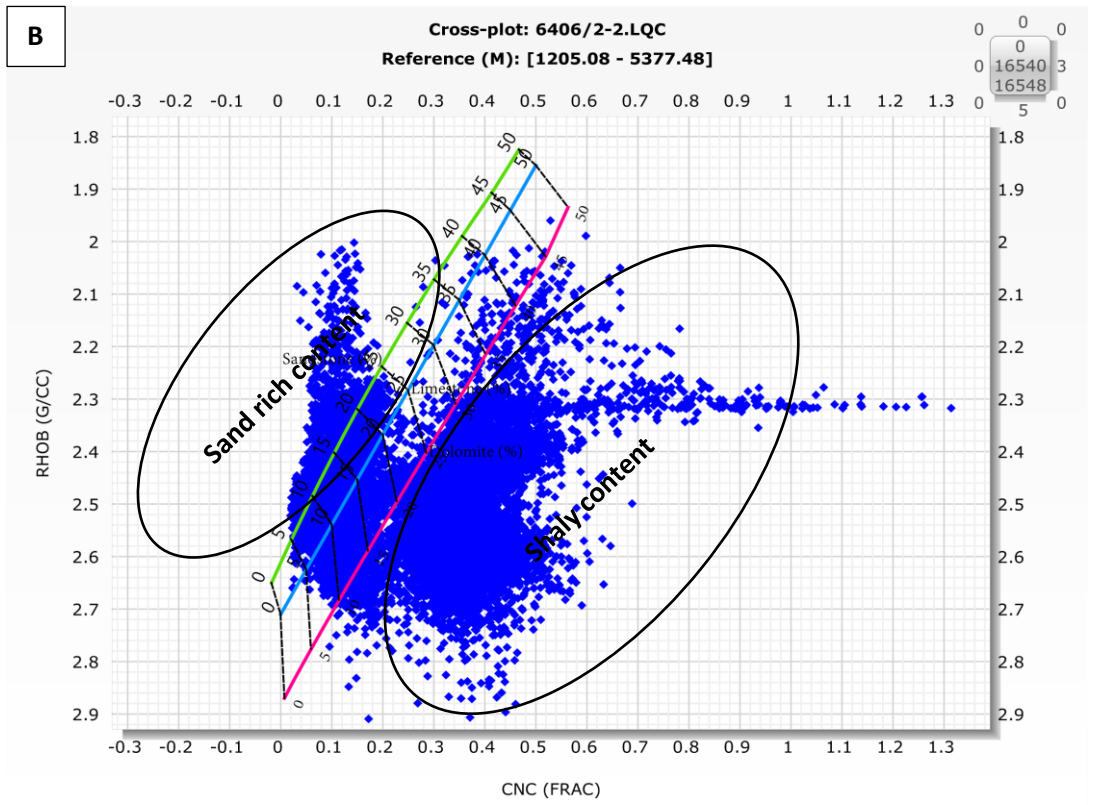

Charts:

Schlumberger, Por-11 & Por-12, Neutron Porosity vs Bulk Density, TNPH (rhof = 1 g/cm3, NaCl = 0 kppm)

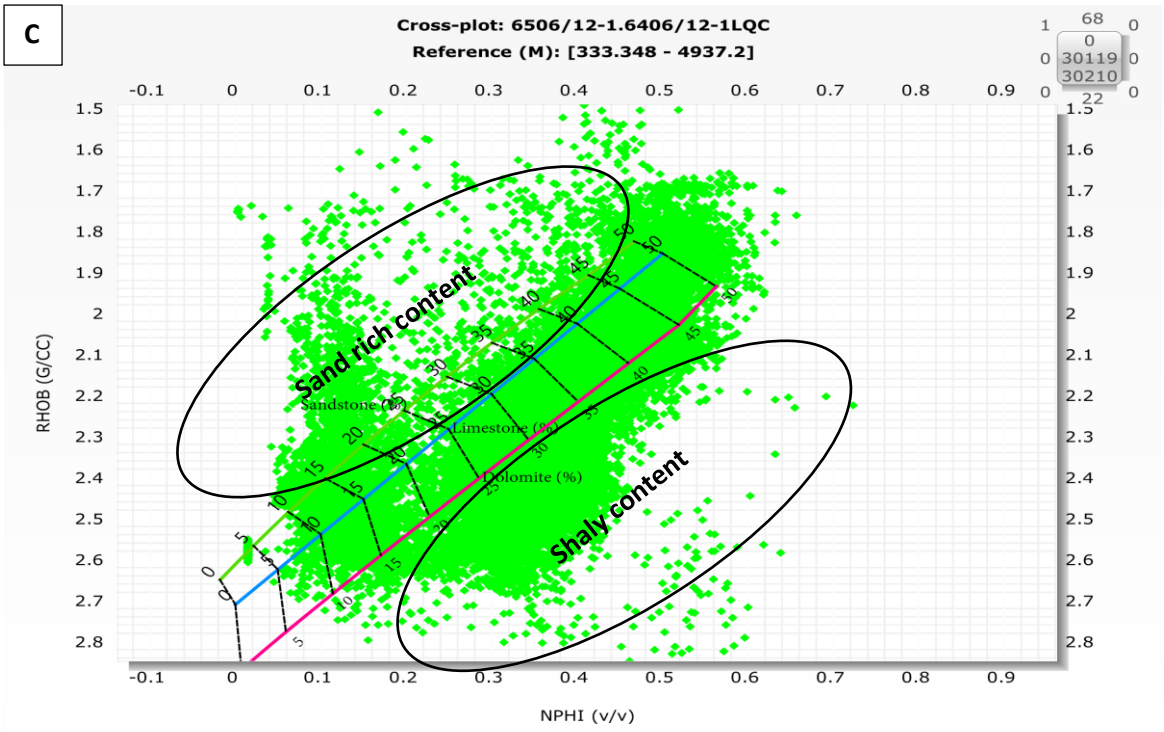

Charts:

Schlumberger, Por-11 & Por-12, Neutron Porosity vs Bulk Density, TNPH (rhof = 1 g/cm3, NaCl = 0 kppm)

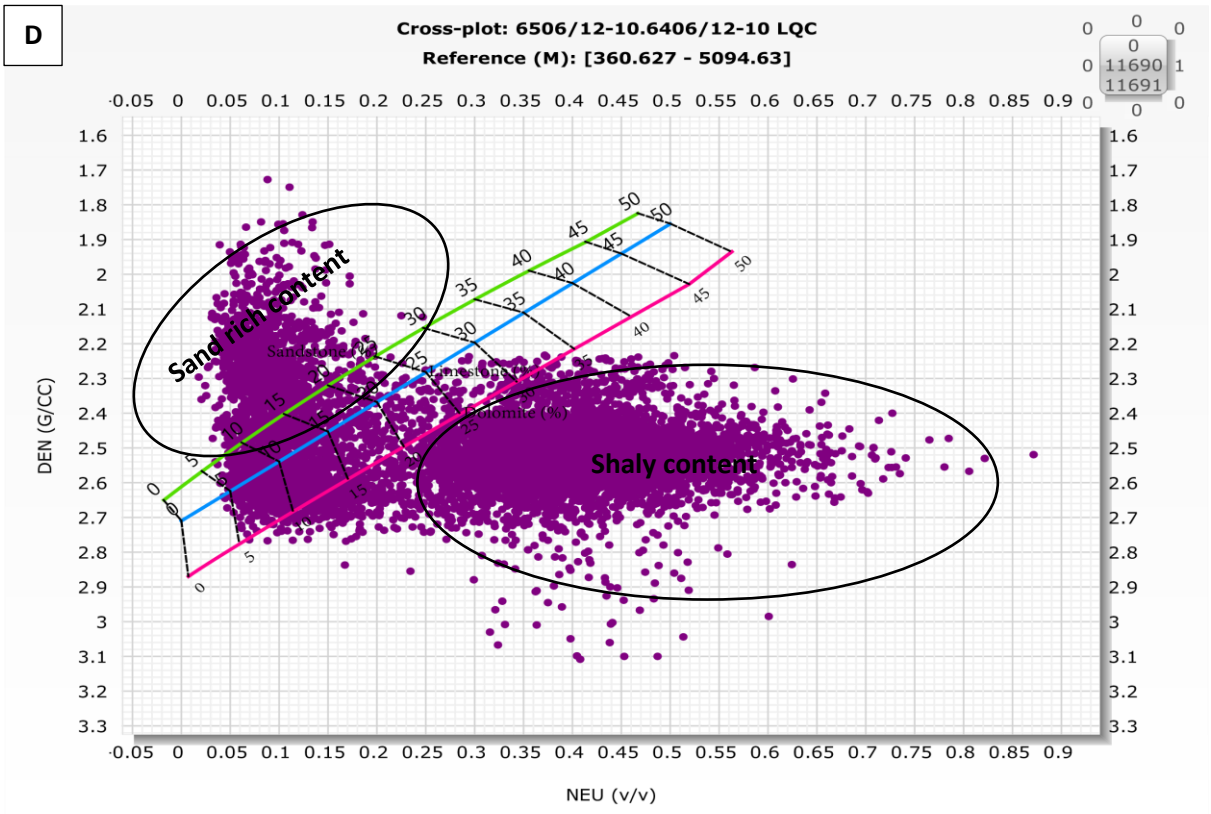

Charts:

Schlumberger, Por-11 & Por-12, Neutron Porosity vs Bulk Density, TNPH (rhof = 1 g/cm3, NaCl = 0 kppm)

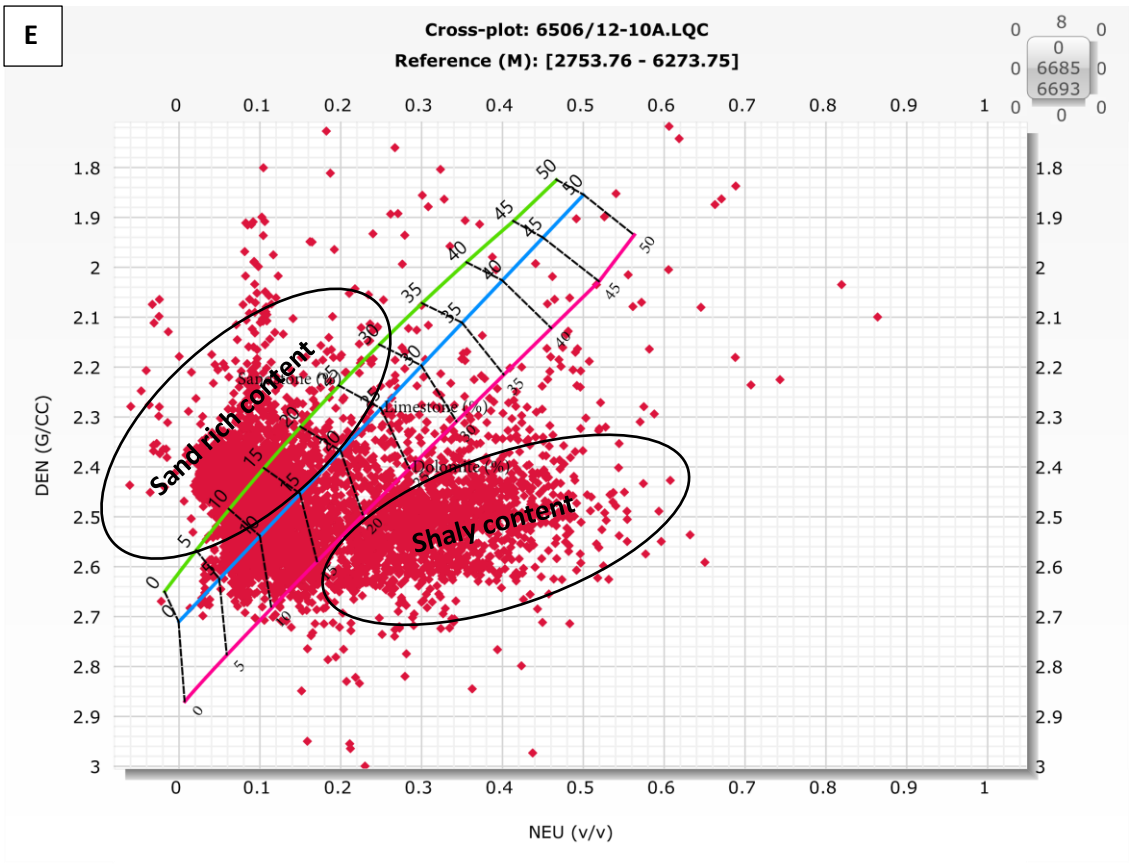

Charts:

Schlumberger, Por-11 & Por-12, Neutron Porosity vs Bulk Density, TNPH (rhof = 1 g/cm3, NaCl = 0 kppm)

Figure 5.1. Lithological interpretation using neutron-density log cross plot (A) well 6406/2-1 (B) well 6406/2-2 (C) well 6506/12-1 (D) well 6506/12-10 (E) well 6506/12-10A

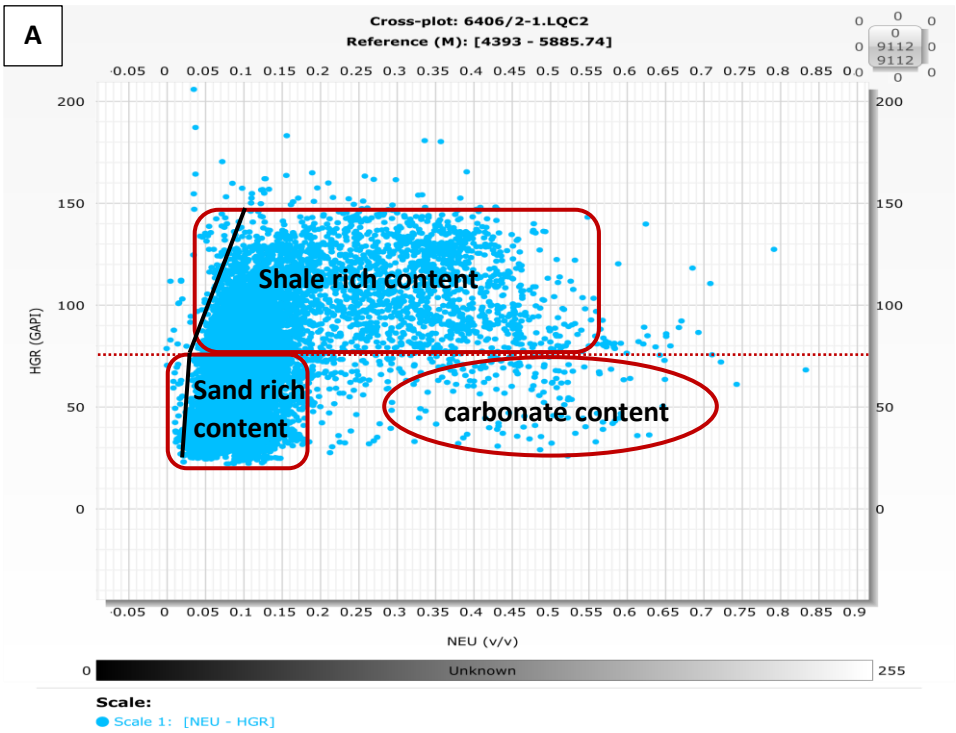

B

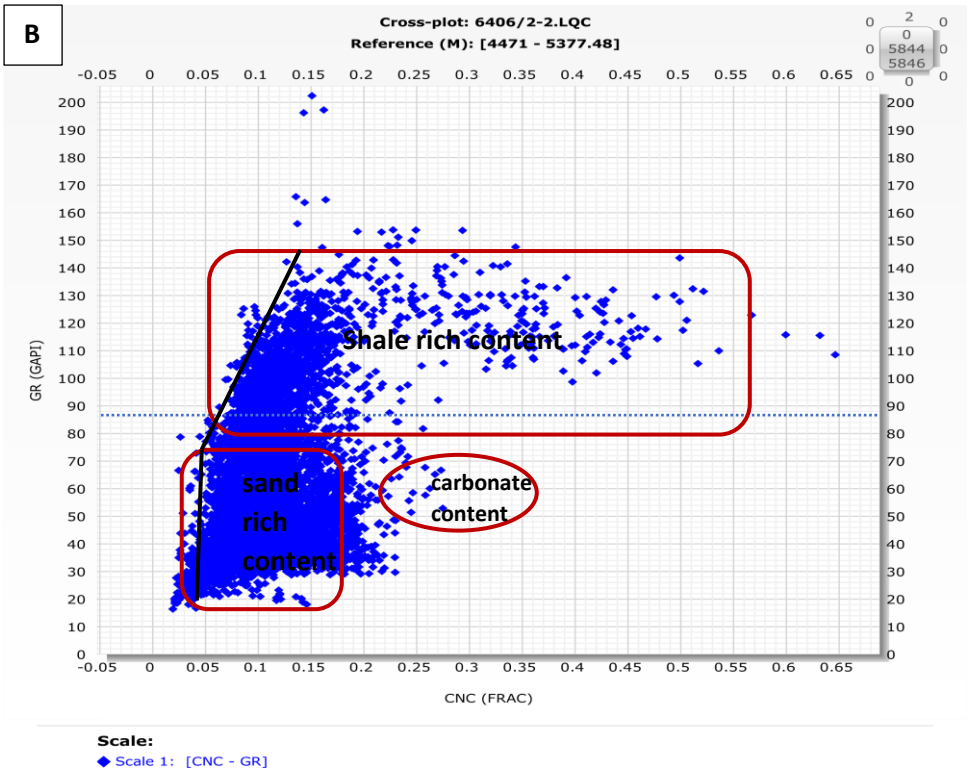

Scale:
◆ Scale 1: [CNC - GR]

C

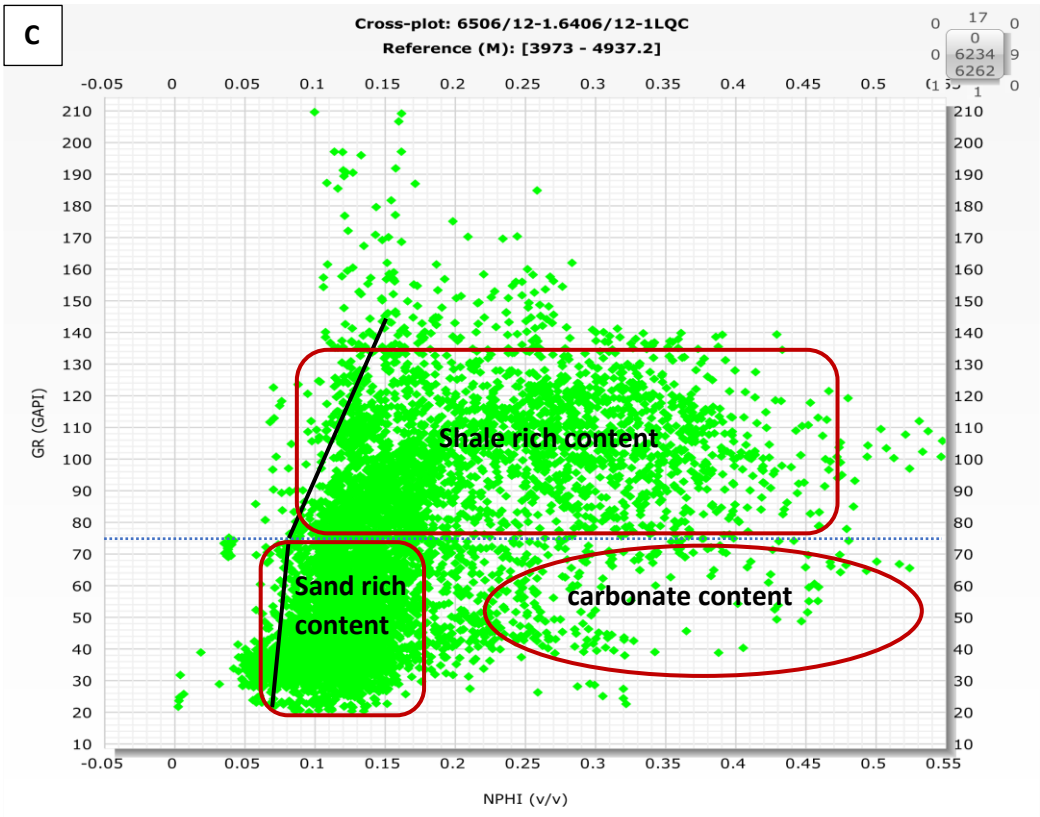

Scale:
◆ Scale 1: [NPHI - GR]

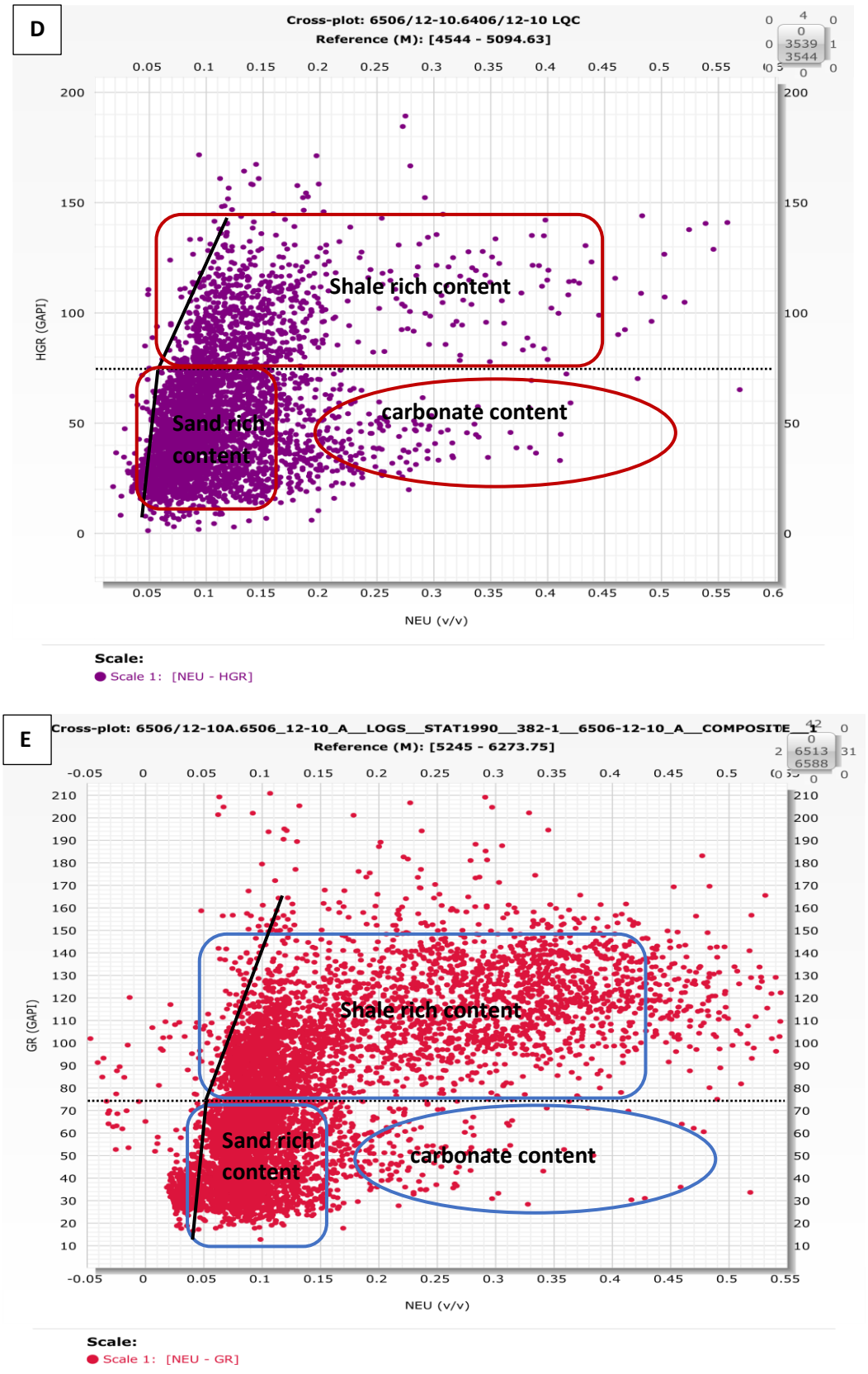

Figure 5.2. Lithological interpretation using neutron-gamma ray log cross plot. Dotted line indicates sand/shale cutoff mark of 75API (A) well 6406/2-1 (B) well 6406/2-2 (C) well 6506/12-1 (D) well 6506/12-10 (E) well 6506/12-10A

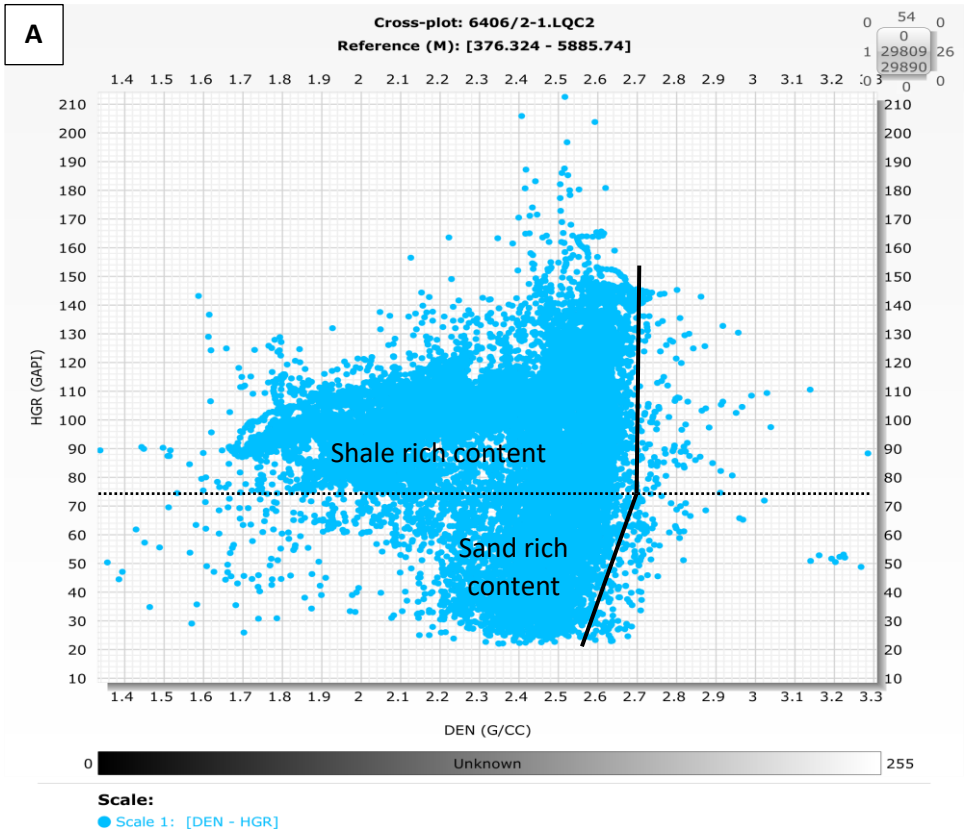
A
Cross-plot: 6406/2-1.LQC2
Reference (M): [376.324 - 5885.74]
HGR (GAPI)
DEN (G/CC)
Shale rich content
Sand rich content
Unknown
Scale:
Scale 1: [DEN - HGR]

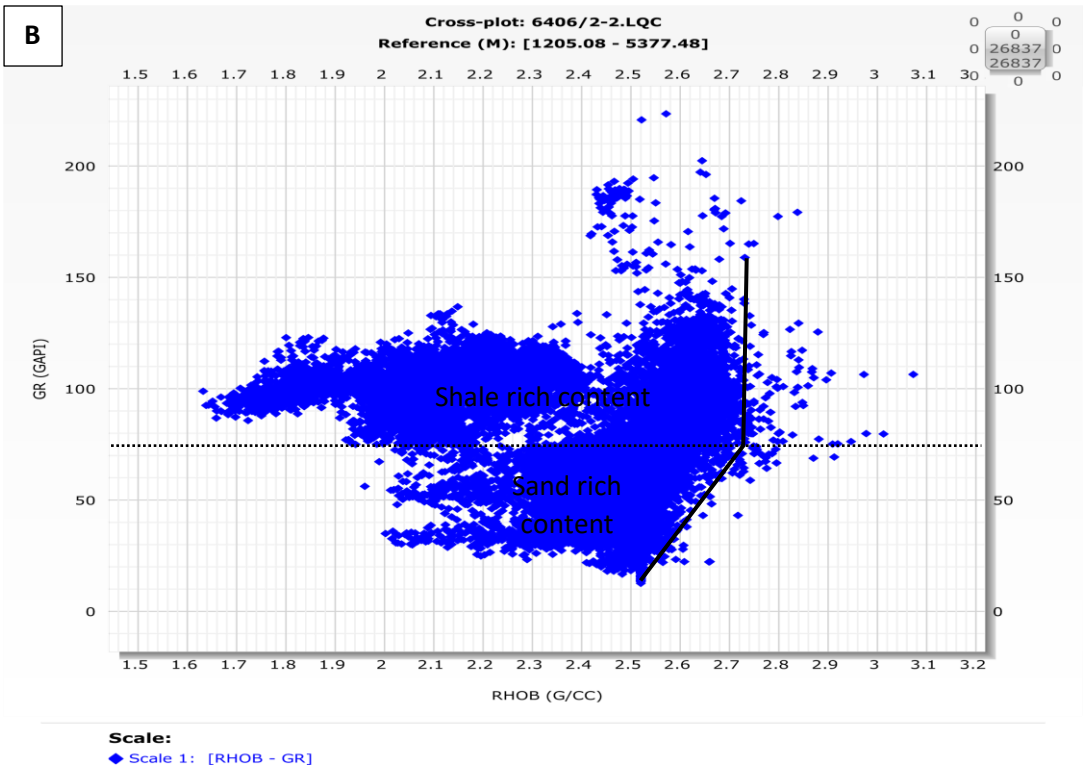
B
Cross-plot: 6406/2-2.LQC
Reference (M): [1205.08 - 5377.48]
GR (GAPI)
RHOB (G/CC)
Shale rich content
Sand rich content
Scale:
Scale 1: [RHOB - GR]

C

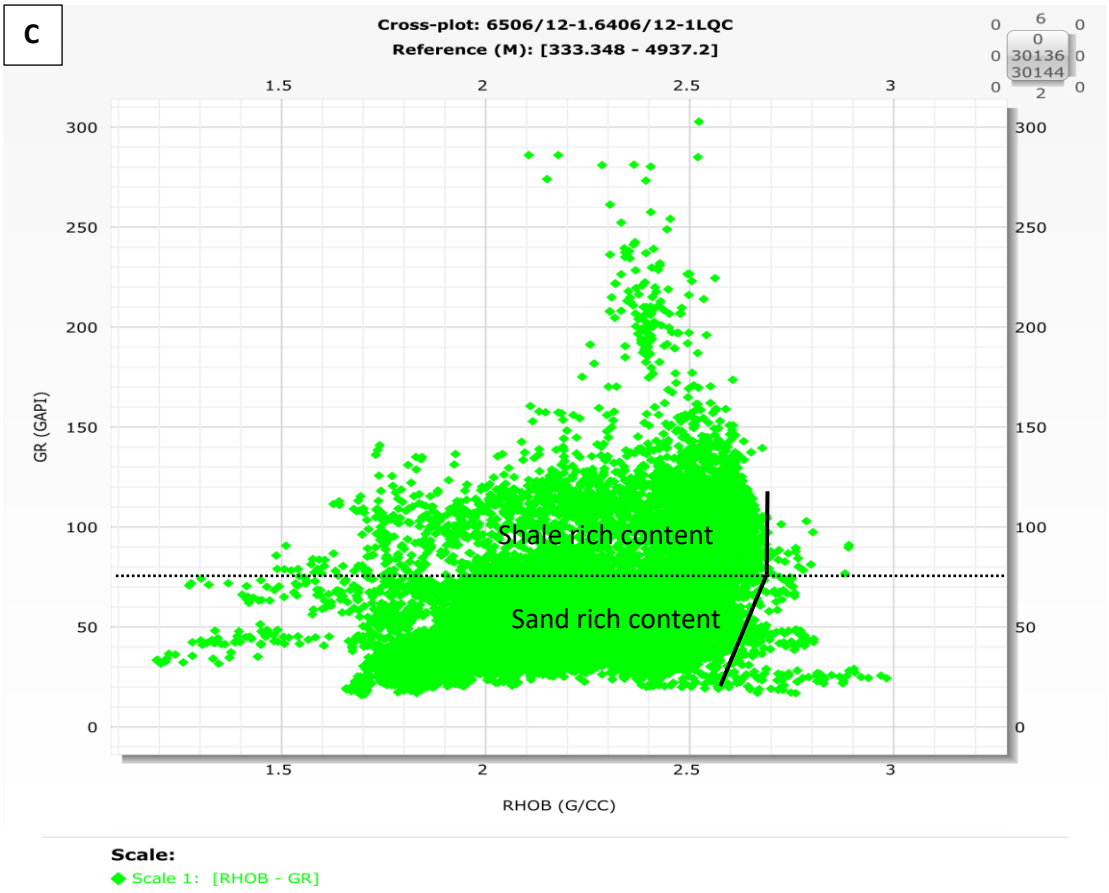
Cross-plot: 6506/12-1.6406/12-1LQC
Reference (M): [333.348 - 4937.2]
GR (GAPI)
RHOB (G/CC)
Shale rich content
Sand rich content
Scale:
Scale 1: [RHOB - GR]

D

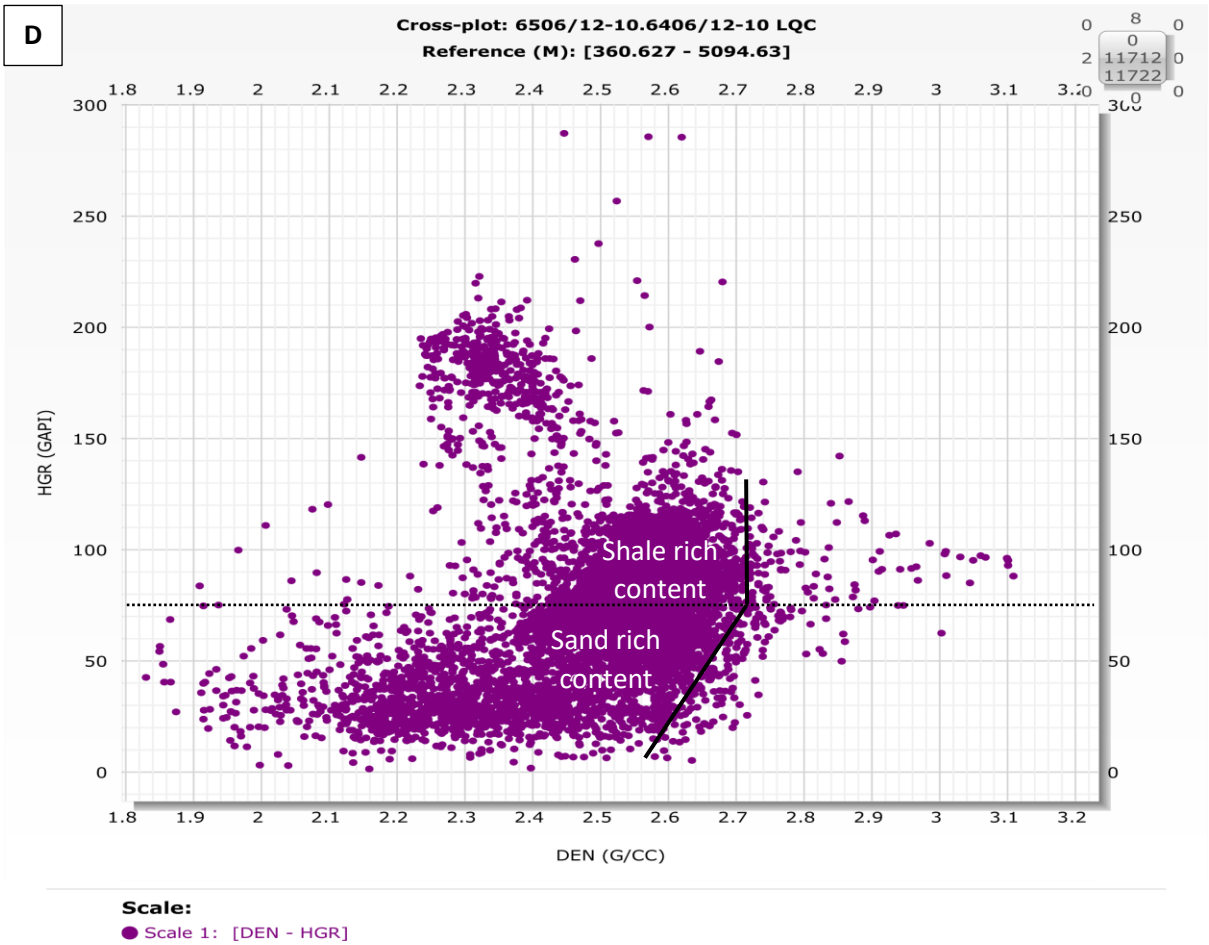
Cross-plot: 6506/12-10.6406/12-10 LQC
Reference (M): [360.627 - 5094.63]
HGR (GAPI)
DEN (G/CC)
Shale rich content
Sand rich content
Scale:
Scale 1: [DEN - HGR]

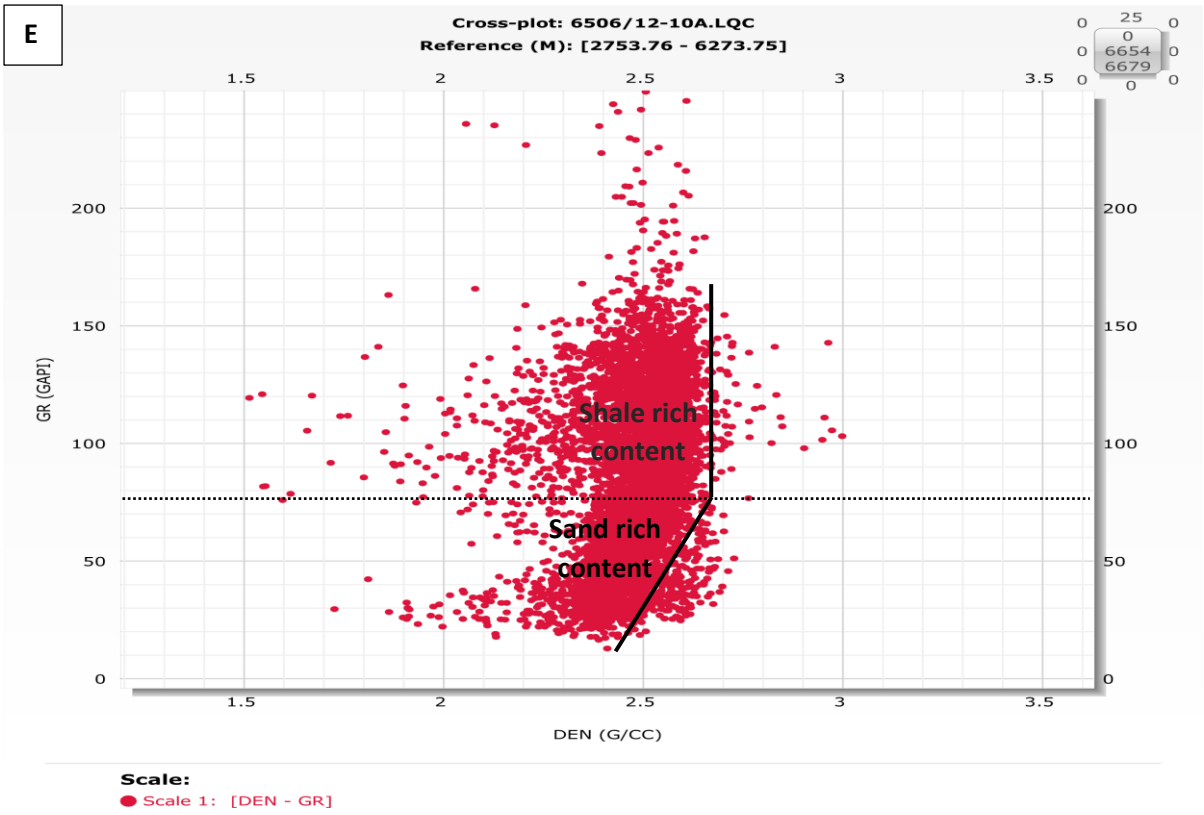

Figure 5.3. Lithological interpretation using density-gamma ray log cross plot. Dotted line indicates sand/shale cutoff mark of 75API (A) well 6406/2-1 (B) well 6406/2-2 (C) well 6506/12-1 (D) well 6506/12-10 (E) well 6506/12-10A

The relationship between neutron-density derived total porosity, and depth in sand rich zones of the five wells revealed porosity is well preserved in these deeply buried sandstones (Figure 5.4). This could be due to the presence of grain coating minerals and mineral dissolution at that depth.

5.3 well correlation

Tilje, Tofte, Ror, and Ile Formations have been correlated laterally across well 6406/2-1, 6406/2-2, 6506/12-1, 6506/12-10, and 6506/12-10A (Figure 5.5). The correlation was based on the formation depth provided on the NPD fact page. Correlation across the five wells showed that the oldest Ror Formation is absent and does not continue lateral in well 6506/12-1. As seen on the well log, Ror formation show low porosity due to the dominant mudstone present in this formation. As a result, petrographic study was not carried out for this formation.

A

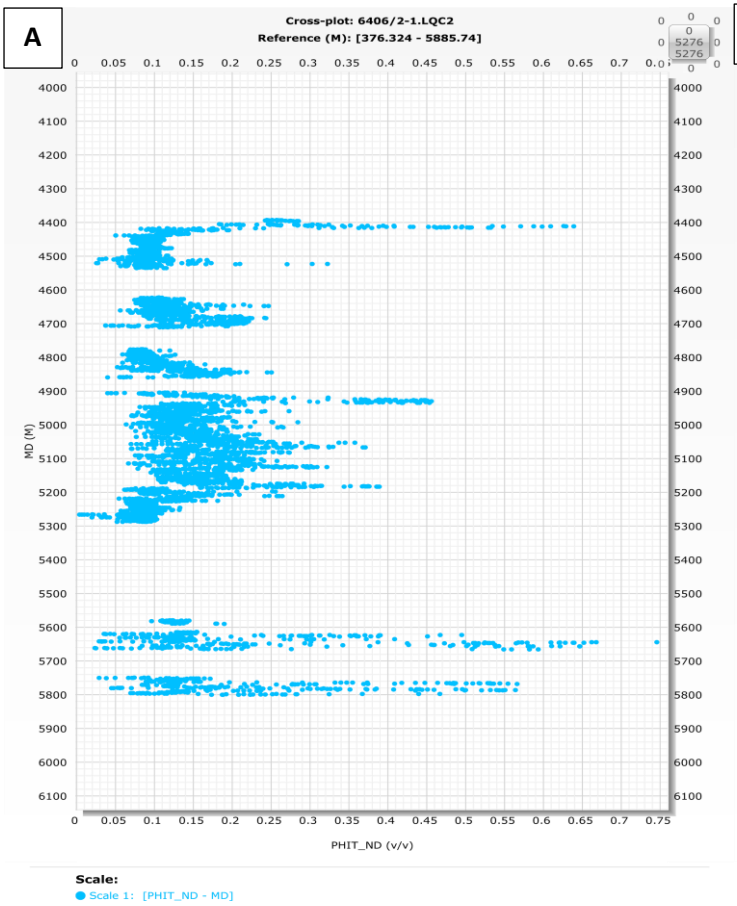
Cross-plot: 6406/2-1.LQC2
Reference (M): [376.324 - 5885.74]
MD (M)
PHIT_ND (v/v)
Scale:
Scale 1: [PHIT_ND - MD]

B

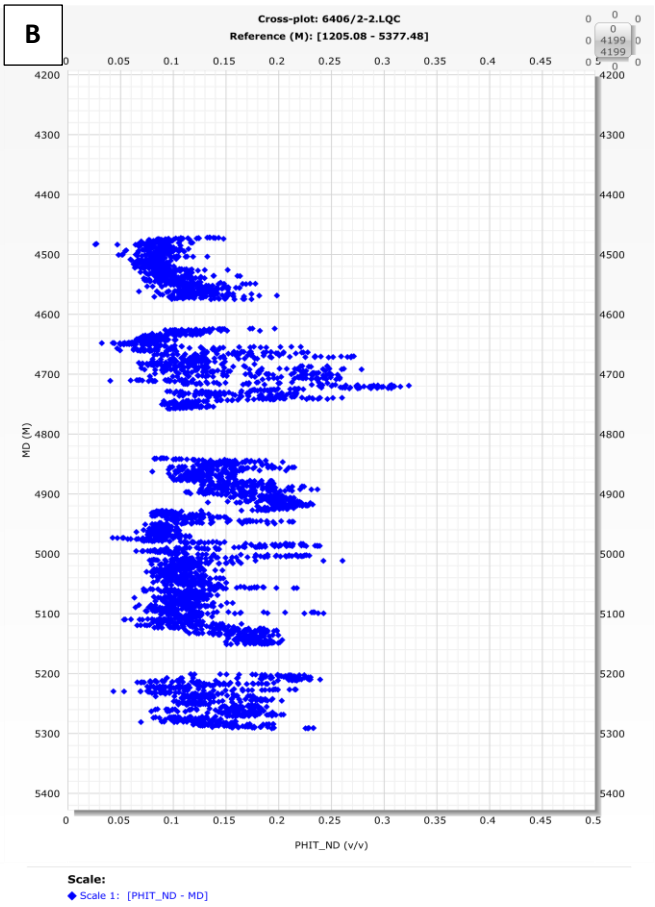
Cross-plot: 6406/2-2.LQC
Reference (M): [1205.08 - 5377.48]
MD (M)
PHIT_ND (v/v)
Scale:
Scale 1: [PHIT_ND - MD]

C

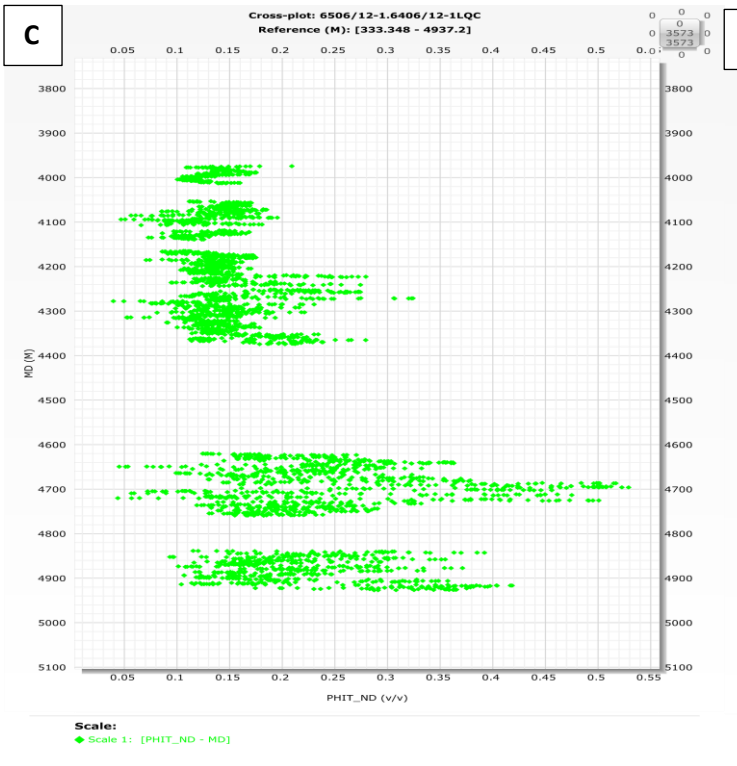
Cross-plot: 6506/12-1.6406/12-1LQC
Reference (M): [333.348 - 4937.2]
MD (M)
PHIT_ND (v/v)
Scale:
Scale 1: [PHIT_ND - MD]

D

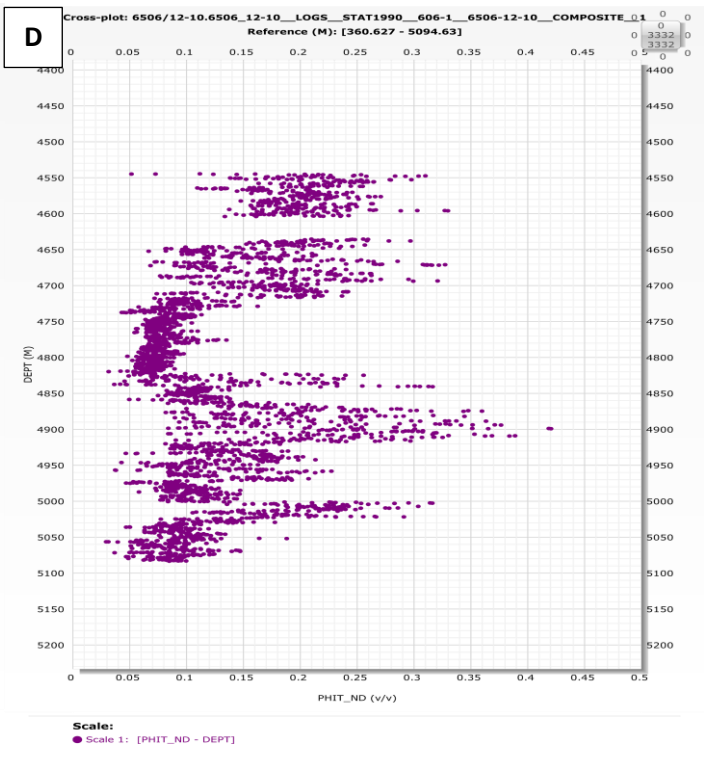
Cross-plot: 6506/12-10.6506_12-10__LOGS__STAT1990__606-1__6506-12-10__COMPOSITE_1
Reference (M): [360.627 - 5094.63]
DEPT (M)
PHIT_ND (v/v)
Scale:
Scale 1: [PHIT_ND - DEPT]

Figure 5.4. Cross plot showing the relationship between neutron-density porosity and depth. (A) well 6406/2-1 (B) well 6406/2-2 (C) well 6506/12-1 (D) well 6506/12-10 (E) well 6506/12-10A

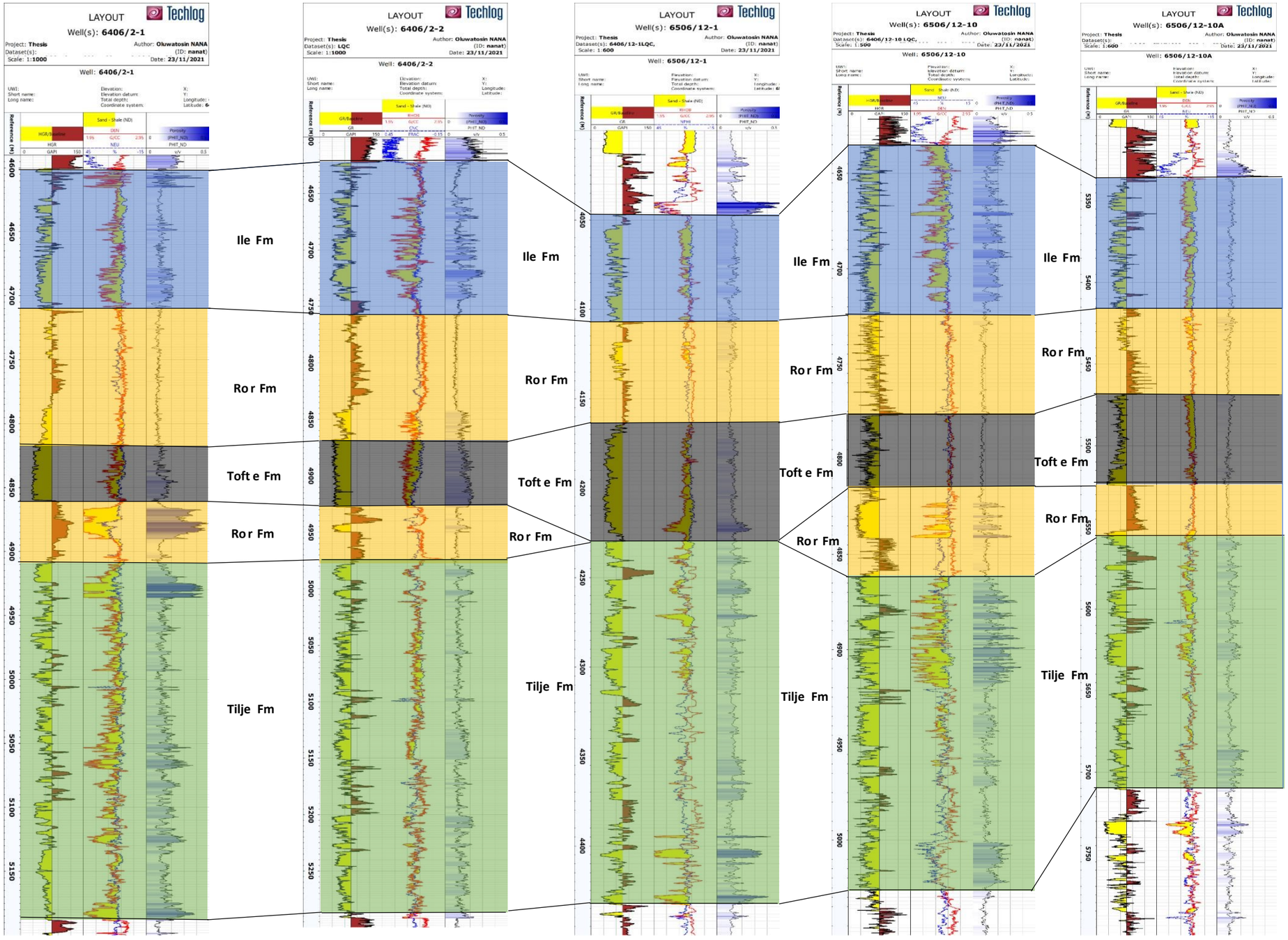

Figure 5.5. Correlation of Ile, Ror, Tofte, and Tilje Formation across well 6406/2-1, 6406/2-2, 6506/12-1, 6506/12-10, and 6506/12-10A

Chapter Six: Petrographic Analysis Results

6.1 Introduction

Petrophysical analysis gives an indication of high porosity preservation in the deeply buried early to middle Jurassic sandstones of offshore Mid-Norway. Hence, this chapter focuses on petrographic and mineralogic study using thin section analysis, point counting, and SEM analysis carried out on the selected samples from the six wells chosen for this study. The purpose of these analyses is to classify the sandstone, determine the texture and mineral composition of the sandstone and to make a description of porosity distribution in relation to the distribution of authigenic clay, types and effectiveness of grain coating minerals, and quartz and carbonate cementation in the deeply buried sandstone.

6.2 Point count

Pont counting was carried out on 27 thin sections with the objective of quantifying the mineralogical composition of the sandstone for the purpose of classifying the sandstone and to determine other diagenetic minerals and factors that might affect the general quality of this sandstone. This point counting analysis was based on the framework composition (quartz, feldspar, and lithic fragment), porosity, coatings, authigenic clays, matrix, and cements.

The result of this point count (Table 6.1) shows a high percentage of quartz grain and a relatively high percentage of lithic fragment compared to feldspar grain in all the six wells selected for this study. Intergranular volume (IGV) has been calculated based on the information gathered from this point count. A graphic representation (Figure 6.1) showing the percentage composition of the point counted samples is shown below.

Table 6.1. Point counting result of all 27 thin section

Well	Formation	Depth (m)	Framework composition			Cement		Porosity		Authigenic clay			Matrix	Mica	IGV
			Quartz	Feldspar	Rock frag.	Quartz	Carbonate	Primary	Secondary	Chlorite	Illite	Coating			
6406/2-1	Tofte	4844.75	40.3	7.7	7.3	9.3	7.7	12.6	6.65	0.0	0.3	0.0	5.3	2.7	35.2
		4847.50	48.0	8.7	8.3	0.0	7.3	8.7	0.7	2.3	0.0	0.0	13.7	2.3	32
		4850.25	48.7	4.7	8.0	9.7	9.0	11.7	1.3	0.0	0.0	0.0	4.7	2.3	35.1
	Tilje	5101.50	43.0	6.0	15.0	0.3	14.7	9.64	2.66	4.0	0.0	4.0	0.0	1.0	32.64
		5104.00	36.3	4.0	15.7	15.7	0.0	12.7	1.3	4.7	0.0	9.3	0.0	0.3	42.4
6406/2-2	Ile	4706.25	47.3	9.3	7.0	1.27	2.2	15.3	2.8	0.0	1.7	5.73	4.2	2.9	30.4
		4716.25	41.2	5.0	2.2	14.0	0.0	0.99	3.21	0.0	9.5	0.0	5.8	18.0	30.29
		4726.25	46.3	10.9	6.0	3.4	0.0	17.46	3.43	0.0	4.0	4.9	2.0	1.7	31.76
	Tofte	4884.50	44.0	7.7	8.7	8.0	0.0	10.3	0.99	0.0	9.0	7.0	1.0	3.3	35.3
		4897.00	44.3	6.7	7.3	8.3	0.3	2.67	6.33	0.0	8.3	0.0	12.0	3.7	31.57
		4897.75	45.7	6.3	10.3	7.7	0.3	12.67	9.33	0.0	4.7	0.0	1.7	1.3	27.07
		4910.25	42.7	4.7	9.0	4.3	1.33	12.67	6.33	1.67	4.33	6.67	2.0	4.3	32.97
		4919.75	44.3	3.3	16.2	6.3	1.0	7.98	3.32	6.0	1.0	6.0	0.3	4.3	28.58
	Tilje	4984.25	39.7	5.0	8.7	7.3	8.98	14.33	3.67	1.7	0.0	8.23	0.3	2.0	40.84
		4986.75	41.0	1.5	7.8	3.8	40.2	0.0	5.0	0.0	0.0	0.0	0.0	0.8	44
		5124.50	50.0	5.0	8.2	1.8	5.48	15.75	2.25	2.5	0.0	6.72	1.2	1.0	33.45
		5126.50	47.8	2.2	10.4	7.0	3.75	8.78	5.02	6.9	0.25	5.75	1.8	0.8	34.23
6506/12-1	Tilje	4255.00	52.5	3.2	6.8	2.5	6.8	11.2	5.52	0.0	6.0	0.0	4.0	1.3	30.5
		4271.66	51.3	4.7	7.7	11.7	0.0	0.0	11.0	0.0	8.3	0.0	1.0	4.3	21
		4273.66	48.9	4.9	7.5	13.1	0.3	14.38	2.62	0.0	4.6	0.0	0.3	3.3	32.68
6506/12-10	Tilje	4943.25	49.7	3.7	7.3	2.7	9.3	8.9	4.32	1.0	5.7	5.3	0.0	2.0	32.9
		4962.66	50.5	2.5	11.0	4.2	7.5	9.0	5.5	2.0	0.0	7.0	0.0	0.8	29.7
		5012.85	46.2	2.8	4.2	2.2	14.2	10.75	3.25	5	0.5	8.2	0.0	2.5	40.85
6506/12-10A	Tilje	5686.85	45	4.0	6.2	7.4	0.8	10.4	4.0	9.0	0.0	10.4	0.0	2.8	38
		5694.50	46.1	2.0	3.7	11.4	18.4	6.1	6.1	2.7	0.0	0.0	0.2	3.3	38.8
6506/11-5S	Tilje	4554.54	51.3	2.7	8.3	18.7	0.0	0.0	9.3	0.0	5.3	0.0	4.0	0.3	28
		4703.28	52.7	1.3	11.0	23.0	0.7	1.33	6.97	0.0	1.3	0.0	0.3	1.3	26.63

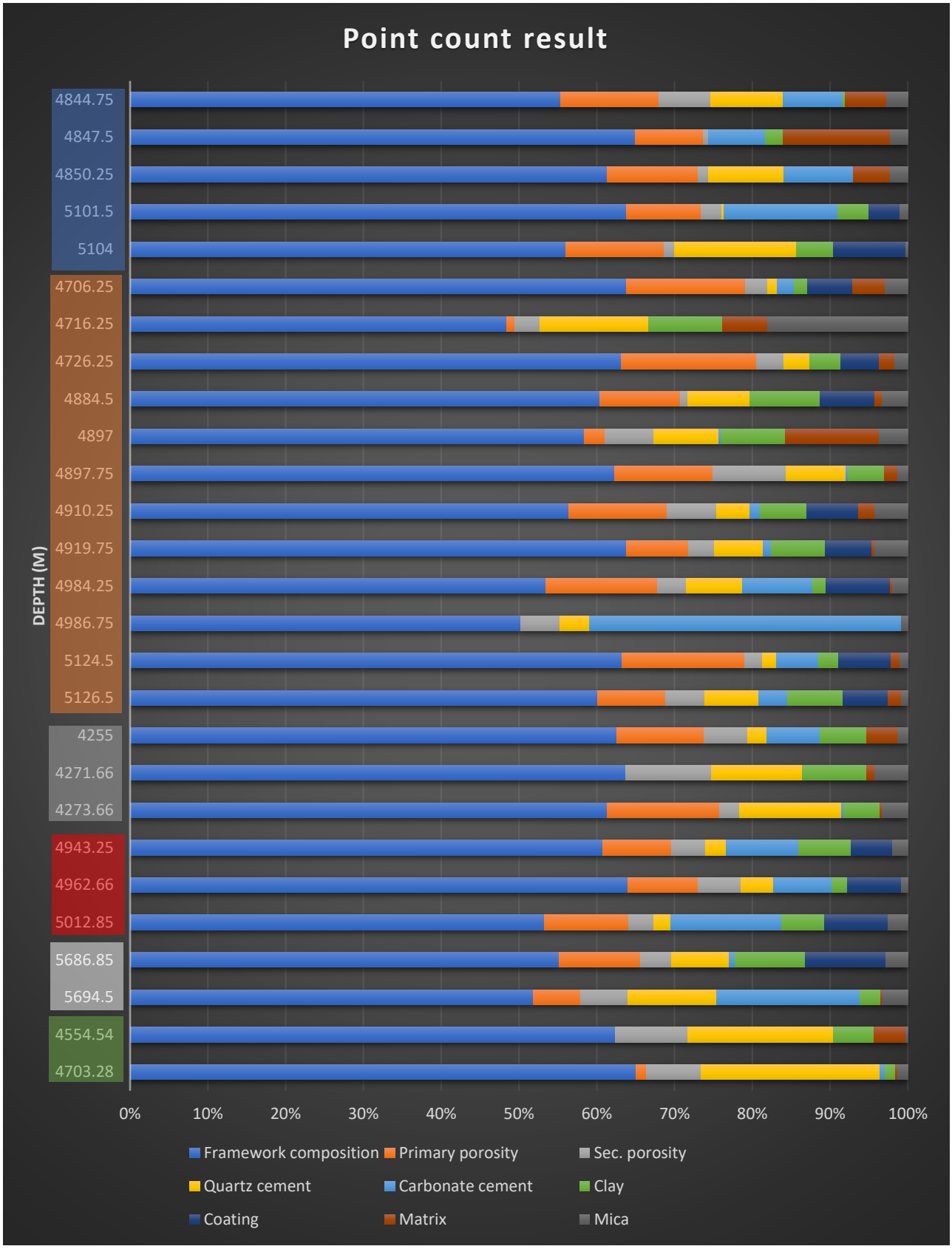

Figure 6.1. Point counting result showing the composition of the sandstone. Coloured rectangle on the right depicts individual well depths; Blue- well 6406/2-1, Orange- 6406/2-2, Grey-6506/12-1, Red-6506/12-10, White- 6506/12-10A, and Green-6506/115S.

6.3 Sandstone classification

More than 50 different methods have been proposed for sandstone classification. However, most of those currently in use involve a framework classification based on quartz, feldspar, and lithic fragment ternary plot (Figure 6.2). For this study, Dott (1964) ternary diagram was used for sandstone classification.

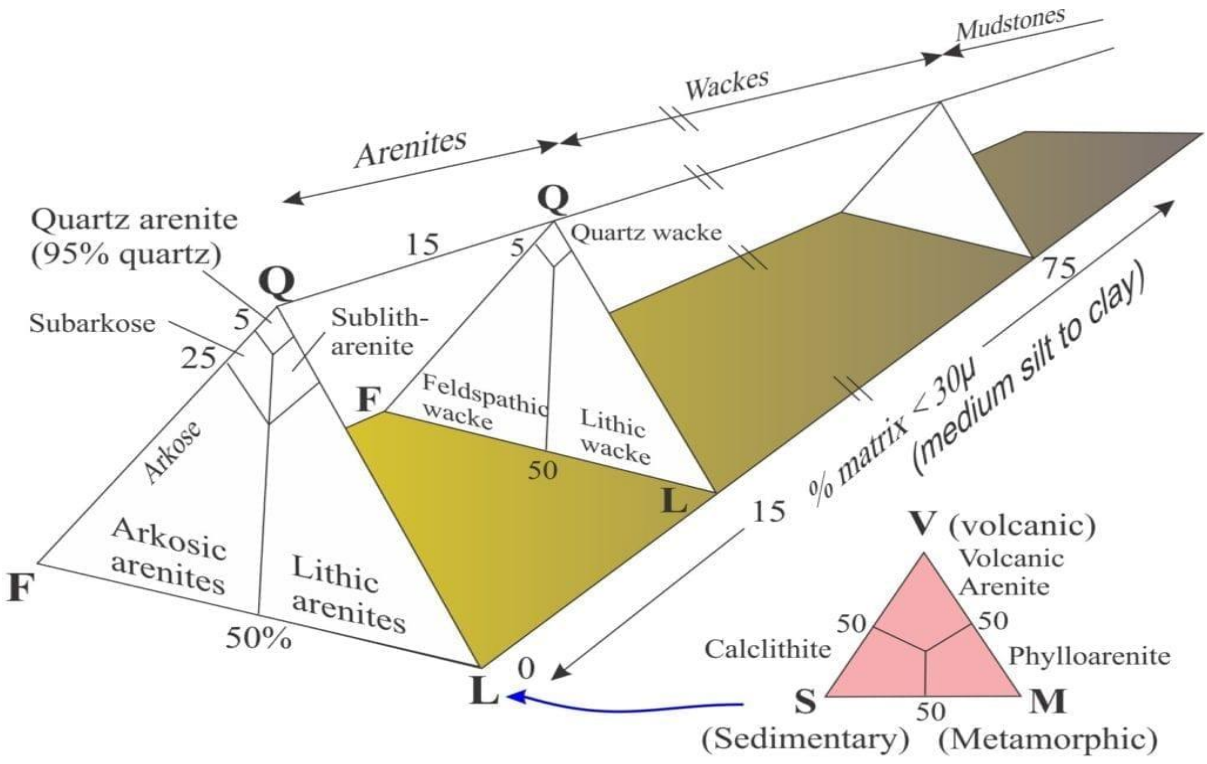

Figure 6.2. Classification of terrigenous sandstone, from Pettijohn, Potter, and Siever, 1973, who in turn modified a diagram from R.H Dott, 1964. Q = quartz, F=feldspar, L=lithic fragment. (Sourced from geological digression).

The quantified quartz, feldspar, and lithic fragment (QFL) from the point count result were plotted in the QFL diagram of Dott (1964). The result shows that sandstones of Tilje and Tofte formations are classified mainly as sublithic arenite and Ile formation is classified as subarkosic sandstone (Figure 6.3). A relatively high percentage of lithic fragment compared to feldspar grain is observed in all six wells except in the upper part of well 6406/2-2 (Ile Formation) where feldspar grain is relatively higher than lithic fragment. Samples depth 4884.75m and

4847.5m in well 6406/2-1 overlap to the subarkose area due to the slightly high percentage of feldspar to lithic fragment (about 2.5% difference).

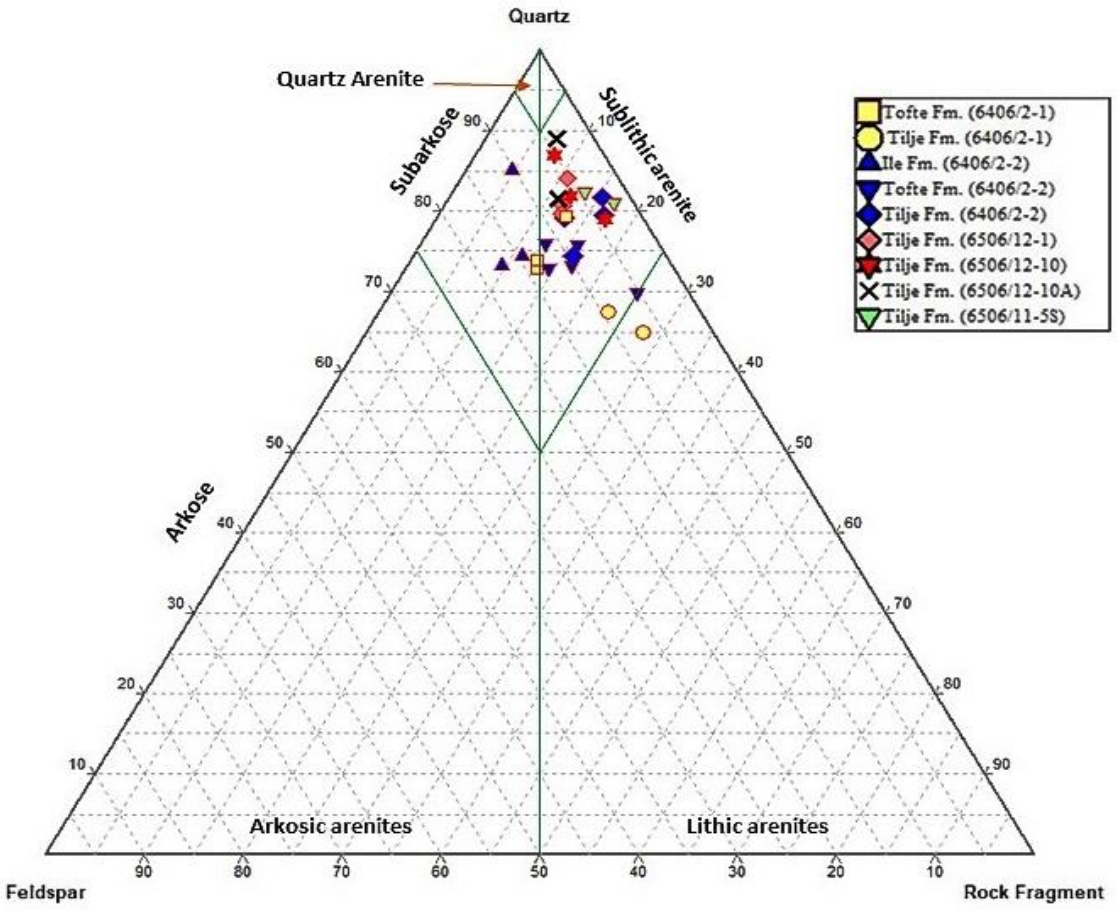

Figure 6.3. classification of Ile, Tofte, and Tilje sandstones according to Dott (1964).

6.4 Texture Description and Maturity.

Textural analysis of these clastic rocks is described for their grain size, grain shape, and sorting (Table 6.2). These parameters are useful for the interpretation of the depositional environment and the transport process of the sediment.

Folk 1951 defined four stages of textural maturity of sandstones (Figure 6.4). This definition is based on the clay content, the degree of sorting, and the degree of rounding. The stages are described below:

1. Immature stage: Poorly sorted and angular grains containing a considerable amount of clay and fine mica.
2. Submature stage: Poorly sorted and angular grains with little or no clay.

3. Mature stage: Sediment contains no clay, and it is well sorted but with subangular grains.
4. Supermature stage: Sediments contain rounded and well-sorted grain, and no clays are present.

To properly determine the textural maturity of sandstone, Folk 1980, further described some key steps to follow (Figure 6.5). These key steps are stated below.

Step 1. Determine the percentage of clay (including mica)

a. If the rock has over 5% percent clay, it is IMMATURE.
b. If the rock contains less than 5% clay, go to Step 2.

Step 2. Determine the sorting of the rock

a. If it is not well sorted with σ over 0.5ϕ (very poorly, poorly, and moderately sorted), it is SUBMATURE.
b. If it is well sorted with σ under 0.5ϕ, go to Step 3.

Step 3. Determine the roundness of quartz grains of sand size

a. If the grains are subangular to very angular with ρ under 3.0, it is MATURE.
b. If the grains are sub-round to well-rounded with ρ over 3.0, it is SUPERMATURE.

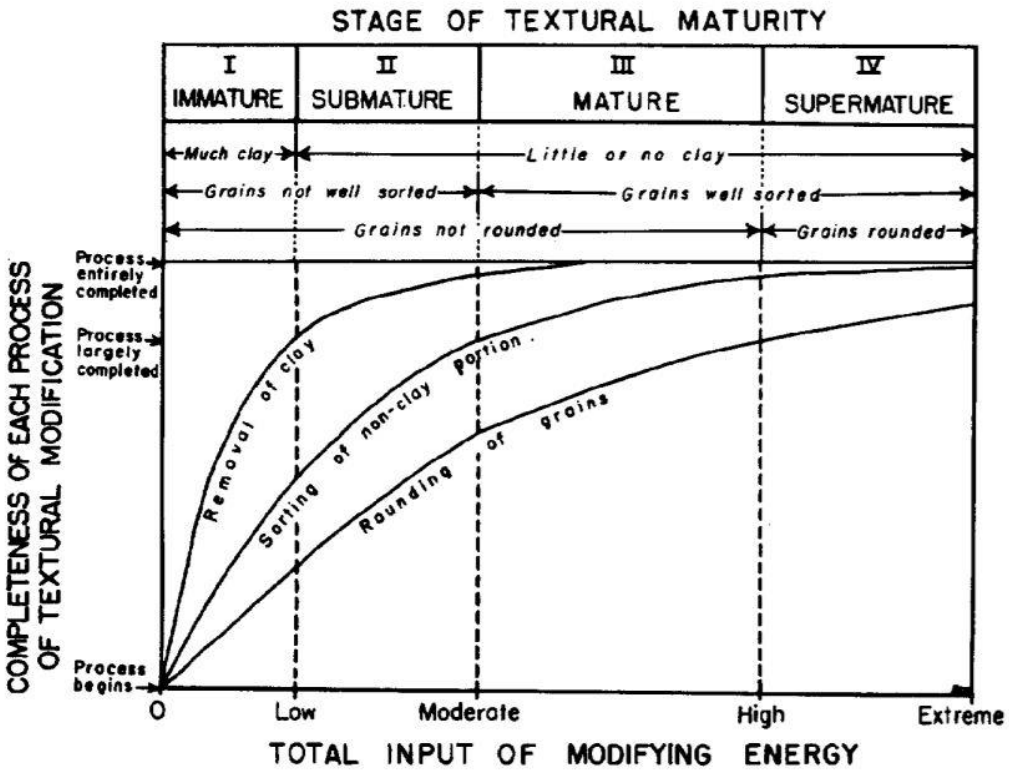

Figure 6.4. textural maturity flow sheet (Folk 1980)

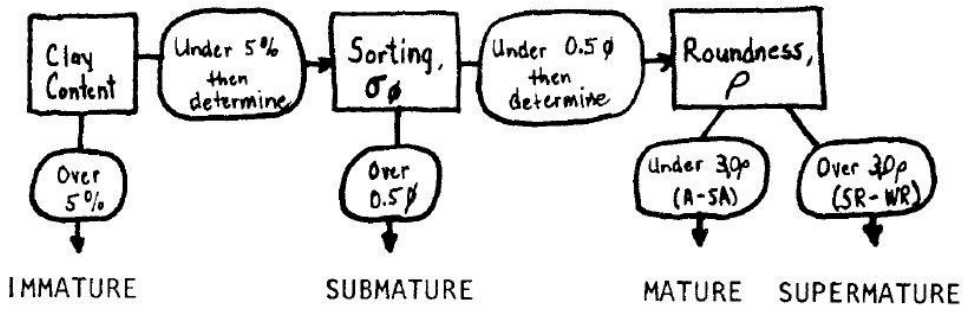

Figure 6.5. textural maturity flow sheet (Folk 1980)

Following the steps stated above, samples from Tilje and Tofte Formation in well 6406/2-1 are described as submature (stage 2). Samples from Tilje, Tofte, and Ile Formation in well 6406/2-2 are described as submature (stage 2) with an exception to sample at depth 4716.25m which is described as immature (stage 1) to mature (stage 3) due to distinction between poorly sorted grain (over 5% of Mica) and well sorted grain respectively in Ile Formation. This sample at depth 4716.25m can also be described as bimodal mature (Folk 1980). Well 6506/12-1 samples are described as supermature (stage 4). Well 6506/12-10 samples are described as submature (stage 2). In well 6506/12-10A, the sample at depth 5686.85m is described as supermature (stage 4), and sample at depth 5694.50m is described as submature (stage 2). And well 6506/11-5S samples are described as submature (stage 2) (Figure 6.6).

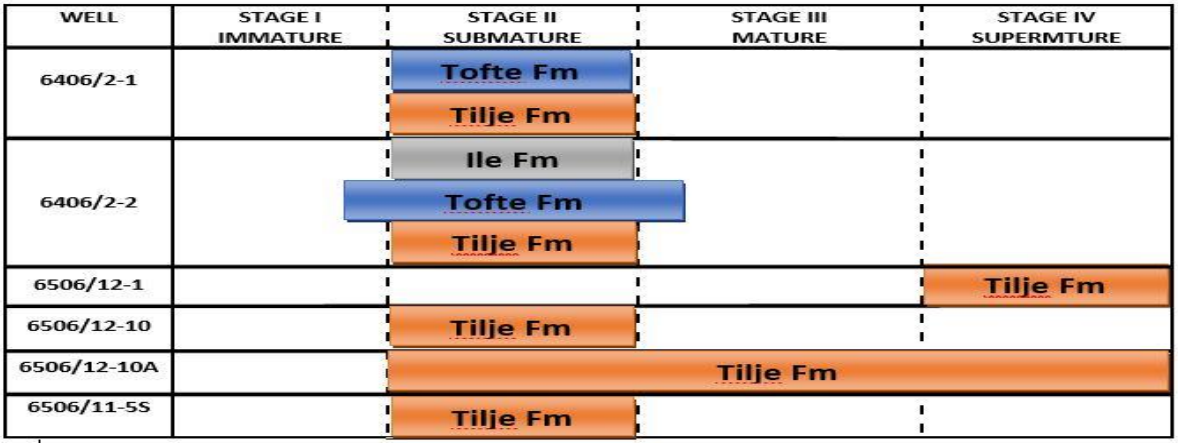

Figure 6.6. Textural maturity of all formations in the well

Table 6.2. average grain size, shape and sorting of all samples in the six wells

Well	Formation	Depth (m)	Average grain size		shape	Sorting
			Millimetres (mm)	Wentworth size class		
6406/2-1	Tofte	4844.75	0.46	Medium	Sub-angular to sub-rounded	Moderate
		4847.50	0.41	Medium	Sub-angular to sub-rounded	Moderate
		4850.25	0.36	Medium	Sub-angular to sub-rounded	Moderate
	Tilje	5101.50	0.42	Medium	Sub-rounded	Moderate
		5104.00	0.37	Medium	Sub-angular to Sub-rounded	Moderate
6406/2-2	Ile	4706.25	0.39	Medium	Sub-angular to subrounded	Moderate
		4716.25	0.08-0.35	V.fine – Medium	Sub-angular to sub-rounded	Poor and Well
		4726.25	0.46	Medium	Sub-rounded to rounded	Moderate
	Tofte	4884.50	0.51	Coarse	Sub-rounded	Moderate
		4897.00	0.47	Medium	Sub-angular to subrounded	Moderate
		4897.75	0.37	Medium	Sub-rounded	Moderate
		4910.25	0.36	Medium	Sub-rounded	Poor
		4919.75	0.30	Medium	Sub-rounded	Moderate
	Tilje	4984.25	0.3	Medium	Sub-angular to subrounded	Moderate
		4986.75	0.23	Fine	Sub-angular	poor
		5124.50	0.22	Fine	Sub-angular to angular	Moderate
		5126.50	0.28	Medium	Sub-rounded	moderate
6506/12-1	Tilje	4255.00	0.22	Fine	sub-rounded to rounded	Well
		4271.66	0.29	Medium	Sub-rounded	Well
		4273.66	0.23	Fine	Subrounded	Well
6506/12-10	Tilje	4943.25	0.38	Medium	Sub-rounded	Moderate
		4962.66	0.37	Medium	Sub-rounded to rounded	Moderate
		5012.85	0.29	Medium	Sub-angular to subrounded	Moderate
6506/12-10A	Tilje	5686.85	0.23	Fine	sub-rounded	Well
		5694.50	0.13 - 0.19	Fine	Sub-angular to angular	Poor
6506/11-5S	Tilje	4554.54	0.53	Coarse	Sub-rounded to rounded	Moderate
		4703.28	0.46	Medium	Sub-rounded to rounded	Moderate

6.5 Intergranular Volume

The values of intergranular volume (IGV) of all the samples have been calculated from point counting results (Table 6.1), (Figure 6.7). The range and average values of IGV of individual wells are presented in the table below (Table 6.3).

Table 6.3. IGV values of individual well

Well	IGV range	Average value
6406/2-1	**32% - 42.4%**	**35.5%**
6406/2-2	**27.07% - 44%**	**33.4%**
6506/12-1	**21% - 32.68%**	**28.06%**
6506/12-10	**29.7% - 40.85%**	**34.5%**
6506/12-10A	**38% - 38.8%**	**38.4%**
6506/11-5S	**26.63% - 28%**	**27.3%**

Slightly higher IGV values of *42.4%*, *40.84% & 44%*, *40.85%*, and *38% & 38.8%* observed in well 6406/2-1, 6406/2-2, 6506/12-10, and 6506/12-10A respectively are most likely due to factors including:

1. Early quartz cementation which reduces mechanical compaction resulting in higher IGV of the sample *(observed in well in all four wells mentioned above).*
2. Carbonate cement from the dissolution of carbonate grain *(observed in well 6406/2-2 and 6506/12-10, and 6506/12-10A).*
3. Increased primary porosity due to chlorite coating of grain and authigenic clay content *(observed in all four wells mentioned above).*

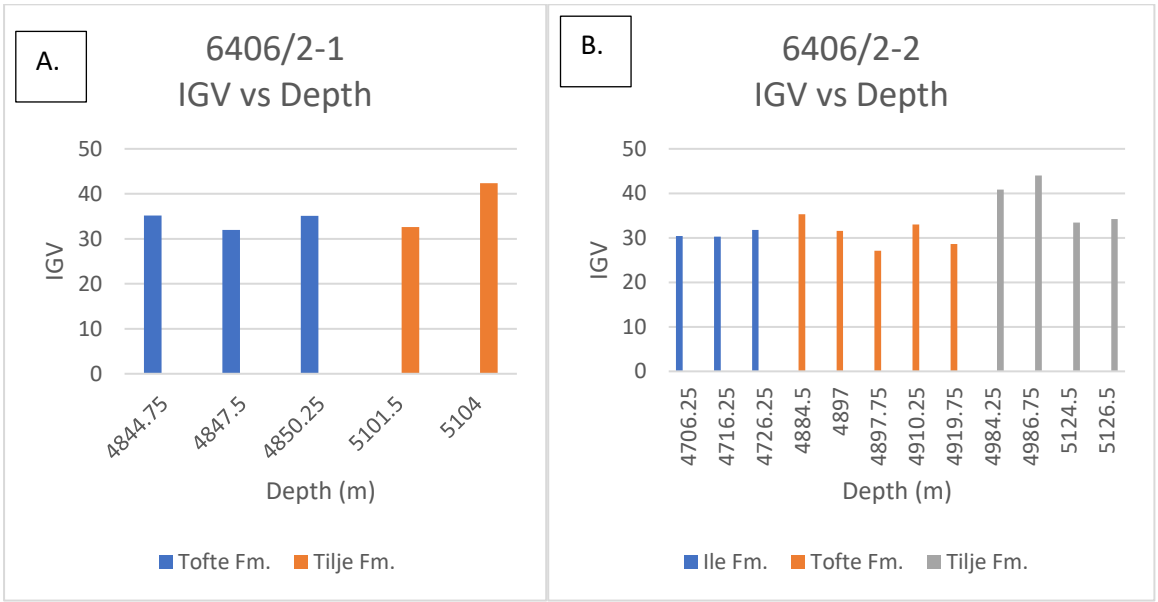

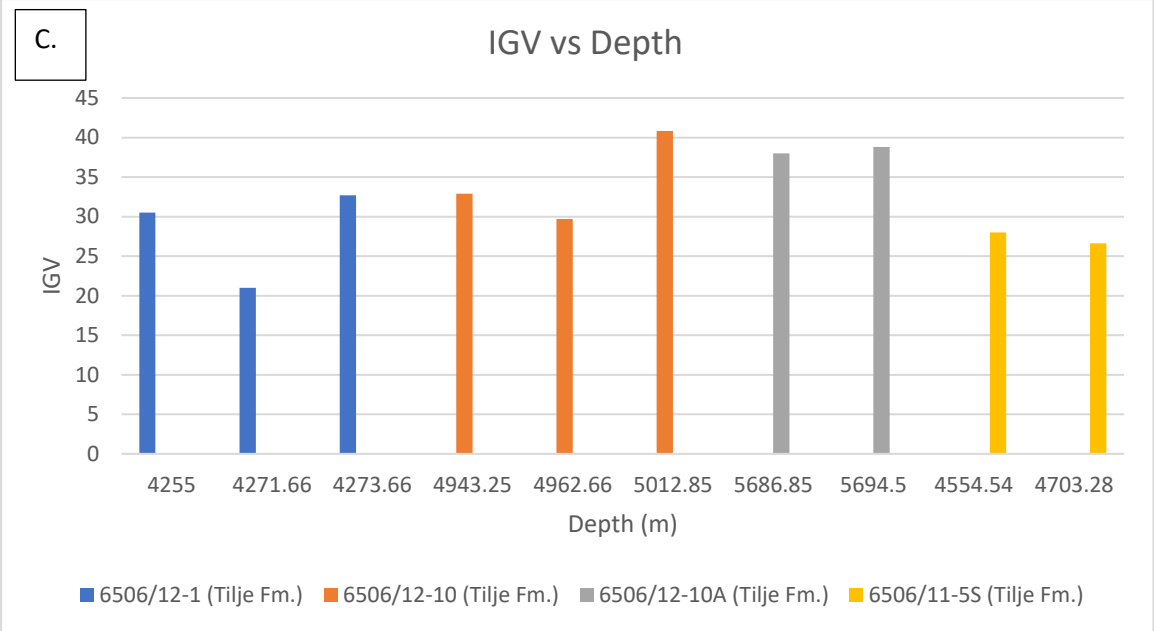

Figure 6.7. Relationship between calculated IGV point counting and depth (a)well 6406/2-1 (b) well 6406/2-2 (c) well 6506/12-1; 6506/12-10; 6506/12-10A; 6506/11-5S

There are assumptions that IGV values are controlled by primary clay content, grain size and textures (Marcussen et al. 2010). Therefore, the relationship between IGV and depth, quartz cement, sorting, authigenic clay, and grain size have been plotted to see how these factors control IGV.

The plots show that IGV calculated from point counting show very little depth dependence (Figure 6.7), IGV values increases with quartz cementation in most of the samples except in well 6506/11-5S (Figure 6.8), an increase in IGV with increasing grain size is seen in Figure 6.9. As against the general understanding that IGV is higher in well-sorted sandstone (Rittenhouse, 1971; Ramm, 1992; Paxton et al. 2002; Chuhan et al. 2003). IGV found in the studied samples shows a negative correlation with sorting in some of the samples (Figure 6.10). The plot between IGV with authigenic clay (Figure 6.11) also show an increase in IGV with authigenic clay, except in well 6506/12-1.

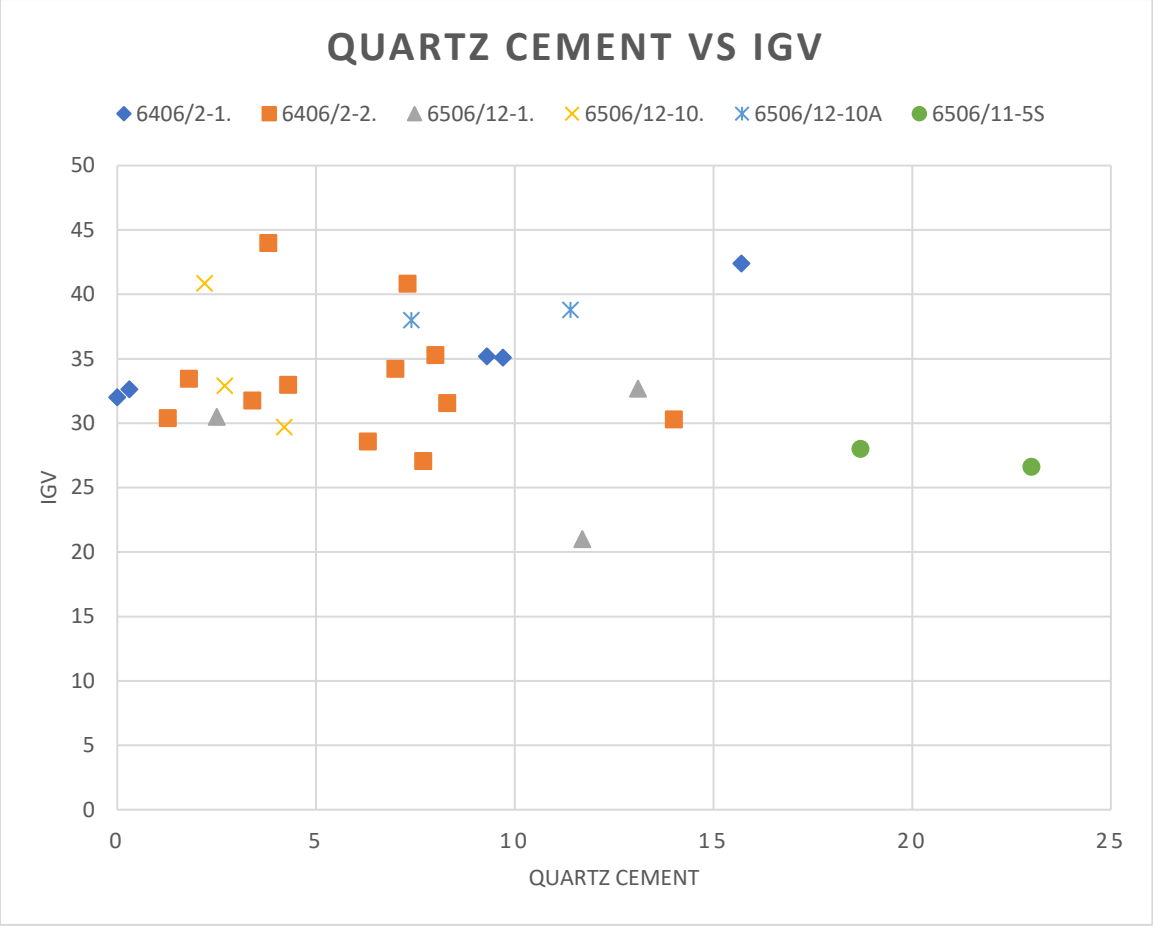

Figure 6.8. Quartz cement vs IGV cross plot

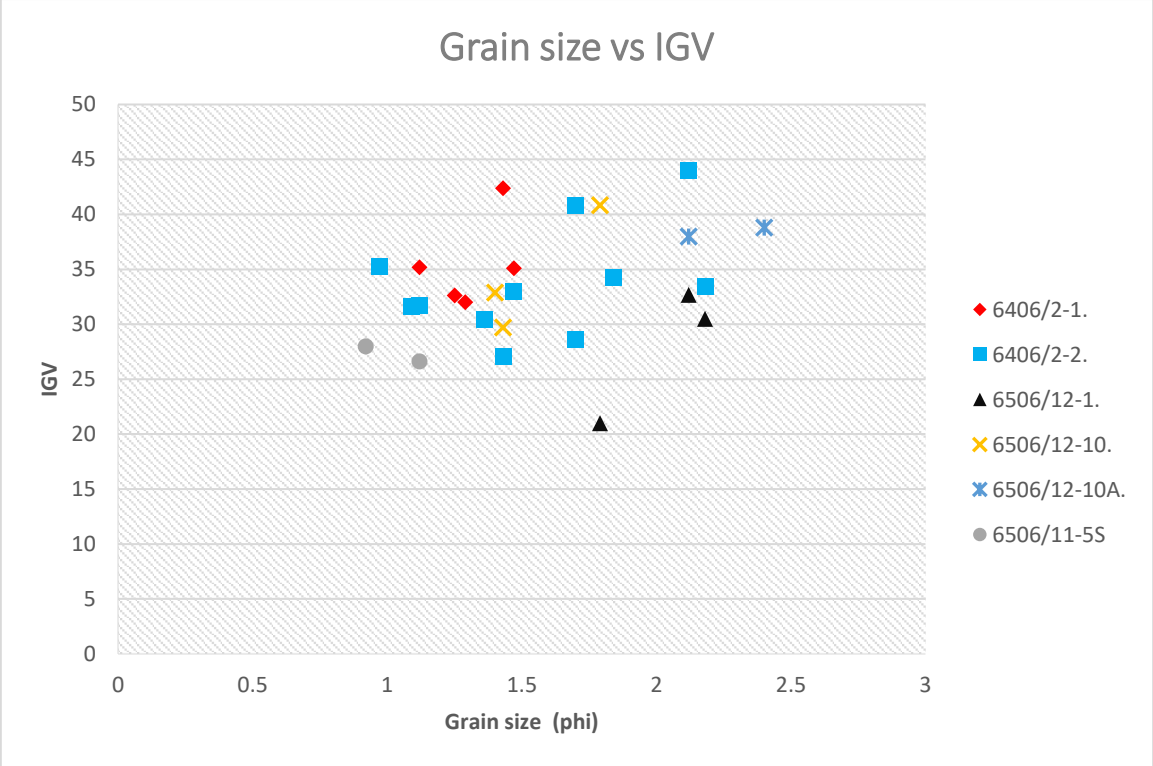

Figure 6.9. Grain size vs IGV cross plot

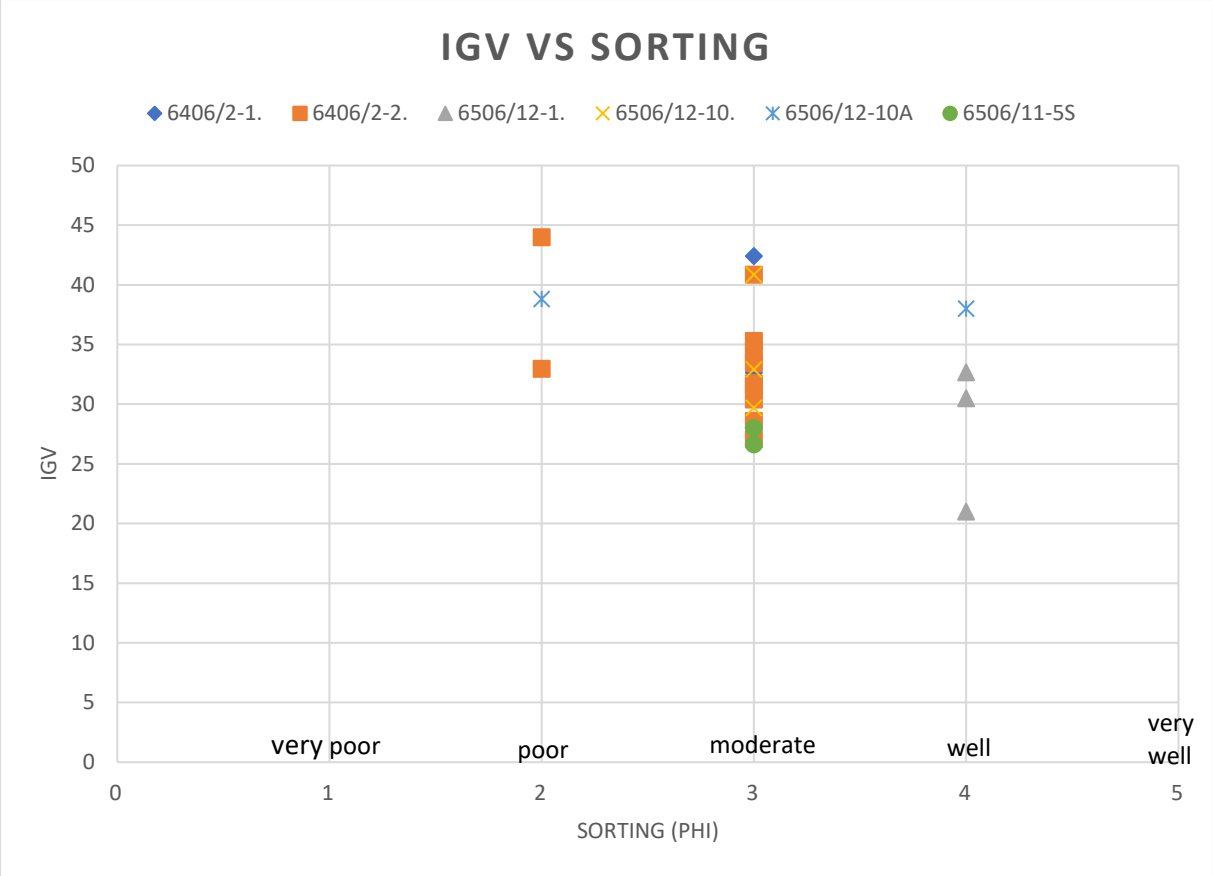

Figure 6.10. IGV vs Sorting cross plot

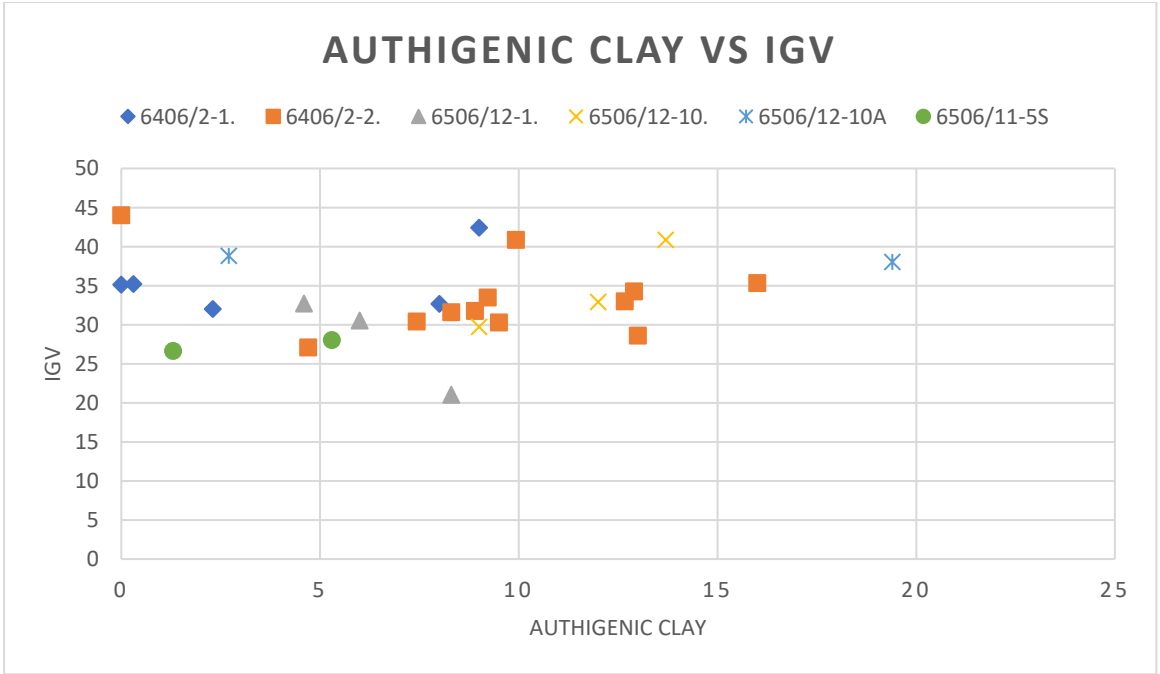

Figure 6.11. Plot of authigenic clay vs IGV

6.6 Thin section and SEM

6.6.1 Quartz cementation

In the studied samples, quartz cementation occurred mainly as overgrowth and pore-filling cement (Figure 6.12). Due to the inaccessibility to cathodoluminescence analysis, quartz cementation was recognized, and point counted on the basis of distinct dust rim separating the detrital quartz from its overgrowth, this might result in the underestimation of quartz cement as some of the samples exhibit no dust rims. Quartz cementation was recognized in all five wells. Quartz cementation in Tilje Formation in well 6506/11-5S was found to be very high (Figure 6.12A & B), drastically reducing the primary porosity of the formation; the only porosity type seen here is secondary porosity (Figure 6.12A). Figure 6.13 shows quartz cementation increases with depth in all wells except well 6506/12-10 where quartz cementation shows no significant change with depth. However, the small amount of sample in well 6506/12-10 is not enough to judge the variation of quartz cementation with depth.

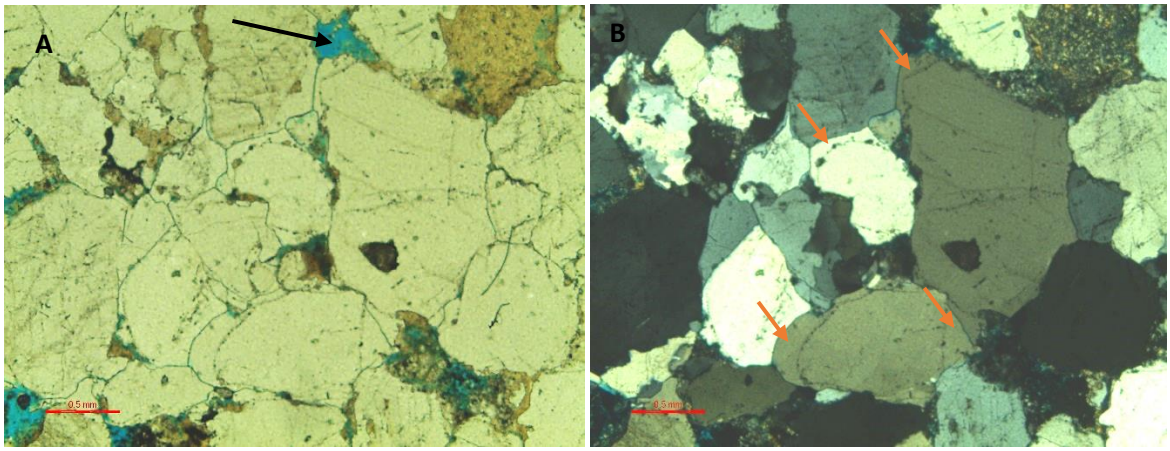

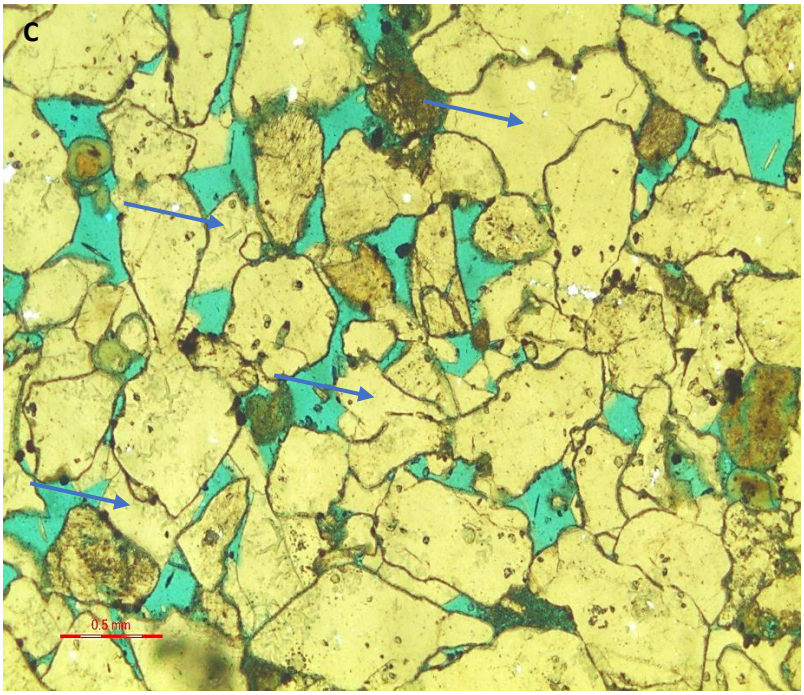

Figure 6.12. Photomicrographs of quartz overgrowth and pore filling quartz cement. Scale bar are all 0.5mm in all views. (A) Tilje Formation, well 6506/11-5S, 4703.28m. Quartz overgrowth in plane polarized (pp), black arrow points to secondary porosity. (B) Same as (A) in crossed polarized (xp), Orange arrow points to quartz overgrowth (C) Tilje Formation, well 6406/2-1, 5104.00m. Blue arrow points to quartz cement filling pore.

.

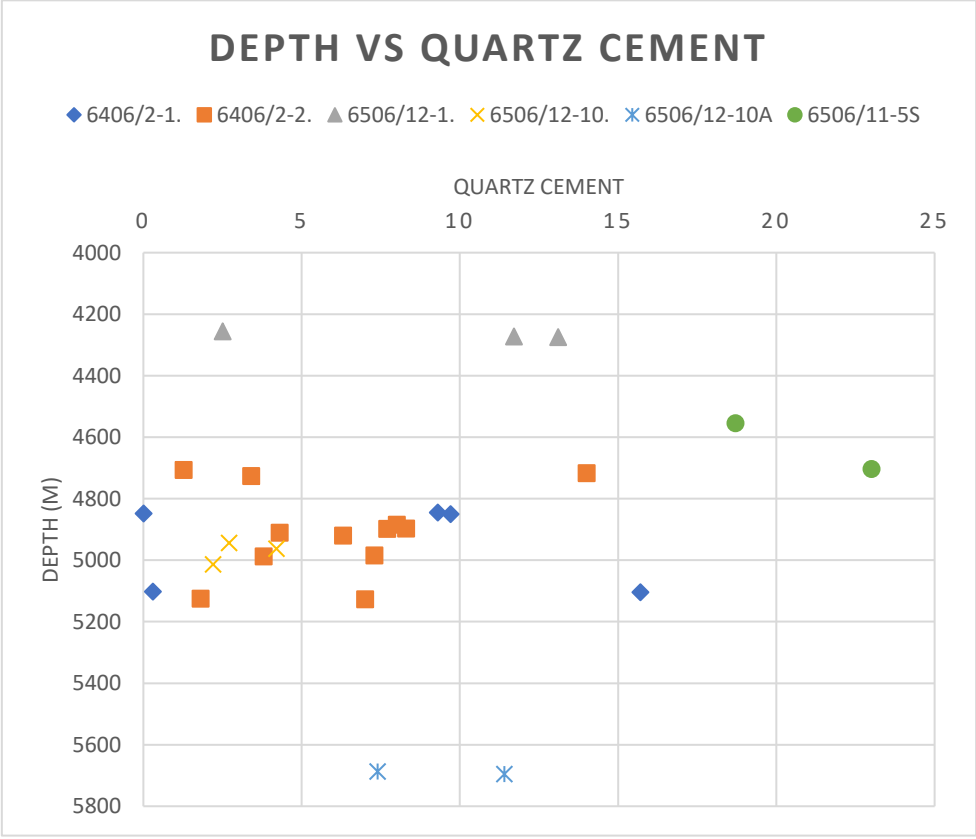

Figure 6.13. Cross plot of Depth vs Quartz cement.

6.6.2 Carbonate cement

The percentage of carbonate cement has been quantified through point count. Result of the point count showed that carbonate cement was observed in all the wells, with the Tilje formation having the highest amount of carbonate cement. However, four of the wells, namely 6406/2-1, 6406/2-2, 6506/12-10, and 6506/12-10A, contains a high amount of carbonate cement, and the highest amount of carbonate cement counted in each of the four wells are 14.7% at 5101,50m, 40.2% at 4986.75m, 14.2% at 5012m, and 18.4% at 5694.50m respectively.

The carbonate cements present in these well are calcite, siderite and ankerite. With the aid of SEM analysis, siderite and ankerite were confirmed as the dominant carbonate cement in the studied well intervals (Figure 6.24A, Figure 6.14). These cements occur mainly as pore-filling (Figure 6.14A, E and Figure 6.24A) and replacement mineral. The replacement is shown by the presence of quartz grain floating in a carbonate matrix (Figure 6.15).

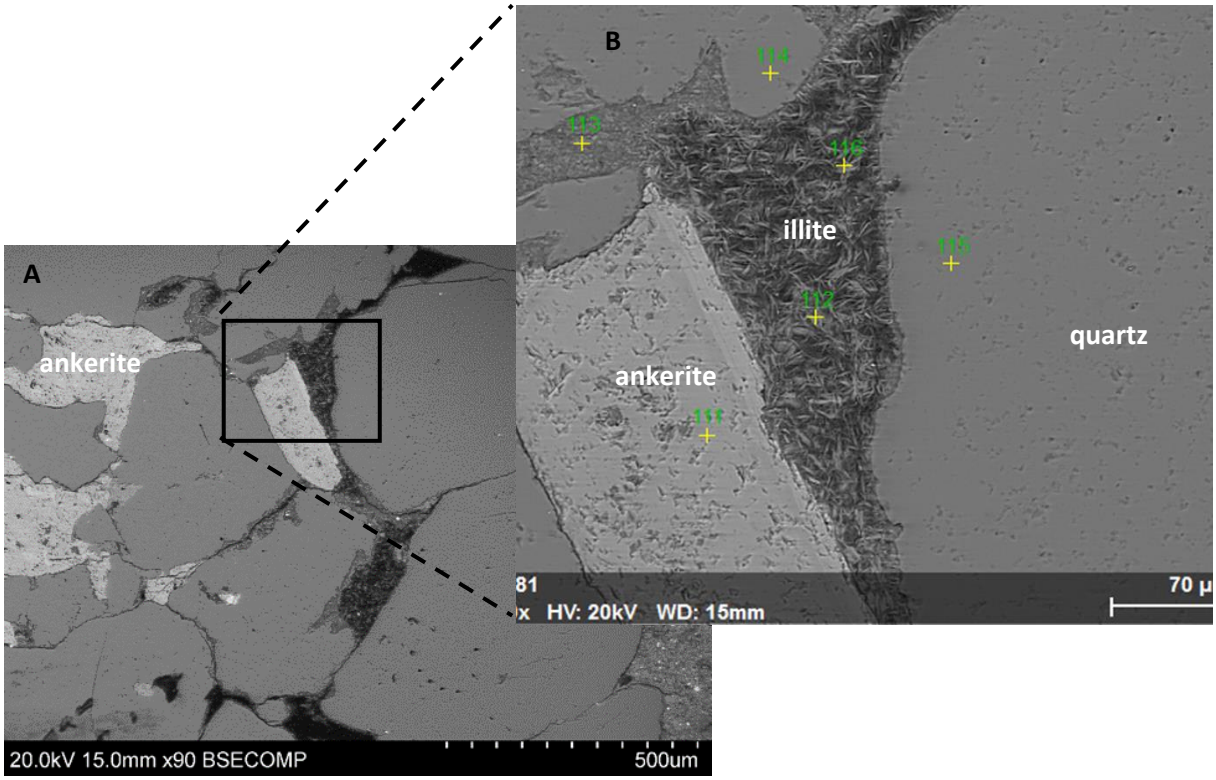

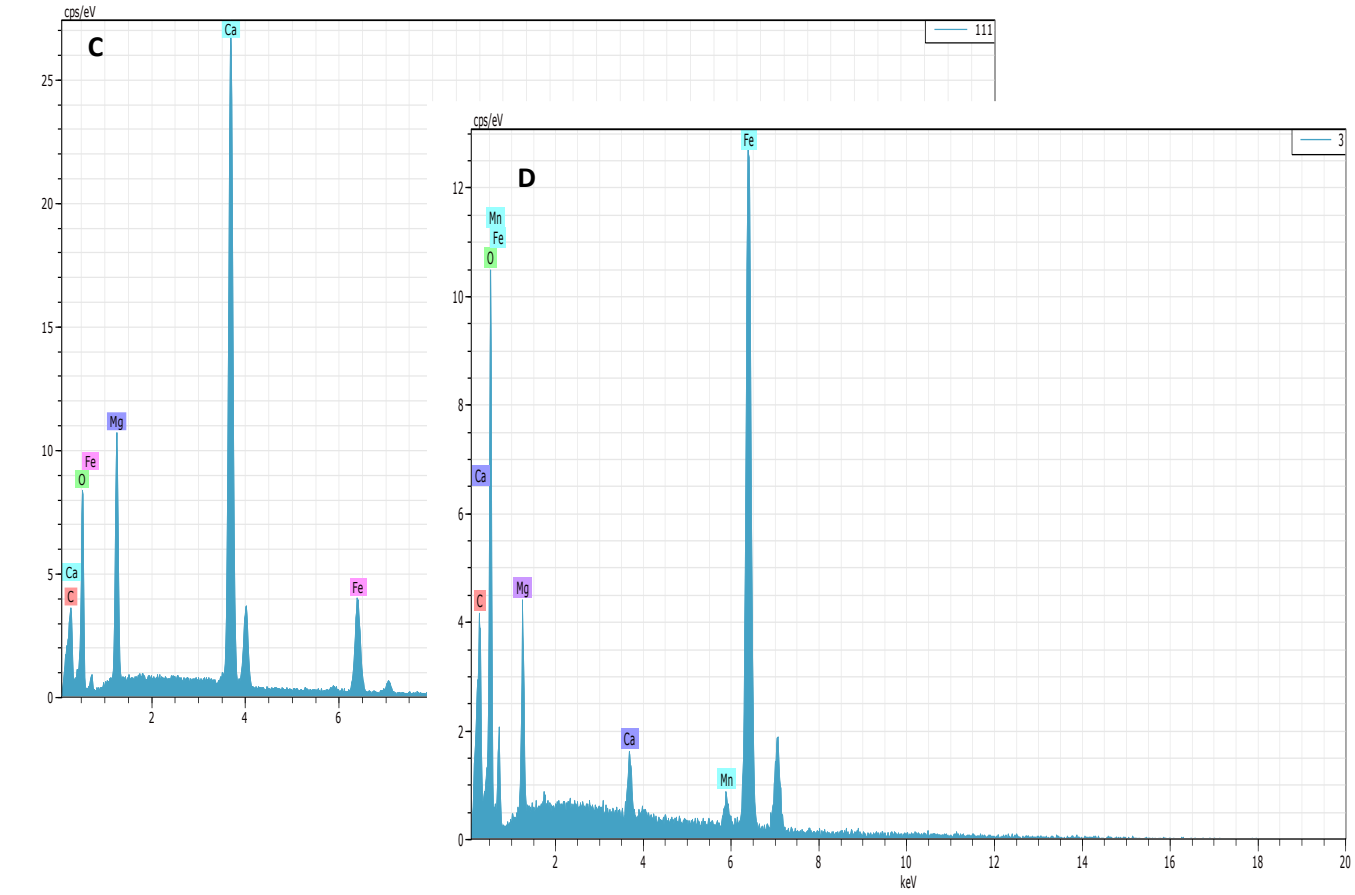

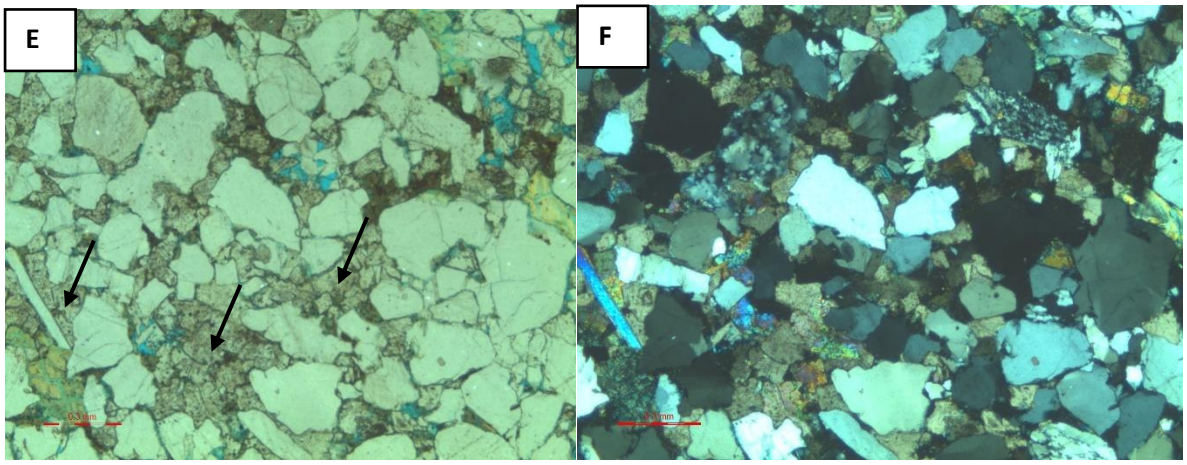

Figure 6.14. Pore filling carbonate cements (A and B) Tilje Formation, well 6506/12-10, 4943.25m. SEM photomicrographs ankerite filling pore (C) EDS image showing spectrum of for ankerite. (D) EDS image showing spectrum for siderite in Figure *6.24A. (E and F) Tofte Formation, well 6406/2-1, 4850.25m. photomicrograph of pore filling calcite cement in pp and xp light respectively. Black arrow points pore filling calcite. Scale bar is 0.5mm in both views.*

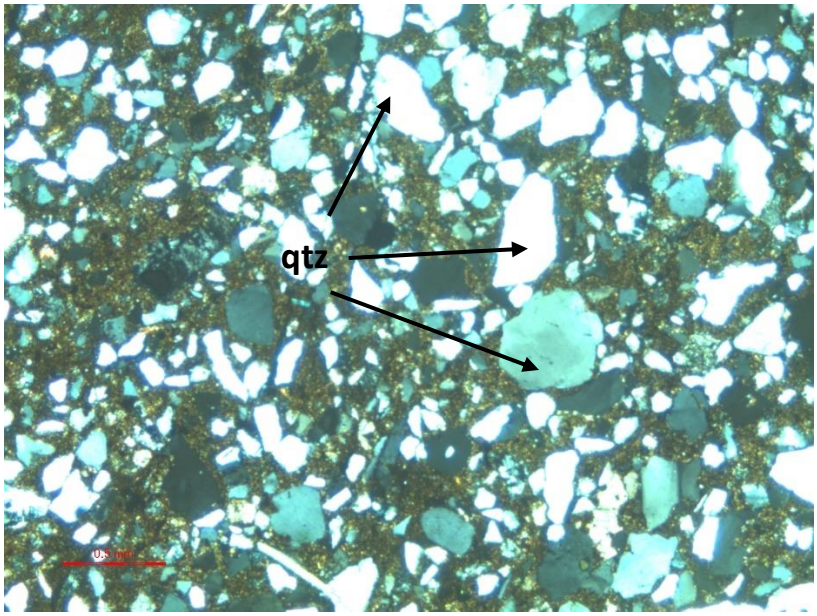

Figure 6.15. Tilje Formation, well 6406/2-2, 4986.75m. Photomicrograph of carbonate cement replacement shown by the presence of quartz grain (qtz) floating in the carbonate matrix. Scale bar is 0.5mm.

6.6.3 Authigenic clay

A good number of authigenic clay minerals were observed and counted under the petrographic microscope. They occur as pore-lining (grain coating) and pore-filling clay in all the wells except in well 6506/12-1 and well 6506/11-5S, where they only occur as pore-filling clay. Concentrically laminated Fe-rich clay ooids and ooidal grain coatings were observed in the samples, and in some cases, the concentrically laminated ooidal clays are coated by radial chlorite (Figure 6.19A). The observed morphology of the clays during SEM analysis and their respective EDS spectrum confirmed the authigenic clay minerals are illite and chlorite (Figure 6.16, Figure 6.17, Figure 6.18). Pellets, which consist of structureless, or randomly oriented clay confined to a rounded mass are also observed (Figure 6.19D)

It is observed that authigenic illite may have formed from dissolution of K-feldspar (Figure 6.16) and alteration of muscovite (Figure 6.17). Where the clays occur as pore filling, they partially destroy porosity, for instance, in places where there is excessive growth of coatings on grain to the extent that they block pore throats and fill pores (Figure 6.23A). However, in some cases, they completely obliterate porosity. For example, Fe-ooid coating and pellets are seen to completely fill pore space, as seen in some of the samples (Figure 6.20).

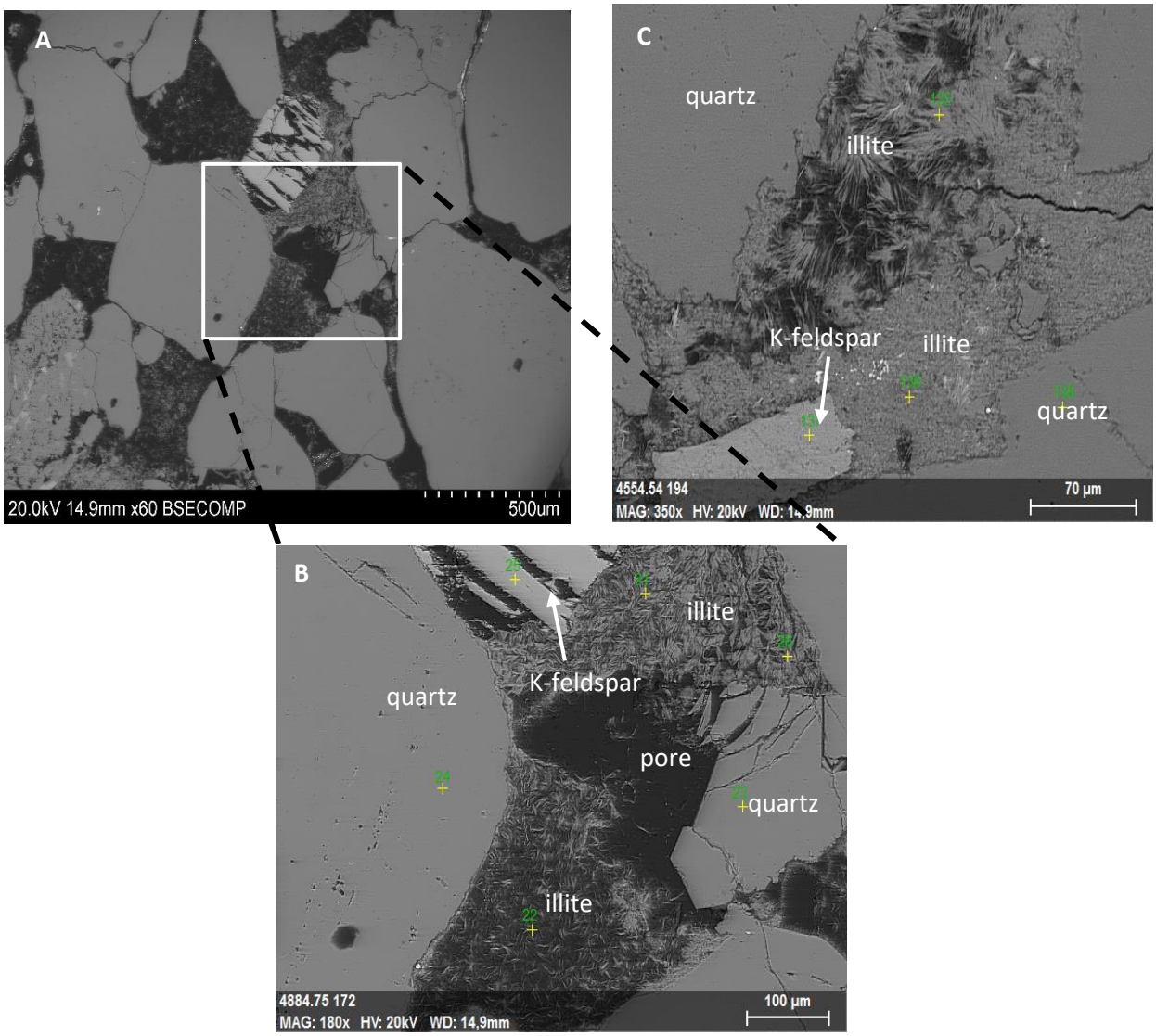
A
20.0kV 14.9mm x60 BSECOMP
500um
C
quartz
illite
K-feldspar
illite
quartz
4554.54 194
MAG: 350x HV: 20kV WD: 14,9mm
70 µm
B
illite
K-feldspar
quartz
pore
quartz
illite
4884.75 172
MAG: 180x HV: 20kV WD: 14,9mm
100 µm

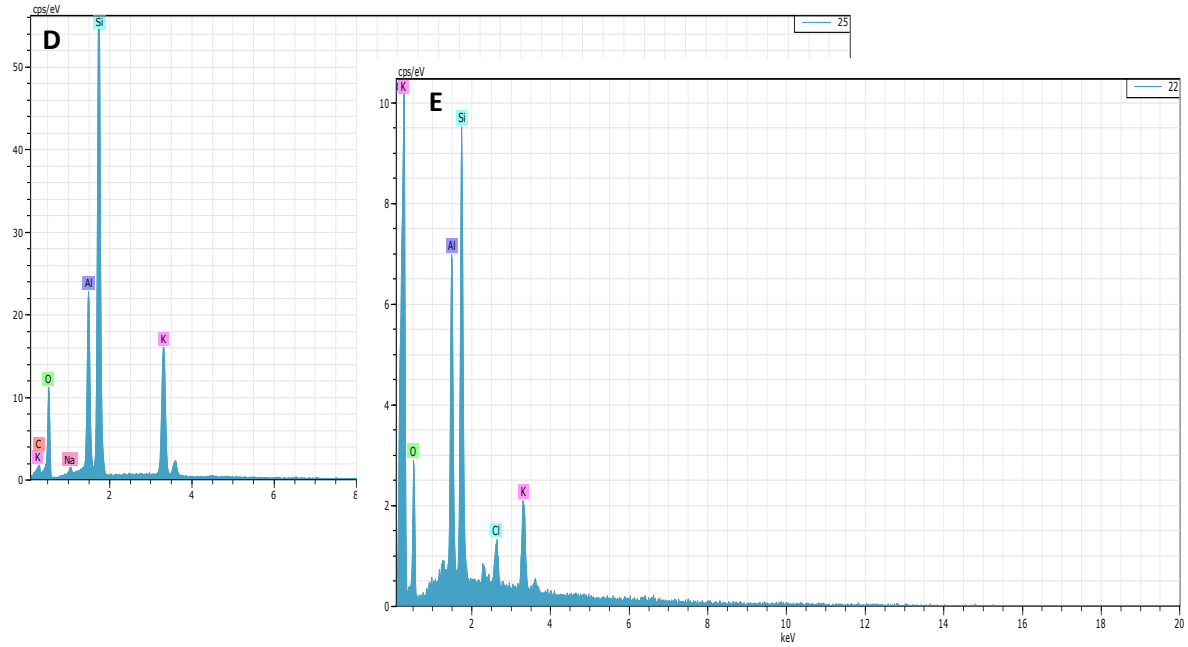

Figure 6.16. (A and B) Tofte Formation, well 6406/2-2, 4884.50m. SEM photomicrographs of Pore filling authigenic illite from K-feldspar dissolution reactio with kaolinite (C) Tilje Formation, well 6506/11-5S, 4554.54m. SEM photomicrographs of Pore filling authigenic illite from K-feldspar dissolution (D) EDS image showing spectrum for K-feldspar in Figure *6.16B (E) EDS image showing spectrum for illite in* Figure *6.16B.*

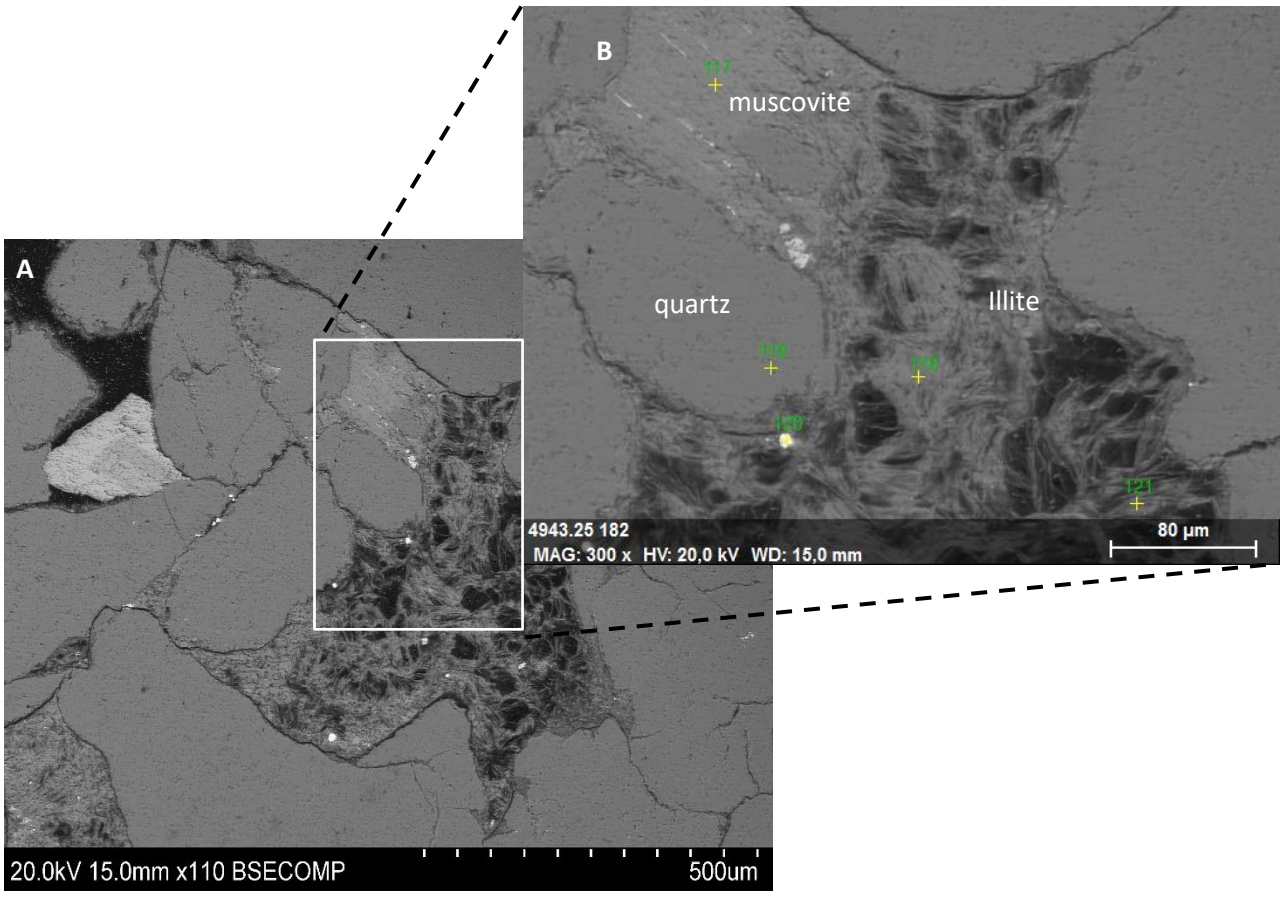

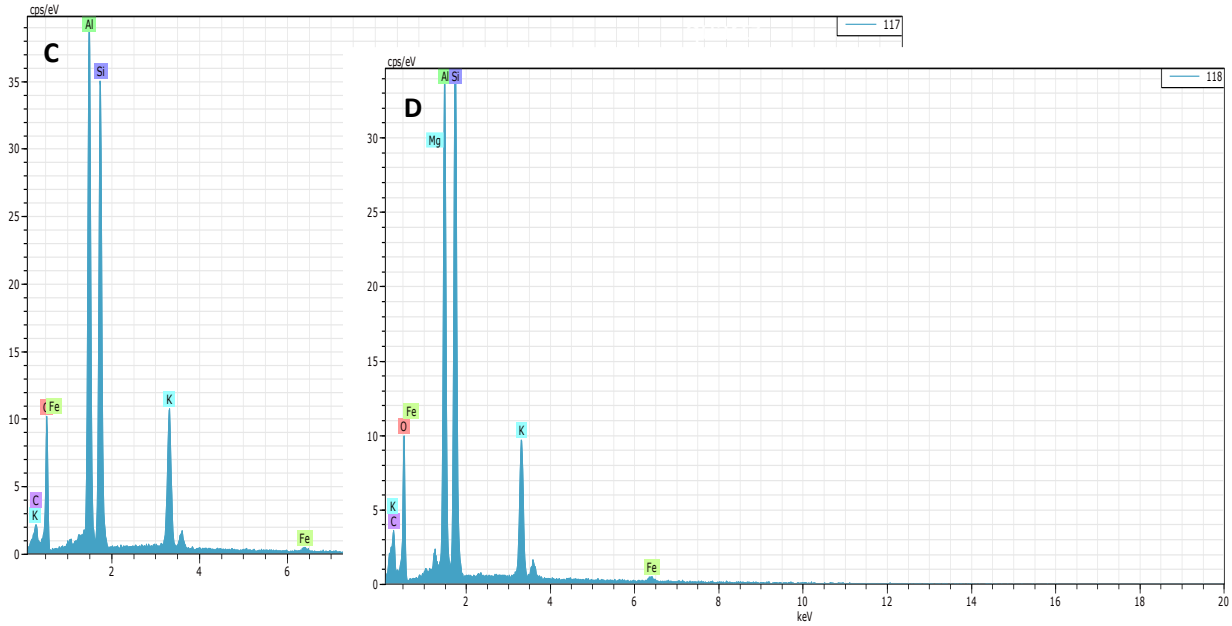

Figure 6.17. (A and B) Tilje Formation, well 6506/12-10, 4943.25m. SEM photomicrographs of Pore filling authigenic illite from muscovite alteration to illitinised smectite (C) EDS image showing spectrum for altered muscovite in Figure *6.17B (D) EDS image showing spectrum for illite in* Figure *6.17B.*

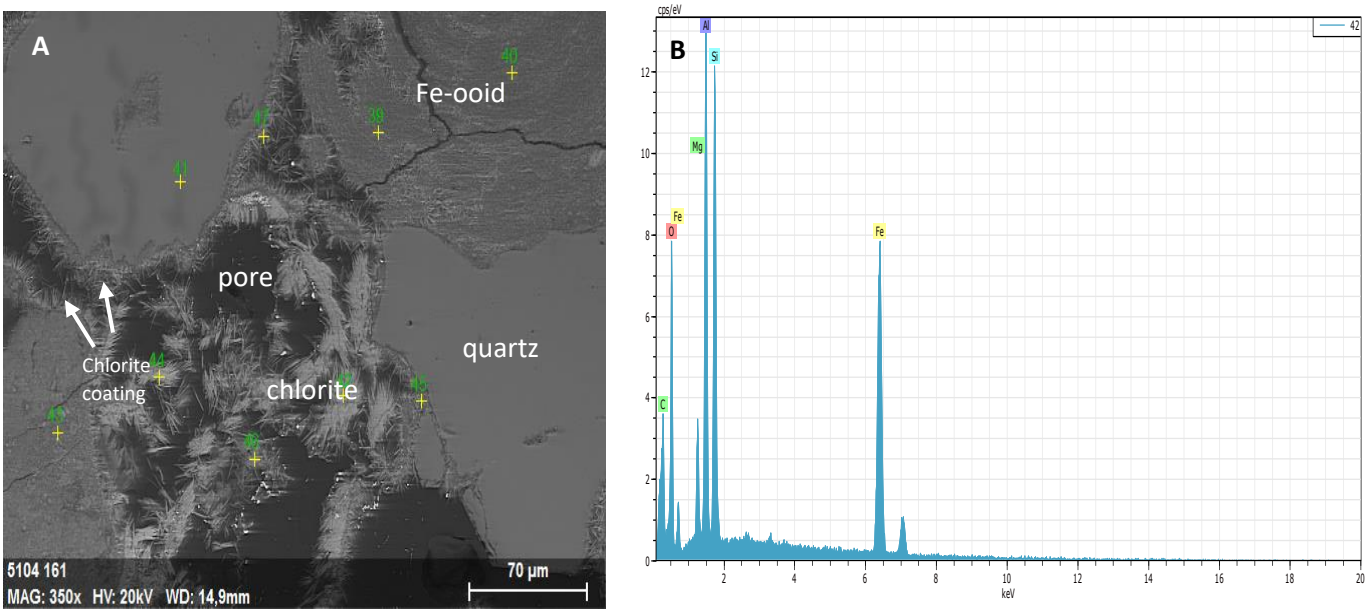

Figure 6.18. (A) Tilje Formation, well 6406/2-1, 5104m. SEM photomicrographs of Pore filling authigenic chlorite (B) EDS image showing spectrum for chlorite in Figure *6.18A.*

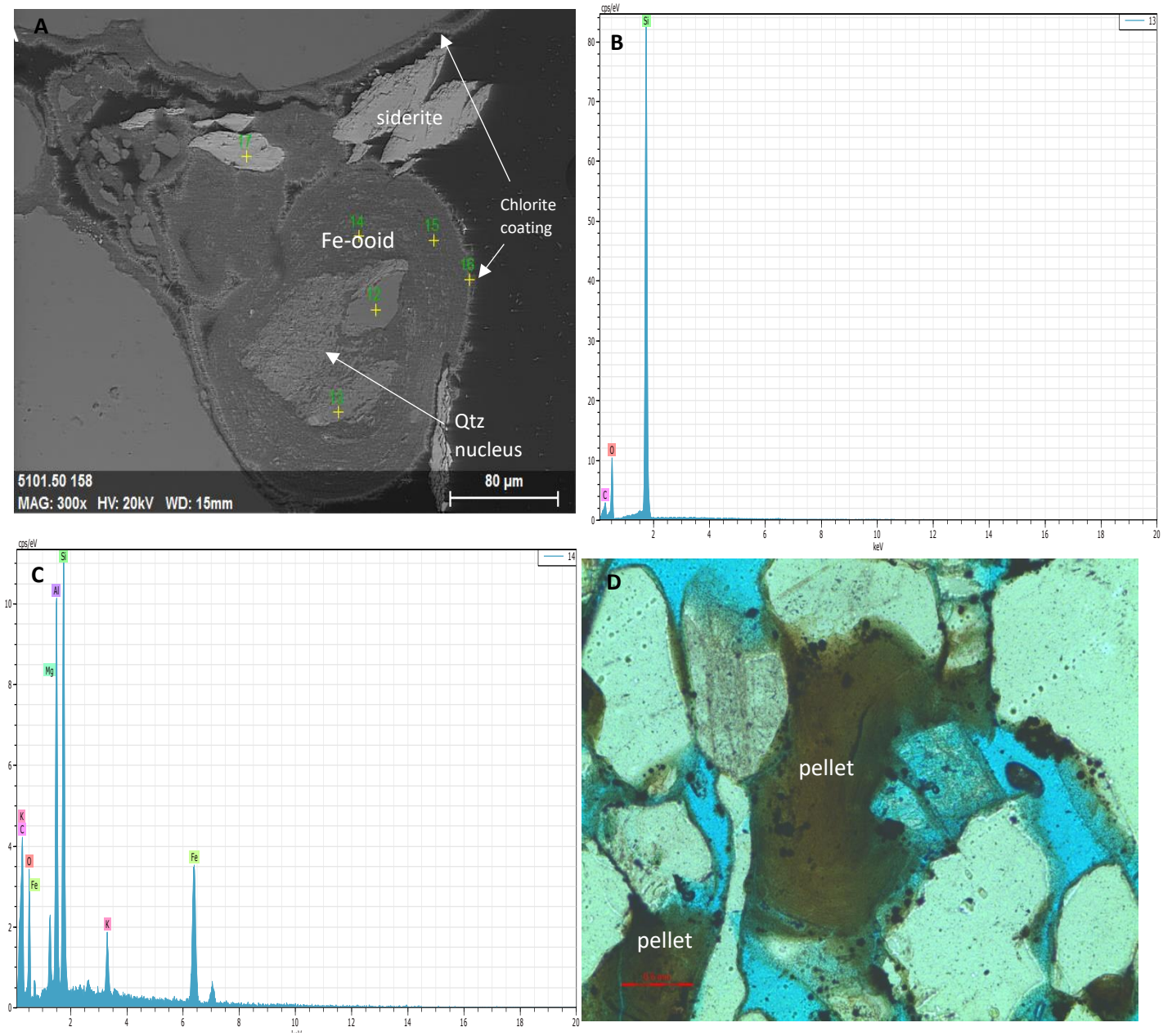

Figure 6.19. (A) Tilje Formation, well 6406/2-1, 5101.50m. SEM photomicrographs concentrically laminated Fe-rich ooidal grain coatings and some case with radial chlorite coating (B) EDS image showing spectrum for quartz in Figure *6.19A (C) EDS image showing spectrum for Fe-rich ooidal coating in* Figure *6.19A (D) Tilje Formation, well 6406/2-2, 5126.50m. photomicrograph of chlorite pellet. Scale bar is 0.5mm.*

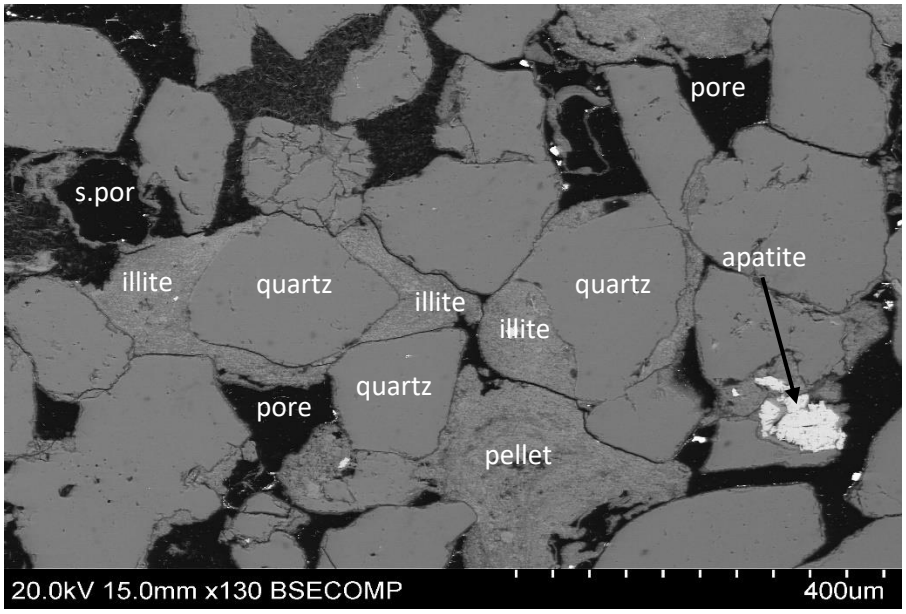

Figure 6.20. Tilje Formation, well 6506/12-1, 4255.00m. SEM photomicrograph of fe-ooid coating and pellets seen to completely fill pore space (s.por = secondary porosity)

6.6.4 Grain coating

Grain coatings observed under the petrographic microscope was quantified through point counting of coating (Table 6.1). The coatings were analyzed under SEM to determine the extent and type of coating. The SEM analysis results indicate chlorite and illite coatings (Figure 6.23 and 6.25). Clay rims with a mixture of illite and chlorite were also observed on some of the grains (Figure 6.24). In some samples, the clay rims are coated by authigenic chlorite (Figure 6.23 & 6.24)

A plot of observed coating against primary porosity depicts an association of high porosity with chlorite-coated intervals (Figure 6.21). The coating vs quartz cement plot (Figure 6.22) also showed a positive correlation between grain coating and quartz cementation, illustrating a tendency towards a reduction in quartz cement in samples rich in grain coating. However, some of the samples are characterized by high abundance of quartz cement despite the presence of grain coating in the samples. Table 6.4 shows the coverage of grain-coated samples in the different wells, some examples of these coating coverages are shown in Figure 6.26.

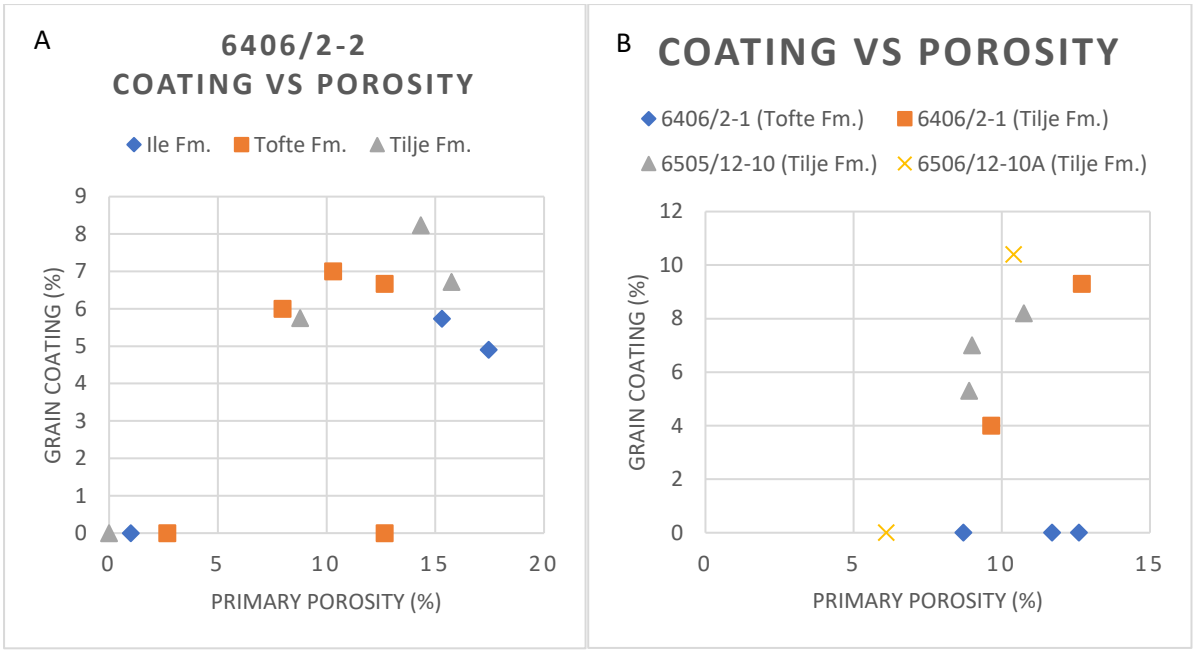

Figure 6.21. Primary porosity vs grain coating cross plot (a) well 6406/2-2 (b) well 6406/2-1, 6506/12-10, and 6506/12-10A

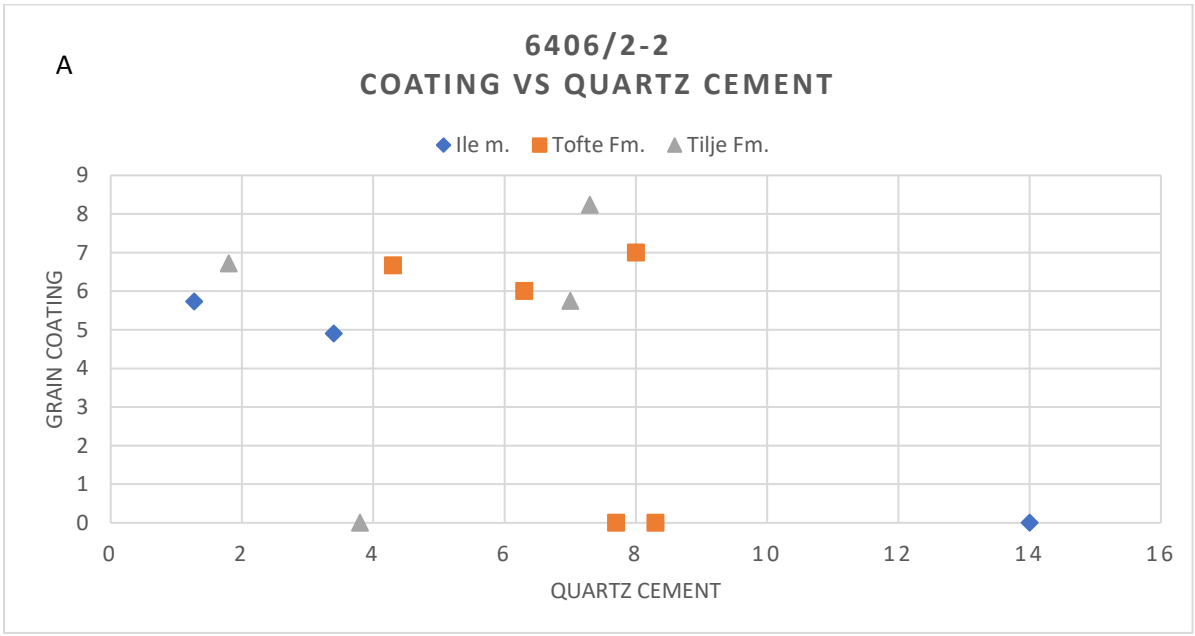

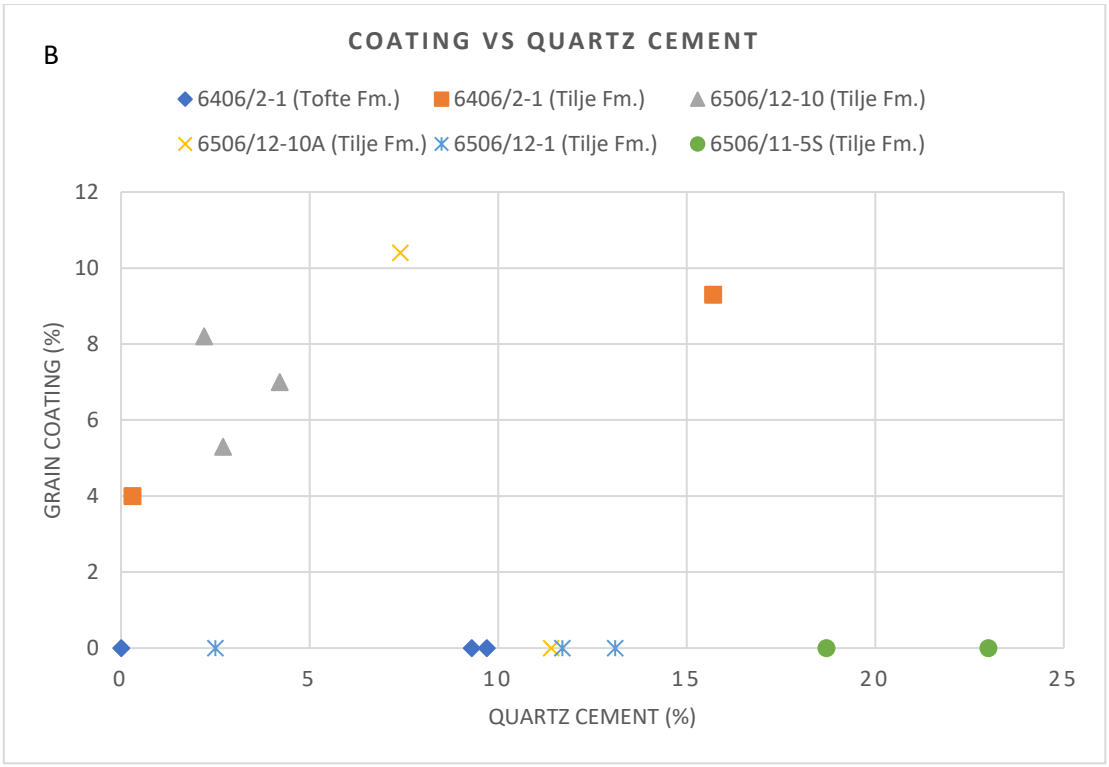

Figure 6.22. Quartz cement vs grain coating crossplot (a) well 6406/2-2 (b) well 6406/2-1, 6506/12-10, 6506/12-10A, and 6596/11-5S.

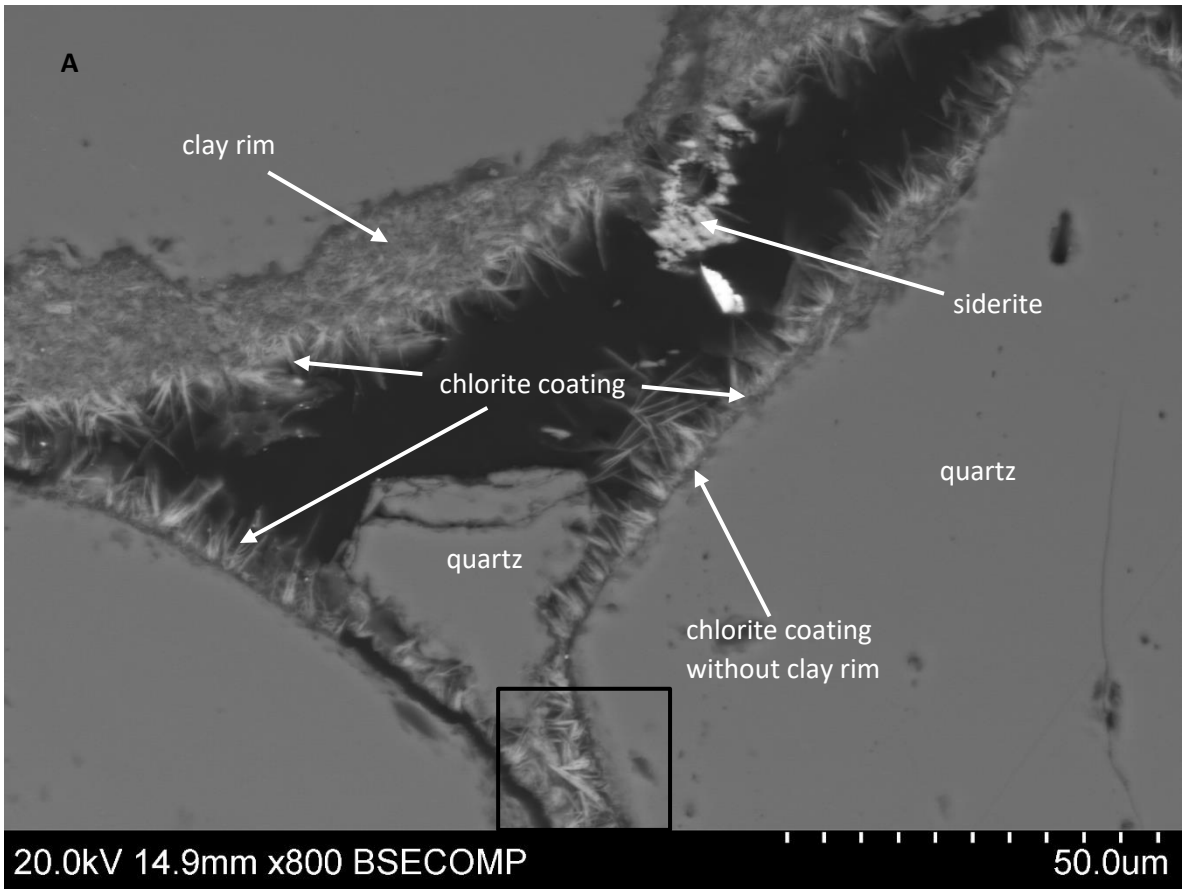

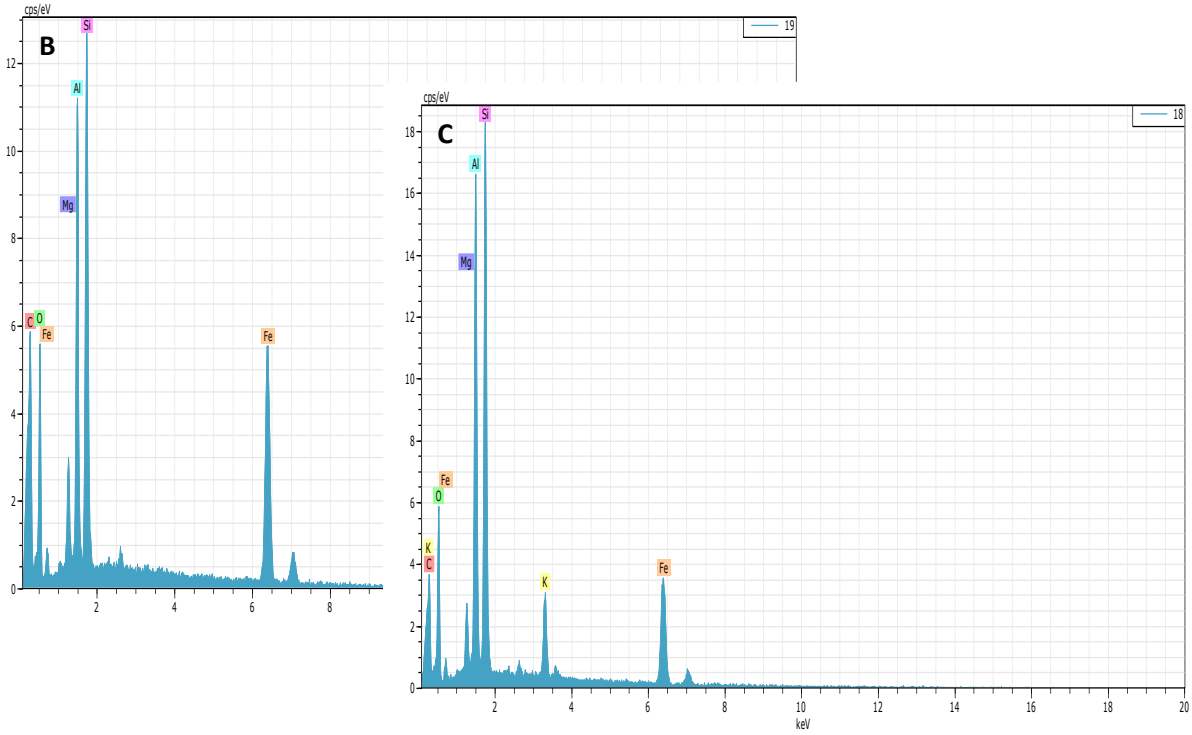

Figure 6.23. (A)Tilje Formation, well 6406/2-1, 5104.00m. SEM photomicrograph of chlorite coating on quartz grain and clay rims coated with authigenic chlorite (boxed area, extensive grain coating blocking porosity) (B) EDS image showing spectrum for chlorite coating in Figure *6.23A (C) EDS image showing spectrum for mixed chlorite/illite rim in* Figure *6.23A*

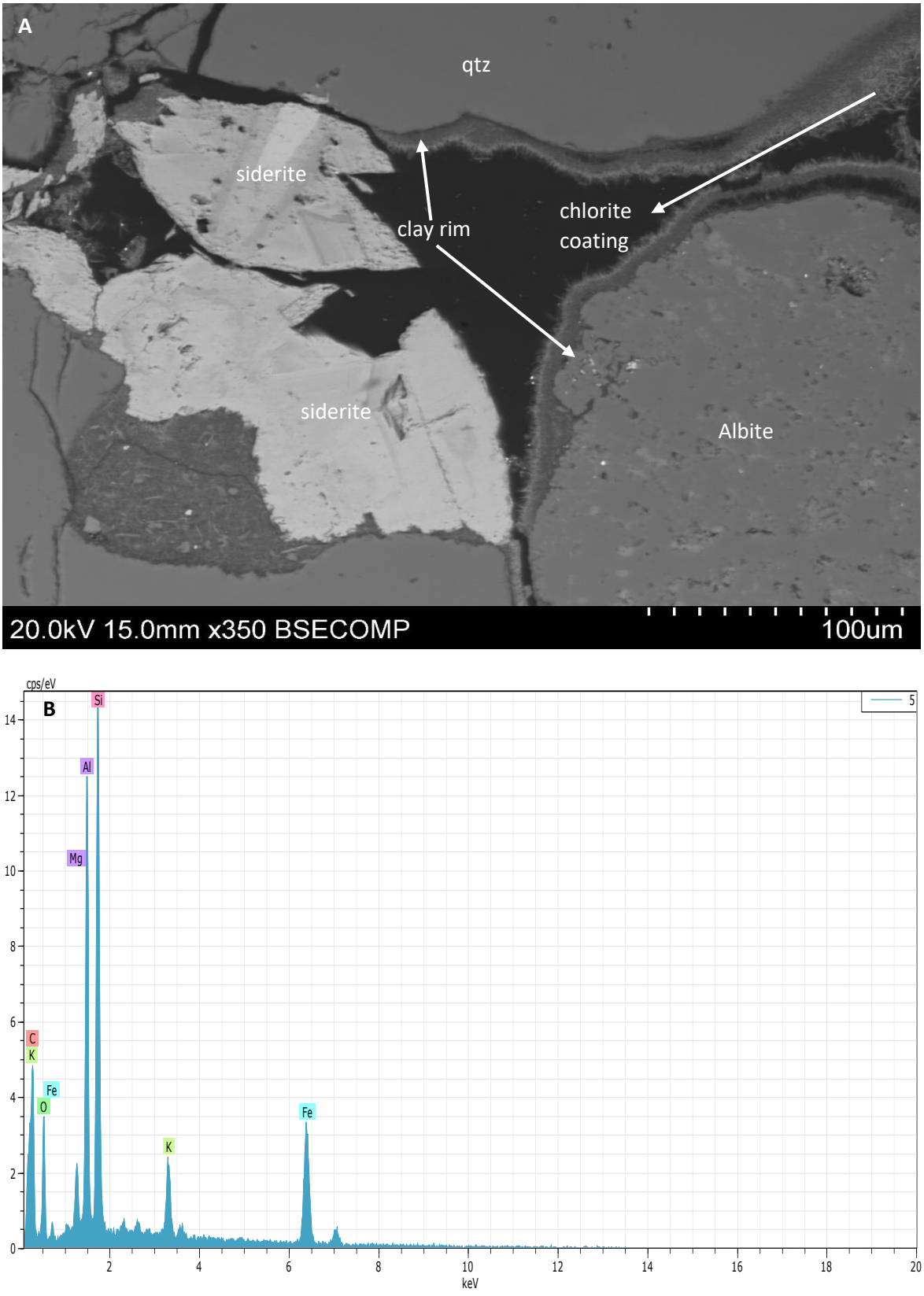

Figure 6.24. (A) Tilje Formation, well 6406/2-1, 5101.50m. SEM photomicrograph of clay rims with a mixture of illite and chlorite and siderite cement (B) EDS image showing spectrum for mixed chlorite/illite rim in figure 6.24A

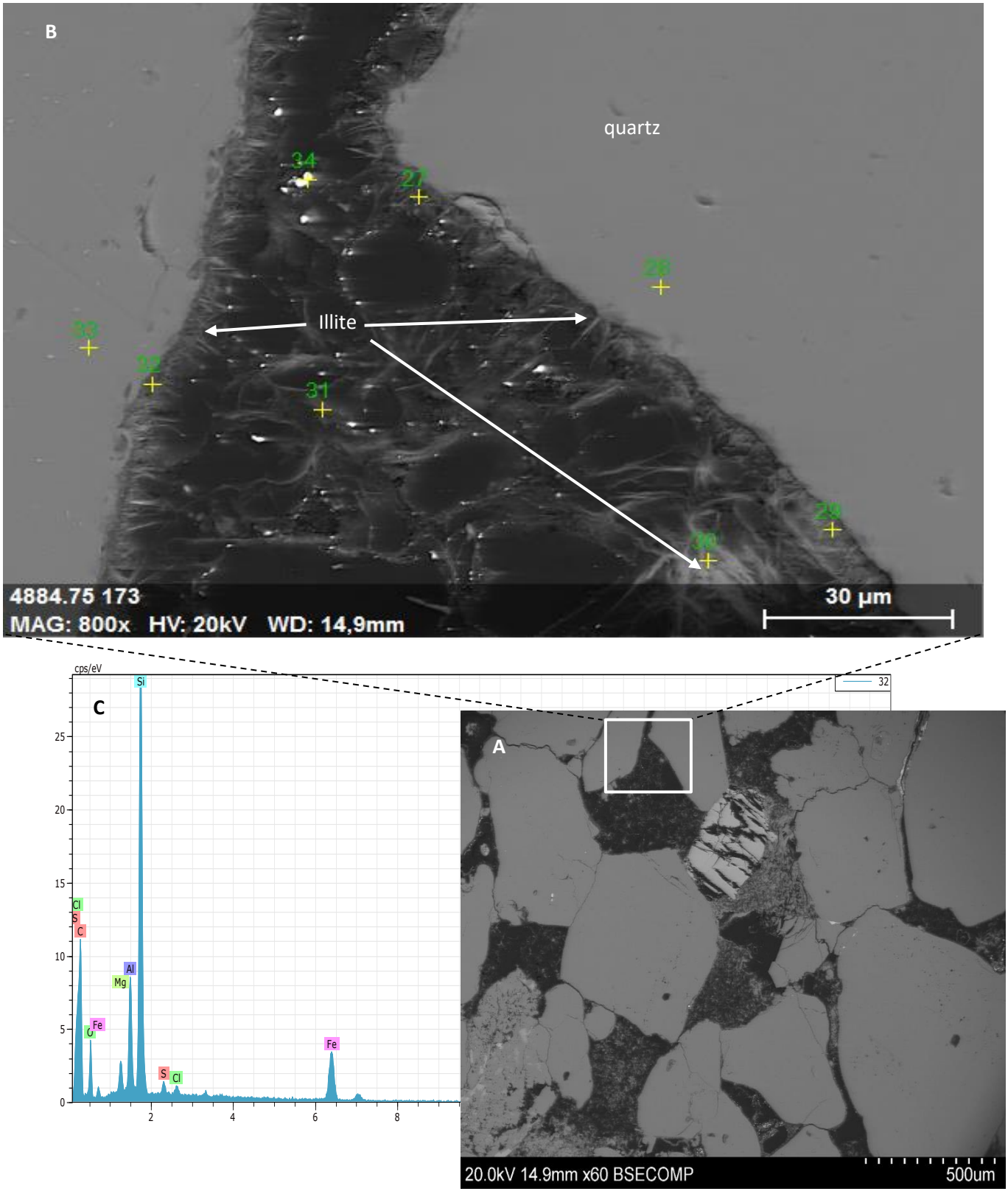

Figure 6.25. (A and B) Tofte Formation well 6406/2-2, 4884.50m. SEM photomicrograph of illite coating on quartz grain (C) EDS image showing spectrum for illite coating in Figure *6.25B*

Table 6.4. Grain coating coverage

Well	Formation	Depth (m)	Comment
6406/2-1	Tilje Formation	5101.50	Good coating, with high amount of siderite cement
6406/2-1	Tilje Formation	5104.00	Good coating, with some pore filling quartz cement
6406/2-2	Ile Formation	4706.25	Very good coating, with carbonate cement and clay
6406/2-2	Ile Formation	4726.25	Very good coating, with carbonate cement and clay
6406/2-2	Tofte Formation	4884.50	Poor coating
6406/2-2	Tofte Formation	4910.25	Moderate coating, with high amount of clay
6406/2-2	Tofte Formation	4919.75	Good coating, with some pore quartz cement
6406/2-2	Tilje Formation	4984.25	Good coating
6406/2-2	Tilje Formation	5124.50	Very good coating, with secondary porosity due to chlorite coating on dissolved grain
6406/2-2	Tilje Formation	5126.50	Good coating, with carbonate cement and chlorite pellet reducing porosity
6506/12-10	Tilje Formation	4943.25	Good coating, with carbonate cement
6506/12-10	Tilje Formation	4962.66	Good coating, with carbonate cement
6506/12-10	Tilje Formation	5012.85	Very good coating, with carbonate cement
6506/12-10A	Tilje Formation	5686.85	Very good coating, with chlorite pellets reducing porosity.

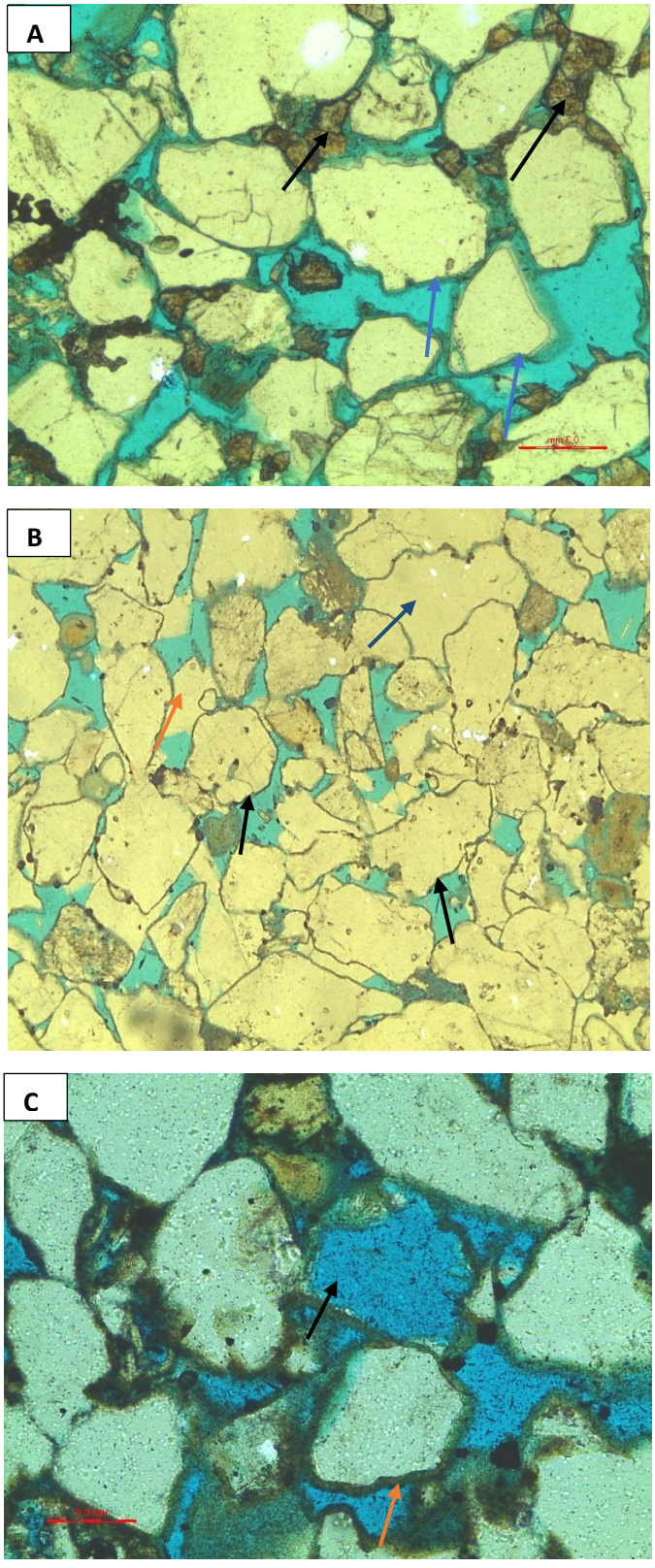

Figure 6.26. (A)Tilje Formation, well 6406/2-1, 5101.50m. photomicrograph of good coating (blue arrow), with high amount of siderite cement (black arrow) (B) Tilje Formation, well 6406/2-1, 5104m. photomicrograph of good coating (black arrow), with some pore filling quartz cement (dark blue arrow) (C) Tilje Fomation, well 6406/2-2, 5124.50m. photomicrograph of very good coating (orange arrow), with secondary porosity (black arrow) due to chlorite coating on dissolved grain. Scale bar are all 0.3mm

6.6.5 Feldspar

Feldspar minerals identified under a petrographic microscope and through SEM analysis are K-feldspar, albite. Underestimation of feldspar quantity is most likely due to the difficulty in differentiating untwined albite grain and quartz grain, as both grains exhibit similar optical features. Bulk of the feldspar grain have undergone feldspar dissolution forming secondary porosity, and have also been replaced by sericite and illite, albitization of K-feldspar is common in the samples (Figure 6.27).

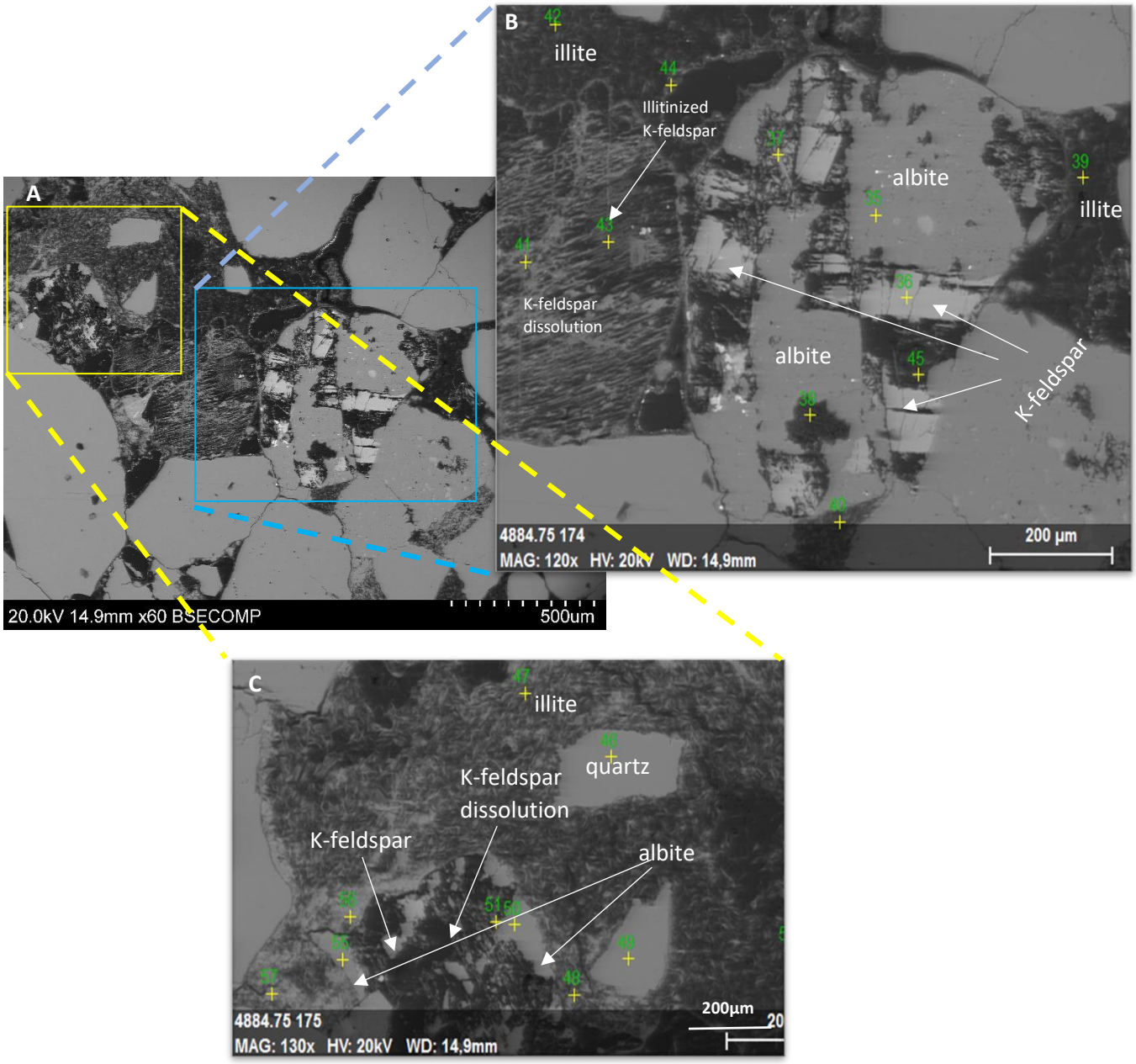

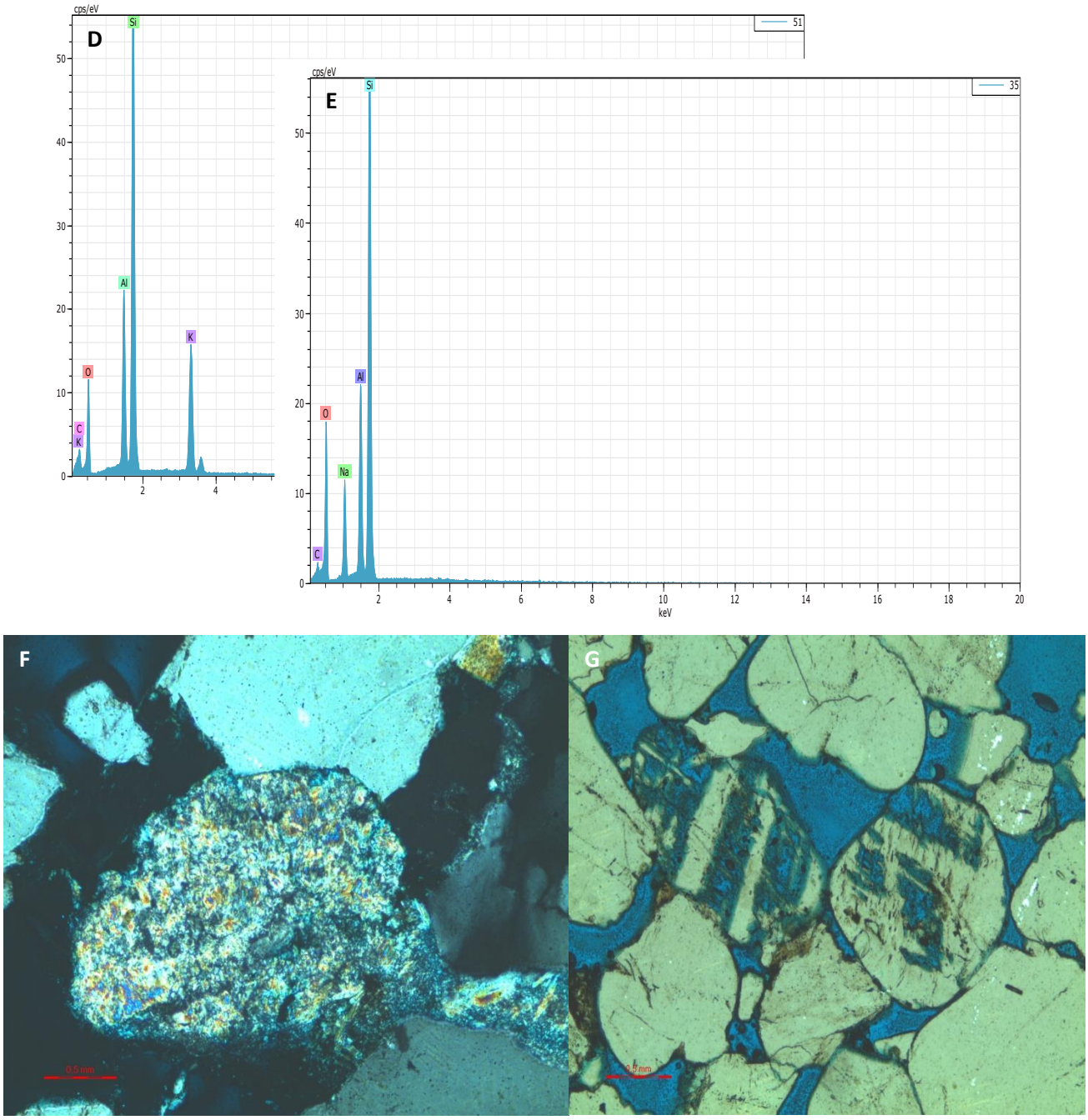

Figure 6.27. (A, B, and C) Tofte Formation, well 6406/2-2, 4884.50m. SEM photomicrograph showing albitization of K-feldspar and illitization of K-feldspar (D) EDS image showing spectrum for K-feldspar in Figure *6.27A (E) EDS showing spectrum for Albite in* Figure *6.27A (F) Tilje Formation, well 6506/11-5S, 4703.28m. photomicrograph of feldspar grain replaced by sericite (G)Ile Formation, well 6406/2-2, 4726.25m. photomicrograph of microcline dissolution forming secondary porosity*

6.6.6 Heavy minerals

Heavy minerals like pyrite, rutile, and apatite (Figure 6.20) were found in small patches alongside clay minerals and mica in almost all the wells. However, at depth 4703m in well 6506/11-5S a broad pyrite vein was encountered containing pure quartz grain (Figure 6.28).

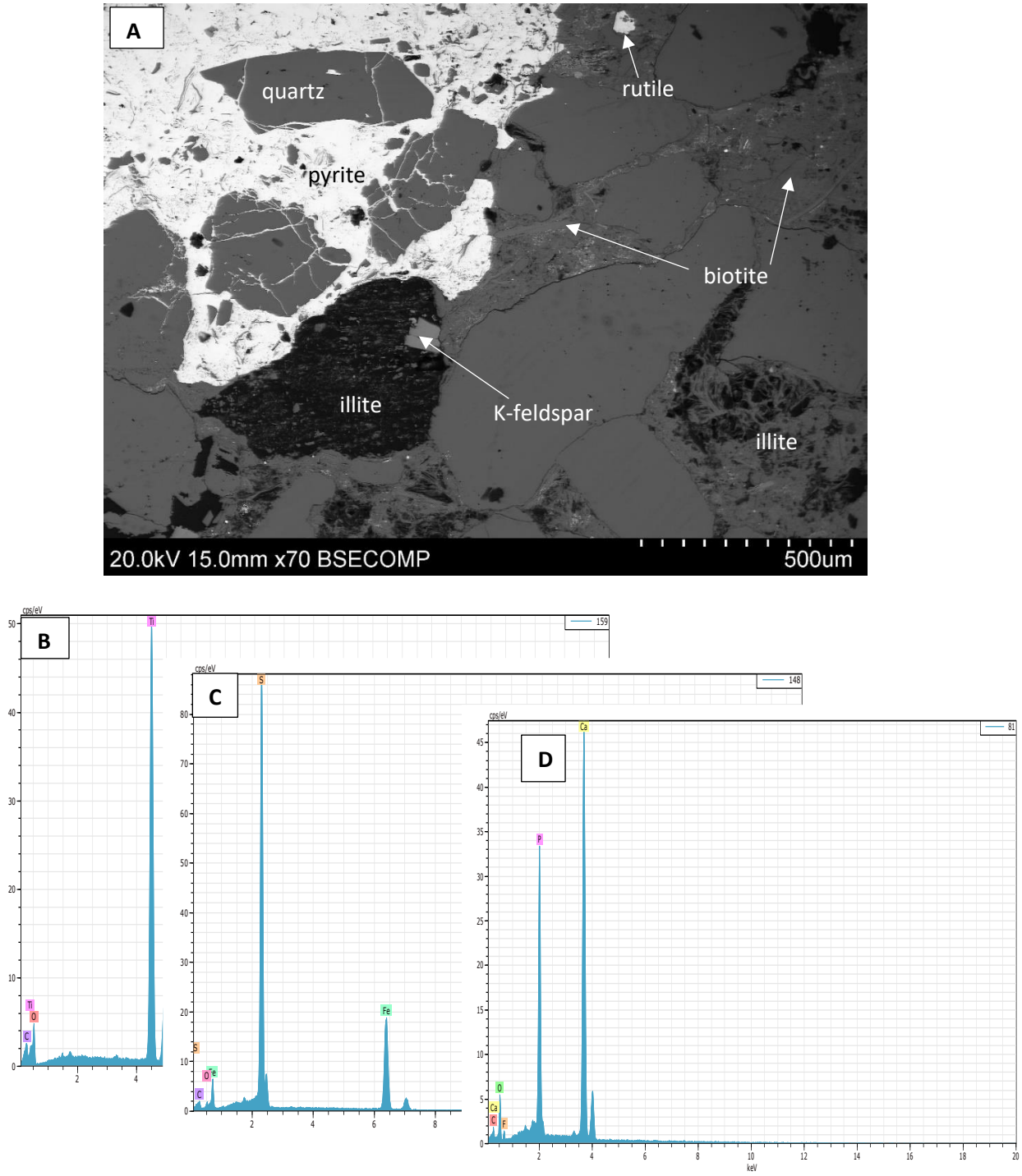

Figure 6.28. (A) Tilje Formation, well 6506/11-5S, 4703.28m. SEM photomicrograph of Pyrite vein (B) EDS image showing spectrum of rutile in Figure *6.28A (C) EDS image showing spectrum of pyrite in* Figure *6.28A (D) EDS image showing spectrum of apatite in* Figure *6.20*

Chapter Seven: Discussion

7.1 Mechanical compaction

At shallow depth, mechanical compaction is the dominant porosity reducing process in siliciclastic sediments. The process of mechanical compaction involves grain rearrangement and repacking, plastic deformation of grains, and fracturing of brittle grain. Therefore, they depend on the mineralogy, grain size, shape, sorting, and fluid composition of the siliciclastic sediments. These processes have effect on the intergranular volume (IGV) of the sandstone (Bjørlykke and Jahren 2010; Houseknecht, 1987).

According to Paxton et al. (2002), uncompacted sandstone has intergranular volume (IGV) of 40 to 42% at the surface, and it reduces to 26% at 1500 to 2500m depth. The (IGV) observed in the studied Tilje Formations ranges from 21% to 44%. These IGV values reflect a degree of compaction ranging from nearly uncompacted to highly compacted. Tofte and Ile Formation show a moderate degree of compaction. Fracture of brittle grain and the plastic deformation of mica grain in the formations of the studied wells suggests the grains were subjected to mechanical compaction (Figure 7.1).

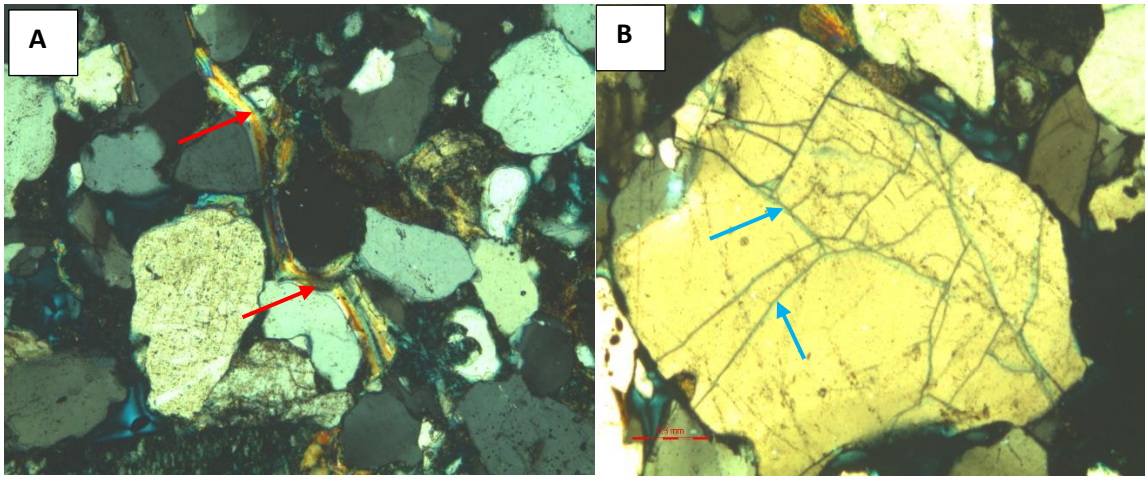

Figure 7.1. Photomicrograph of the grains showing (a) the plastic deformation of mica grain (red arrows) (b) fractured grain (blue arrow) due to increased burial depth. Scale =0.3mm.

From the petrographic result of this study, it is observed that a high IGV value shows a positive correlation with fine to medium grain-sized samples (Figure 6.9). Chuhan et al. (2002), in their experiment, showed that coarse-grained sand promotes compaction and fine-grained material suppresses compaction. As against finer grain sandstone which has good intergranular contact

and less susceptible to crushing, the coarse-grained sand exhibits high forces per grain contact due to the small intergranular contacts between the grains, resulting in a high degree of grain crushing in coarse grain rocks. This analogy explains why many of the analysed fine and medium grain samples have high IGV. In addition to grain size, grain sorting also plays an essential role in the compaction of siliciclastic sediments. However, due to the difficulty of accurately measuring sorting, an underestimation of compaction is possible. The following authors Rittenhouse, (1971); Ramm, (1992); Paxton et al. (2002); Chuhan et al. (2002, 2003), have shown in their study that IGV is higher in well-sorted sandstone. The relationship between IGV and sorting in this study agrees with these previous authors' works as most of the samples exhibit well to moderate sorting with good IGV values (Table 6.1 and 6.2). However, a negative correlation between IGV and sorting is seen in some poorly sorted samples with high IGV at depth 4910.25m and 4986.75m in well 6406/2-2, and 5694.50m in well 6506/12-10A, respectively. At depth 4271.66 in well 6506/12-1, well-sorted sample is seen to have a low IGV value (Figure 6.10) (Table 6.1 and 6.2). The negative correlation at depth 4986.75m and 5694.50m is probably due to high early carbonate cementation, which reduces the effect of mechanical compaction by stiffening the grain framework. While the negative relationship between IGV and sorting in the sample at depth 4910.25m is probably due to the presence of authigenic illite resulting from the alteration of feldspar and mica (Figure 6.11). Low IGV counted in the well-sorted sample at depth 4271.66m is likely due to the late quartz cementation of the grains in the sample.

7.2 Mineralogy and Diagenetic Processes

7.2.1 Quartz Cementation

Most of the samples are found to have quartz cementation in the form of overgrowth on detrital quartz grain and precipitation of quartz cement within pore space (Figure 6.12). In the Halten Terrace area, quartz cementation increases at depth below 2.5-3.0km (Bjørlykke, Aagaard, Egeberg, & Simmons, 1995; Ehrenberg, 1990; Ramm, 1992). All the studied samples in all wells are from depths below 4km, and they agree with the general notion of an increase in quartz cementation with depth. However, samples containing a reasonable amount of pore filling carbonates and authigenic chlorite and illite do not follow the increasing quartz cementation/depth trend (Figure 6.13). Hence, the amount of quartz cementation in most of the studied sample is clearly a function of carbonate cement precipitation and the occurrence or absence of chlorite/illite coating and authigenic clay minerals present in the sample.

At the onset of quartz cementation, mechanical compaction reduces or seizes because quartz cementation works to stabilize the rocks at a much faster rate than the increase in vertical stress from the overburden, with only about 2-4% quartz cement needed to stop further mechanical compaction (Bjørlykke and Jahren 2010). A study of the relationship between high IGV values and quartz cementation in Tilje, Tofte, and Ile Formations in all six wells (Figure 6.8) reflects possible precipitation of quartz cement in the early stage of burial below 2.5km, as most of the samples in the studied well interval show more than 2% quartz cement, which according to (Bjørlykke and Jahren 2010) is considered adequate to stop mechanical compaction.

A good amount of quartz cement is observed in most of the samples in all formation since the grain size of the sample is predominantly fine to medium grain, with an exception to the Tilje Formation in well 6506/11-5S, where heavy quartz cement is seen in the coarse-grained sample of this formation. Considering the relationship between quartz cementation and grain size, studies by different authors (Fuchtbauer, 1967a; Stephan 1970; Walderhaug, 1994) have shown that the amount of quartz cementation in a sample is primarily a function of the grain surfaces available for quartz precipitation, and by default heavy quartz cementation is predominant in areas with finer-grained sizes due to the greater abundance of surface area in fine-grained sands. McBride (1989), however, outlined that this principle does not apply to all formations and can also depend on other factors different from the increased surface area of the fine-grained sample. Furthermore, in his study, McBride (1989) showed the experiment of Heald and Renton (1966), which further explained that with freely circulating cement fluids, quartz cementation is faster in coarse-grained sand than in finer-grained sand. This experiment probably demonstrates the heavy quartz cementation in the coarse-grained samples of Tilje formation in well 6506/11-5S.

Intergranular pore spaces have been completely occluded by pore-filling quartz cement and quartz overgrowth in the analysed samples in the Tilje Formation in well 6506/11-5S. In some of the samples in Tilje, Tofte, and Ile Formation (6406/2-1, 6406/2-2, 6506/12-1, 6506/12-10, and 6506/12-10A), intergranular pores have also been considerably reduced by pore-filling quartz cement and quartz overgrowth resulting in reduced porosity (Figure 7.3). However, the presence of grain coating authigenic clays has been able to preserve porosity to some extent. In addition, according to Bjørlykke and Jahren (2010), a thin layer of authigenic chlorite has proven to be very effective in preventing quartz overgrowth.

Oelkers et al. (1996), in their study, mentioned the work of Fuchtbauer (1983), who summarized the sources of quartz cement within sandstones to be from the dissolution of quartz

associated with siltstones, replacement of feldspar by clay minerals, pressure solution coupled with stylolites, and alteration of smectite to illite. However, McBride (1989) outlined that different authors have described pressure solution of quartz grains as the most common and important source of silica for quartz cement in moderate to deeply buried sandstones. Considering the mica and illite content of the sample (Table 6.1), the sources of quartz cement in Ile, Tofte, and Tilje Fomation can be attributed to pressure solution along mica and illitic clay/quartz contact (Figure 7.2) and silica released during the dissolution of K-feldspar and reaction with kaolinite to form illite. The dissolution of K-feldspar follows an irreversible reaction (Equation 7.1) (Thyne et al. 2001).

$$KAlSi_3O_8 + 2/3\ H^+ \longrightarrow 2/3K^+ + 1/3KAl_3Si_3O_{10}(OH)_2 + 2SiO_2(aq) \quad \text{Equation. 7.1}$$

(K-spar) (Illite)

At depth 5104.00m in the Tilje Formation in well 6406/2-1, high quartz cementation with only a minimal amount of mica and no illites were observed. Although no stylolites were observed at this depth, the source of silica for the high quartz cement in this formation may be explained by pressure solution from neighboring stylolites. Oelkers et al. (1996) also stated that the bulk of the quartz cement in Jurassic quartzose sandstones from the North Sea and mid-Norwegian continental shelf is sourced from quartz dissolution at mica or illitic clay/quartz interfaces in adjoining stylolites.

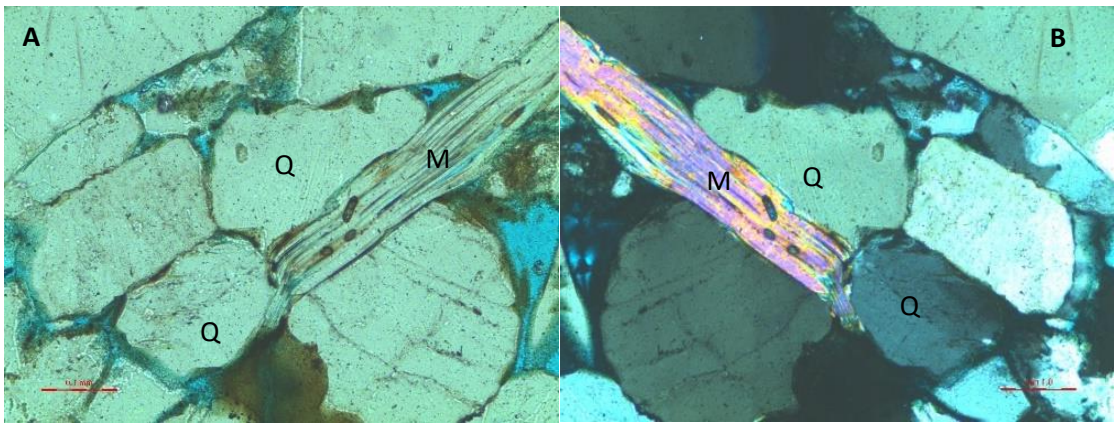

Figure 7.2. Mica/Quartz interaction in Tilje Formation at depth 5126.50m in well 6406/2-2 with scale of 0.1mm (A) Plane polarized image (B) Crossed polarised image. Scale = 0.1mm.(M-Mica, Q-Quartz).

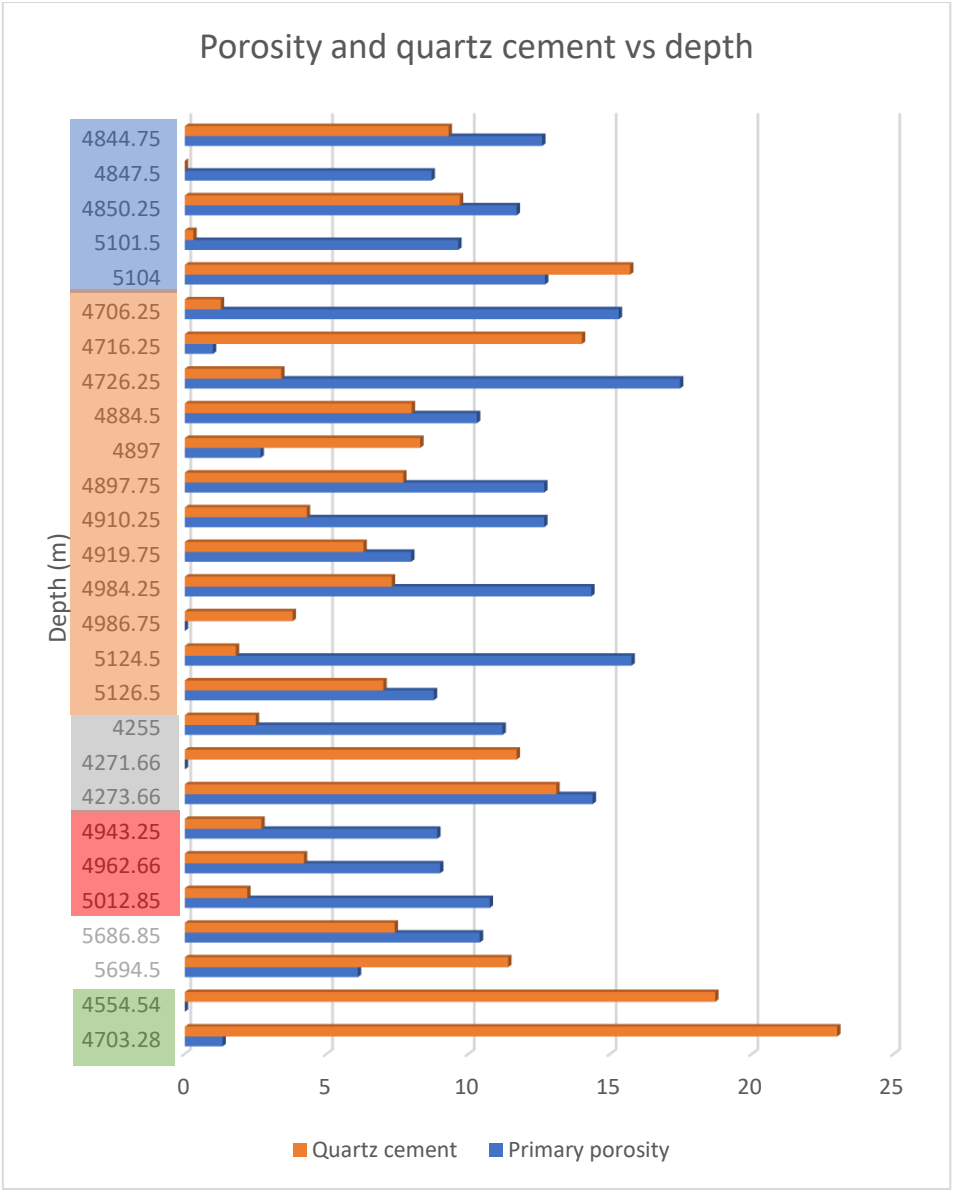

Figure 7.3. Relationship of quartz cementation to porosity. Coloured rectangle on the right depicts individual well depths; Blue- well 6406/2-1, Orange- 6406/2-2, Grey-6506/12-1, Red-6506/12-10, White- 6506/12-10A, and Green-6506/11-5S.

7.2.2 Chlorite and Chlorite Coatings

The formation of chlorite coatings on grains requires an iron-rich precursor. Therefore, understanding these chlorite precursors will aid in the interpretation of the different processes responsible for the formation of chlorite coatings on grains. Ehrenberg (1993), in his study, explained that the formation of chlorite coatings on sand grains is dependent on the depositional environment. However, Bloch et al. (2002) outlined that the formation of chlorite coatings on sand grains is not just a function of the depositional environment but incorporates other factors, including a good source of iron, adequate grain size, and absence of a late carbonate killer cement.

Chlorites observed in the Tilje, Tofte, and Ile Formations occur mainly as pellets, ooids, and coatings arranged perpendicularly on detrital grain and clay rims. However, point counting results showed that the proportion of pellets and ooids vary considerably in the different formations. A good number of pellets is present both in Tilje and Ile Formation, while a high amount of ooids were observed majorly in the Tilje Formation. In the studied samples, chlorite coating has been found to be effective in inhibiting the overgrowth of quartz on detrital quartz.

According to Ehrenberg (1993), the occurrence of ooids and pellets is considered important in the interpretation of chlorite enrichment and depositional environment. The ooids and ooidal grain coatings recognised in the formations are Fe-rich and are concentrically laminated with an appearance that shows a mechanical buildup of clay as the grains were rolled by water currents. The high Fe-content of these ooids depicts an Fe-rich precursor clay was concentrated in the sand at the time of deposition (Ehrenberg, 1993). The concentration of iron in seawater is considered very low; hence a source of iron in seawater is needed for chlorites to form. In most Tilje Formation samples, siderite cement frequently occurs alongside chlorites (Figure 6.23 & 6.24). The sandstones of the Tilje Formation have been described to have a depositional setting corresponding to tidally influenced, shallow marine and shoreface setting Formation and delta lobe progradation (Haq et al. 1987; Hallam, 1988; Surlyk 1990; Ehrenberg, 1993 Swiecicki et al. 1998). In marine environments, siderites cement precipitation is favoured by iron activity and (meteoric-water influx) and anoxic and oxic pore fluid alternation in near shore sediments (Bloch et al. 2002). Consequently, the association of these iron-rich siderites with chlorites in most of the samples of the Tilje Formation further suggests a meteoric-water source of iron, and the depositional setting explains the occurrence of ooids which are representative of high depositional energy in a high-energy environment. In some of the samples, detrital sand grains are coated by detrital-clay rims (mixed layer of chlorite and illite) (Figure 6.24) with the growth of chlorite on these clay rims in some samples (Figure 6.23). These clay rims, which also act as a precursor for chlorite coating formation, could have possibly formed from the deposition of detrital clay carried in suspension in the meteoric water. Considering the low potassium contents of the clay rim (Figure 6.24B), berthierine could also be a possible precursor of chlorite. The work of Ehrenberg (1993) showed that with increasing temperature (between 80-100^{o}C), chlorite could be formed from the transformation of berthierine (an iron-rich mineral with low potassium content) to chlorite, while Aagard et al. (2000) experiment on clay rim showed that the precursor clay rim is dominated by berthierine mixed-layer clay.

In the studied samples, the effectiveness of chlorite coating with regards to porosity preservation is a function of the coating thickness, the continuity of coating around grain, and the grain size. Some of the samples show good, thick, and continuous chlorite coatings on grains (Figure 6.26 A & C), while some samples show poor coatings (Table 6.4). Chlorite coating have been effective in inhibiting quartz overgrowth in samples with good chlorite coatings (Figure 6.22). However, regardless of the good chlorite coating, a few numbers of samples still contain pore filling quartz cement (Figure 6.26 B). Considering the form of quartz cement in these samples, it can be said that the chlorite coatings were formed before the sandstones attained a temperature and burial depth where quartz cementation is predominant.

7.2.3 Illite Precipitation and Illite Coating

The illite observed in the studied wells occurs majorly as pore-filling and as coatings on grain. Point counting result shows that illite is more concentrated in the Ile and Tofte Formation than in the Tilje Formation. Since illite usually retains its predecessor's shape, it is observed in this study that illite has retained the sheet-like morphology of kaolinite and the shape of smectite (secondary electron image is needed to ascertain the shape) (Figure 6.16 &6.17) as seen from SEM examination. Although smectite and kaolinite were not identified in any of the samples, it is assumed that the formation of illite is likely attributed to the replacement of kaolinite and the replacement of smectite. Considering the morphology of smectite-derived illite, it is assumed that smectite in the Tofte Formation is related to mica transformation to illite.

Meteoric water flow through the pore space of the sandstones resulted in the alteration of mica mineral and the dissolution of K-feldspar, resulting in the formation of kaolinite (Equation 7.2 & 7.3) in the early stage of diagenesis. At a higher temperature of about 120-140^{o}C, dissolution of the remaining K-feldspar provides the potassium required for the conversion of kaolinite to illite during burial (Equation 7.4) (Bjørlykke, 1994).

$$2KAlSi_3O_8 + 2H^+ 9H_2O \longrightarrow Al_2Si_2O_5(OH)_4 + 2K^+ + 4H_4SiO_4 \quad \text{Equation. 7.2}$$
K-feldspar — Kaolinite

$$2KAl_3Si_3O_{10}(OH)_2 + 2H^+ + 9H_2O \longrightarrow Al_2Si_2O_5(OH)_4 + 2K^+ + 4H_4SiO_4 \quad \text{Equation. 7.3}$$
Mica — Kaolinite

$$KAlSi_3O_8 + Al_2Si_2O_5(OH)_4 \longrightarrow KAL_3Si_3O_{10}(OH)_2 + 2SiO_2 + H_2O \quad \text{Equation. 7.4}$$
K-feldspar — Kaolinite — Illite — Quartz — Water

The temperature requirement for extensive illitization of kaolinite is around 130-140^{o}C (Thyne et al. 2001). All the studied samples from Ile, Tofte, and Tilje Formations occur at burial depths below 4000m, and all the formations from each of the wells have a formation temperature

greater than 140^{o}C. The factors mentioned above show why no kaolinite is observed at these depths. And this is simply due to the complete illitization of early-formed kaolinite within the temperature window given by Thyne et al. 2001. According to Bjørlykke and Aagaard (1992), the source of potassium needed to convert kaolinite to illite for the formation of late-stage illite (at a depth greater than 3500m) seems to be a result of the dissolution of K-feldspar. Point counting result shows that formations that contain illite still have a considerable amount of K-feldspar with the absence of kaolinite. The persistence of K-feldspar here may be due to the slow dissolution rate of the feldspar. Bjørlykke, in his 1994 paper, stated that the amount of kaolinite present as a precursor might be the limiting factor controlling illite growth. Following Bjørlykke, (1994) analogy, it can be said that the abundance of illite in the studied depth also suggests an abundance of kaolinite in the early stage of diagenesis.

In the studied samples, the two precursors of illite identified in the samples show two different patterns: (1) illite coatings associated majorly with illite derived from smectite (Figure 6.25) (2) pore filling illites associated with illite formed from kaolinite (Figure 6.16) and smectite (Figure 6.17). The study of Storvoll et al. (2002) on grain coating illites in the Garn Formation in offshore mid-Norway, showed that illite coatings are not generated from kaolinite-derived illite but rather from smectite-derived illite, for the following reasons:

1. As discussed in the previous paragraph, the illitisation of kaolinite is insignificant at a temperature below 120-140^{o}C. Hence, quartz cementation, which takes place at a temperature and depth ranging between 2.0-2.5km and 70-90^{o}C, respectively, would have developed enough before any significant illite-coating originated from kaolinite is formed.
2. On the other hand, smectite-illite transformation occurs at a low temperature and shallow depth. This suggests that illite-coating originated from smectite would have developed early to prevent quartz cementation.

These outlined reasons from the Storvoll et al. (2002) study could serve as a reasonable explanation why illite coating is associated with smectite transformation. In all the samples, pyrites (Fe-sulphide), a common early diagenetic mineral, are observed alongside smectite-derived illite (Figure 6.25 & 6.28). This association confirms smectite-illite transformation took place at an early stage of diagenesis. Although illite coating is predominantly in the Tofte Formation, minor chlorite coating also occurs with illite in some samples. The amount of grain

coating illite is not abundant in most of the samples when compared to the chlorite coating. However, they are effective in inhibiting quartz overgrowth.

7.2.4 Carbonate Cementation

The result of the point counting analysis showed that carbonate cement was observed at varying proportions in each of the three formations. These carbonate cements are calcite, siderite, and ankerite. SEM analysis confirmed Mg-rich siderite and Ca-rich ankerite as the dominant authigenic carbonate cement in the studied well intervals (Figure 6.24A, Figure 6.14). These cement types occur mainly as pore-filling (Figure 6.14A, E and Figure 6.24A) and replacement minerals. The replacement is shown by the presence of loosely packed quartz grain in a carbonate matrix (Figure 6.15), suggesting these grains were dissolved and replaced by carbonate cement. A second explanation could be that carbonate precipitation predates any significant mechanical compaction in the sandstones of these formations at shallow depth.

Two potential sources of divalent cations (Ca^{2+}, Mg^{2+}, Fe^{2+}) and carbon dioxide (CO_2) namely, internal and external sources, have been described by different authors (Morad et al. 1990; Dutton, 2008; Xi et al. 2015; Pszonka and Wendorff, 2017; Chen et al. 2019). The internal sources include the dissolution of detrital anorthite grains, locally reprecipitated detrital carbonate grains, and bioclasts. External sources include possible CO_2 sourced from the maturation of kerogen and decarboxylation of organic matter from adjacent mudstone or source rocks and conversion of volcanic rock fragment and clay minerals (conversion of smectite or kaolinite to illite), which provides Ca^{2+}, Mg^{2+}, Fe^{2+} ions into the pore fluids. From the petrographic study of the samples, only very few plagioclase feldspar grains and no detrital carbonate grains and bioclasts were observed, possibly ruling out an internal source of the carbonate. A considerable number of illite and few volcanic rock fragments were observed in the studied samples. The illites formed from the conversion of smectite or kaolinite and the very few volcanic rock fragments present could serve as the source of the divalent cations responsible for the formation of siderite, ankerite, and calcite. As seen in the petrophysical analysis (Figure 5.1, 5.2, & 5.3), the formations contain a high volume of mudstones. The mudstone from these formations and adjacent mudstones-dominated Ror Formation (Figure 5.5) could also serve as a source of CO_2 in the carbonates. However, an isotopic analysis to determine the decarboxylation of organic matter in the adjacent mudstones is necessary to ascertain the outlined carbonate sources.

When considering the relationship between carbonate cementation and IGV, it is observed that samples with high IGV values show a correlation with high carbonate cementation, as seen in Table 6.1. An explanation for this correlation can be attributed to the precipitation of carbonate cement at the early stage of diagenesis, restricting to some reasonable extent, further mechanical compaction of the sediments of these formations. An example of this is seen in the Tilje Formation, where the highest IGV of 44% is calculated in a sample at depth 4986.75 meters (well 6406/2-2) as a result of the high amount of carbonate cement (40.2%) counted in this sample. Furthermore, it is observed that samples with a high amount of carbonate cement contain a fewer amount of quartz cement, suggesting the precipitation of quartz cement postdates carbonate cementation in the early stage of diagenesis.

In as much as carbonate cementation reduces the further mechanical compaction of sediments, carbonate cements also act to reduce intergranular porosity in the sandstone reservoirs. A trend corresponding to intergranular porosity reduction with increasing carbonate cement and vice-versa can be seen in all three formations (Figure 7.4).

7.2.5 Albitization of Feldspar

SEM analysis shows albitization of K-feldspar in some samples in the Tofte Formation (Figure 6.27A, B & C). This albitization process indicates the abundance of sodium (Na^{+}) within porewaters of the deeply buried formation. Albitization of feldspar does not have any significant effect on the reservoir properties, however, a limited amount of calcite may precipitate from the Ca^{2+} released from plagioclase feldspar (Bole 1982; Bjørlykke and Jahren 2010).

7.3 Petrophysics

The ratio between sand and shales and the percentage of shale in the sandstone reservoir were analysed using the petrophysical method (Figure 5.1, 5.2 & 5.3). The volume of shale (Vsh) from thin section sample depths used in this study was analysed using 75API cutoff values. Appendix 2 below shows the range of shale volume in the sandstone reservoir intervals of the selected thin section samples. The shaliness of a sandstone reservoir can affect the permeability of the reservoir. The quality of the sandstone reservoir in the studied interval based on the volume of shale present in the reservoir is shown in the Table 7.1 below.

Well	Formation	Depth (m)	Vsh	Quality
6406/2-1	Tofte	4844.75 - 4850	Low	Good
	Tilje	5101.5 - 5104.00	Low	Good
6406/2-2	Ile	4706.25 - 4726.25	Low	Good
	Tofte	4884.50 - 4919.75	Low	Good
	Tilje	4984.25 - 5126.50	High	Poor
6506/12-1	Tilje	4255.00 - 4273.66	Average	Moderate
6506/12-10	Tilje	4943.25 - 5012.85	Average	Moderate
6506/12-10A	Tilje	5686.85 - 5694.50	Low - Average	Good to Moderate

Table 7.1. *Reservoir quality in the studied interval based on the volume of shale present in the reservoir.*

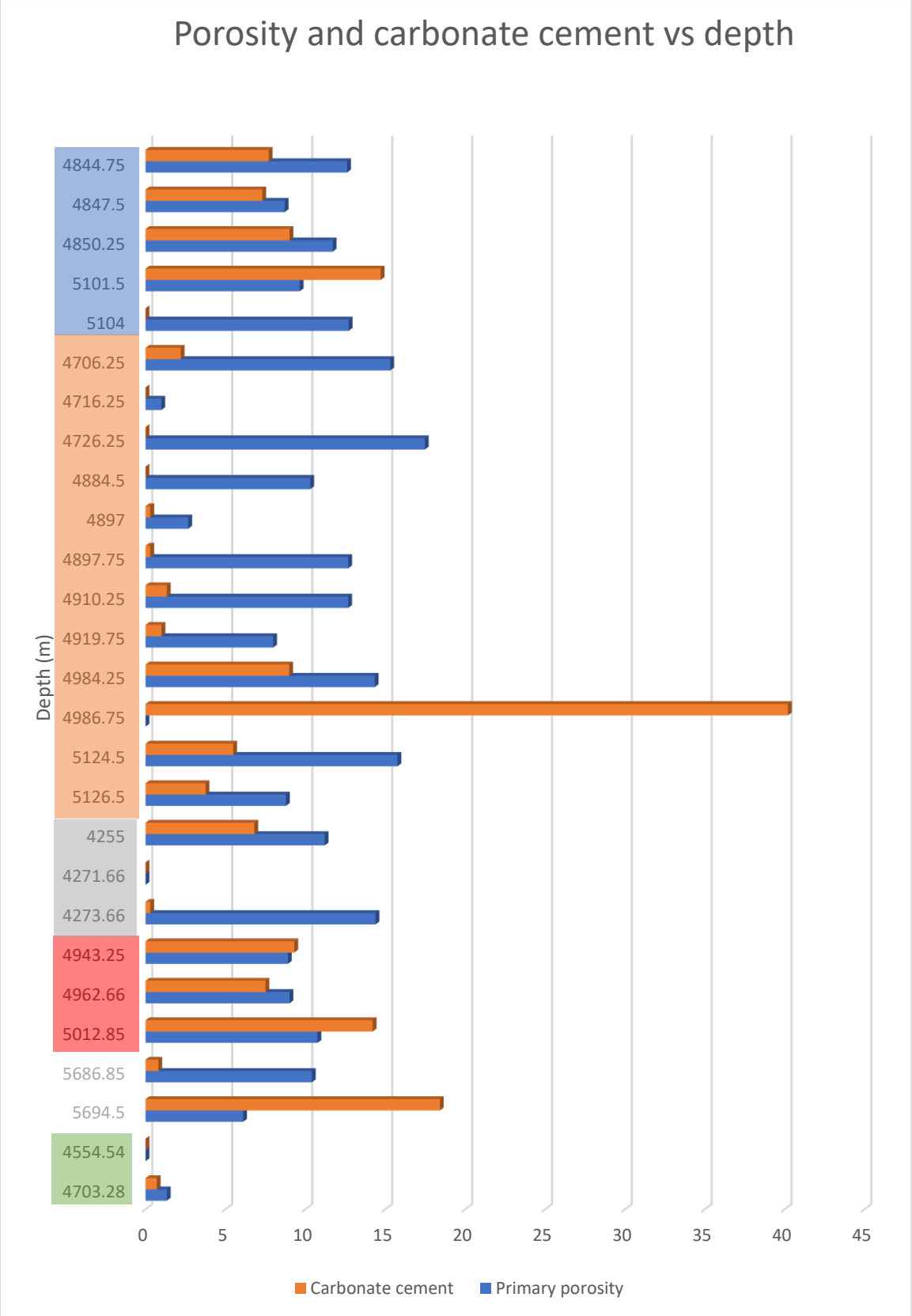

Figure 7.4. Relationship between carbonate cementation and intergranular porosity. Coloured rectangle on the right depicts individual well depths; Blue- well 6406/2-1, Orange- 6406/2-2, Grey- 6506/12-1, Red-6506/12-10, White- 6506/12-10A, and Green-6506/11-5S.

7.4 Impact of Diagenesis on Reservoir Quality

Taking a definition from AAPG, the quality of a reservoir is defined by its storage capacity and deliverability of hydrocarbon. The storage capacity and deliverability are directly related to the porosity and permeability of the reservoir, respectively. Therefore, a good reservoir is characterized by good effective porosity, and permeability and vice-versa. The environment of deposition and diagenesis are the two major factors that contribute to the modification of sandstone reservoir properties. Hence, the development of good porosity and permeability and their destruction is dependent on how these factors combine to influence the reservoir. The diagenetic influence observed in the analysed samples includes compaction, cementation, dissolution, and recrystallization. The study of the mechanical compaction using IGV in the three formations showed that all three formations had undergone a moderate degree of compaction.

Permeability of the sandstone interval was not studied in the formations. Hence, the discussion on reservoir quality in the studied area will focus majorly on porosity. Primary intergranular porosity and secondary porosity (comprising dissolution, fracture, and vuggy porosity) are the porosity types observed from the petrographic and SEM analysis of the studied samples. Porosity in the studied samples is controlled majorly by grain size, grain sorting, grain coating, carbonate and quartz cementation, and the distribution of authigenic clay minerals.

The analysed samples of Tilje, Tofte, and Ile Formation show quartz overgrowth and pore-filling quartz cement have worked to reduce porosity (Figure 7.2), the effect of quartz cementation is seen in the Tilje Formation in well 6506/11-5S. In this well, primary porosity is observed to be totally occluded due to extensive quartz cementation. The only porosity type observed in the Tilje Formation of well 6506/11-5S is secondary porosity. The absence of grain coating and the extensive quartz cementation in this well serves as a background in understanding the influence of grain coating in the preservation of porosity. All the studied samples are from depths below 4000m, chlorite and illite coatings at these depths are observed to be effective in the preservation of porosity through the inhibition of quartz cement growth on detrital grain. Table 6.4 shows grain-coated samples recognized in the three formations show very good to moderate coating. Regardless of the grain coating, some grain coated samples show a negative correlation with intergranular porosity, these samples show porosity of less than 10%. Porosity reduction in these samples can be attributed to the presence of carbonate cement and the distribution of authigenic clay in the pore space (Figures 7.4 and 7.5).

Carbonate cement precipitates at the early stage of diagenesis, occupying pore space, eventually reducing, or destroying the quality of the reservoir. An example is seen in one of the samples of Tilje Formation in well 6406/2-2 at depth 4986.75m, where carbonate cement precipitation in pore space has reduced porosity to zero (Table 6.1). These carbonate cements sometimes minimize the flow of hydrocarbon during production. Although, some carbonate cements precipitated at the early stage of diagenesis were subjected to partial and complete dissolution, leading to the production of secondary porosity. The quality of the reservoir is seen to be reduced due to the presence of authigenic illites precipitated in pore space. In the studied samples, authigenic illite formation tends to reduce permeability due to its fibrous pore-bridging form. In this study, secondary porosities are seen to be associated with the dissolution of feldspar and quartz grain (Figure 6.27 C & G) and microporosities in clay. Molds of chlorite-coated dissolved grains are also observed in the samples (Figure 6.26C).

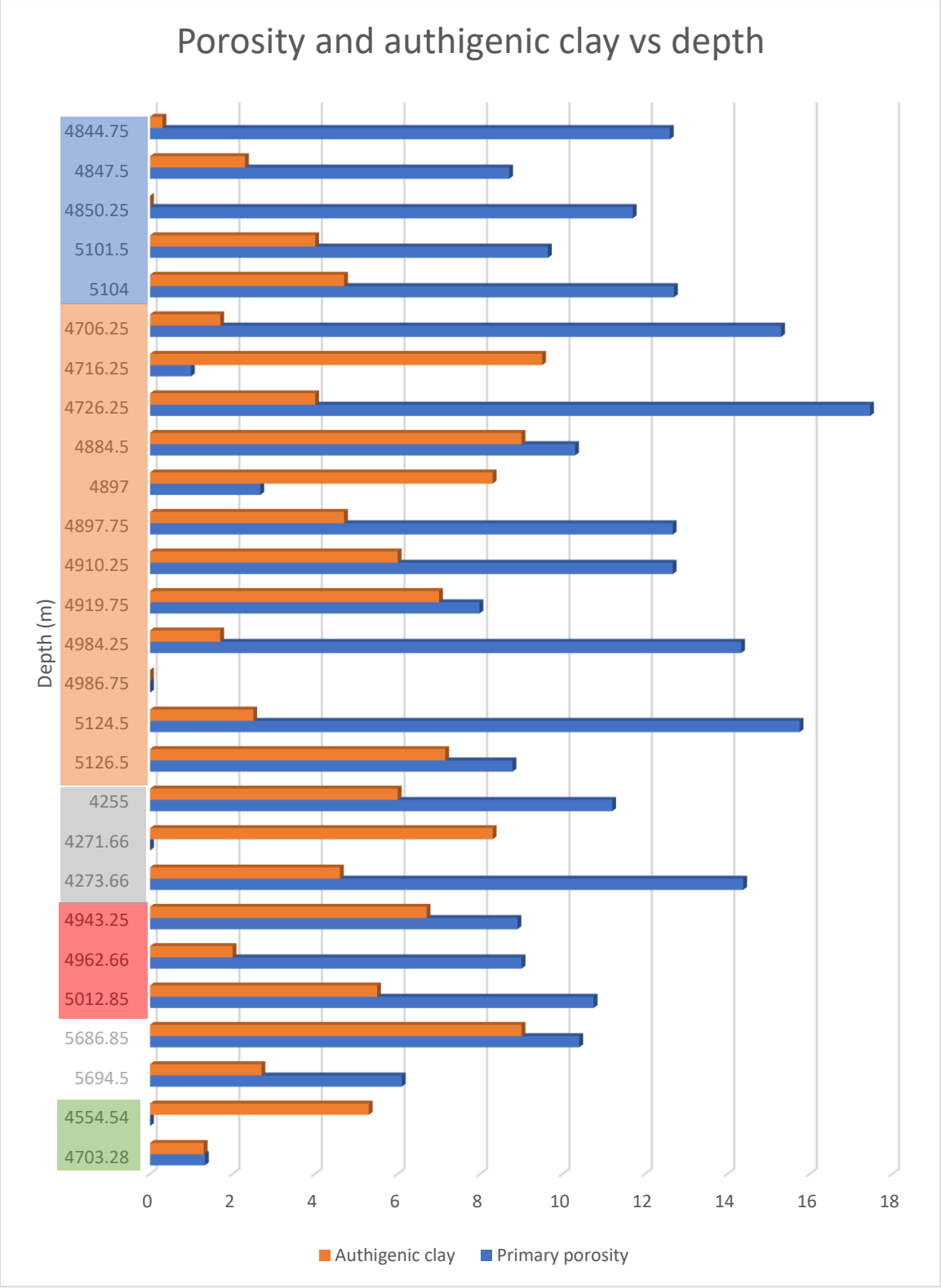

Figure 7.5. Relationship between pore filling authigenic clay and intergranular porosity. Coloured rectangle on the right depicts individual well depths; Blue- well 6406/2-1, Orange- 6406/2-2, Grey- 6506/12-1, Red-6506/12-10, White- 6506/12-10A, and Green-6506/11-5S.

Chapter Eight: Conclusion

The Tilje Tofte, and Ile Formation thin-section samples studied in well 6406/2-1, 6406/2-2, 6506/12-1, 6506/12-10, 6506/12-10A, and 6506/11-5S show a grain size ranging from fine to coarse-grained, and a moderate to well-sorted sample. The majority of the samples were described as medium grain size. Folk's (1951) maturity description of these sandstone samples illustrates a sub-mature sandstone in Ile, Tofte, and Tilje samples in well 6406/2-1, 6406/2-2, 6506/12-10, and 6506/12-10A. And Tilje samples in well 6506/12-1 and 6506/12-10A are described as supermature and submature to supermature, respectively. The sandstones of Tilje and Tofte are classified as sublithic arenite, and the Ile Formation is classified as subarkosic composition.

The calculated intergranular granular volumes in the Tilje formation suggests a degree of compaction ranging from nearly uncompacted to highly compacted. Studied samples from Tofte and Ile Formation show a moderate degree of compaction.

The main diagenetic minerals and processes observed in all three formations are chlorite and illite minerals, quartz and carbonate cementation, and albitization of feldspar, respectively. Chlorite and illite coatings are observed to be effective in the preservation of porosity (8 - 17.5% porosity) in the studied deeply buried sandstone samples through the inhibition of quartz cement growth on detrital grain. However, some grain-coated samples show a negative correlation with intergranular porosity. Porosity reduction in these samples can be attributed to the presence of carbonate cement and the distribution of pore-filling authigenic clay. Considering the association of siderites with chlorites in most of the samples, the Fe-content of chlorite and chlorite coatings suggests a source from meteoric water. Berthierine is interpreted as chlorite precursor where chlorites coatings are associated with low potassium clay rims. Illites observed in these samples are attributed to two precursors (1) illite derived from smectite at a lower temperature (2) illite formed from kaolinite at a much higher temperature.

In addition to reduction of primary porosity by mechanical compaction, intergranular porosity and permeability reduction in the samples is attributed to quartz cementation, carbonate cementation, and authigenic illites in pore spaces. The secondary porosity observed in this

study resulted from fractures and dissolution of less stable minerals like feldspars and carbonate cement.

Petrophysical analysis of the studied sandstone intervals shows that the sandstones contain a low to average volume of shale. An exception is seen in the Tilje Formation (6406/2-2), with high shale volume.

In general, the studied sandstone samples of the Ile, Tofte, and Tilje formation show a good to moderate reservoir quality. However, the heterolithic nature of the Tilje sandstones can be detrimental to the permeability and the flow of fluids in the reservoir.

References

(n.d.).

Aagaard, P., Jahren, J. S., Harstad , A. O., Nilsen, O., & Ramm, M. (2000). Formation of grain coating chlorite in sandstones. Laboratory synthesized vs. natural occurrences. *Clay Mineralogy, 35*(1), 261-269.

Ajdukiewicz, J. M., Paxton , S. T., & Szabo,, J. O. (1991). Deep porosity preservation in the Norphlet Formation, Mobile Bay, Alabama (abs). *AAPG Bulletin, 75*, 533.

Bjørkum, P. A. (1996). How important is pressure solution in causing dissolution of quartz in sandstones? *Journal of Sedimentary Research, A66*, 147-154.

Bjørlykke , K. (1994). Fluid-flow processes and diagenesis in sedimentary basins. In J. Parnell (Ed.), *Geofluids: Origin, Migration and Evolution of Fluids in Sedimentary Basins* (Vol. 78, pp. 127-140). Special Publications of the Geological Society of London.

Bjørlykke , K., & Aagaard, P. (1992). Clay minerals in North Sea sandstones. In D. W. Houseknecht, & E. D. Pittman (Eds.), *Origin, Diagenesis, and Petrophysics of Clay Minerals in Sandstones* (Vol. 47, pp. 65-80). SEPM, Tulsa, OK, Special Publication.

Bjørlykke , K., & Jahren , J. (2010). Sandstones and sandstone reservoirs. Petroleum Geoscience. In *Petroleum Geoscience* (pp. 113-140). Springer Berlin Heidelberg.

Bjørlykke , K., Aagard, P., Egeberg, P. K., & Simmons , S. P. (1995). Geochemical constraints from formation water analyses from the North Sea and the Gulf Coast Basins on quartz, feldspar and illite precipitation in reservoir rocks. *Geological Society, London, Special Publications, 86*, 33-50.

Bjørlykke, K. (2003). Compaction (consolidation) of sediments. In G. V. Middleton (Ed.), *Encyclopedia of Sediments and Sedimentary Rocks* (pp. 161-168). Kluwer Academic Publishers.

Bjørlykke, K., & Egeberg, P. K. (1993). Quartz cementation in sedimentary basins. *AAPG Bulletin, 77*, 1538-1548.

Bjørlykke, K., Nedkvitne, T., Ramm, M., & Saigal, G. (1992). Diagenetic processes in the Brent Group (Middle Jurassic) reservoirs of the North Sea – An overview. *Geological Society, London, Special Publication, 61*, 263–287.

Bjørlykke, K., Ramm, M., & Siagal, G. C. (1989). Sandstone diagenesis and porosity modification during basin evolution. *International Journal of Earth Sciences, 78*, 243-268.

Bloch , S., Lander, R. H., & Bonnell, L. (2002). Anomalously high porosity and permeability in deeply buried sandstone reservoirs: Origin and predictability. *AAPG bulletin, 86*, 301-328.

Blystad, P., Færseth , R. B., Larsen, B. T., Skogseid, J., & Tørudbakken, B. (1995). Structural elements of the Norwegian continental shelf, Part II. The Norwegian Sea Region. *Norwegian Petroleum Directorate Bulletin, 8,* 44.

Boles, J. R. (1982). Active albitization of plagioclase, Gulf Coast Tertiary. *American Journal of Science, 282,* 165-180.

Brekke , H., & Riis , F. (1987). Tectonics and basin evolution of the Norwegian shelf between 62 N and 72 N. *Norsk Geologisk Tidsskrift,, 67,* 295-322.

Brekke, H. (2000). The tectonic evolution of the Norwegian Sea continental margin with emphasis on the Vøring and Møre basins, in Dynamics of the Norwegian Margin. (A. Nøttvedt, Ed.) *Geology Society Special Publication, 167,* 327-378.

Brekke, H., Sjulstad , H. I., Magnus, C., & Williams, R. W. (2001). Sedimentary environments offshore Norway — an overview. In O. J. Martinsen, & T. Dreyer (Eds.), *Norwegian Petroleum Society Special Publications* (Vol. 10, pp. 7-37). Bergen: Elsevier Science.

Bukovics, C., Shaw , N. D., Cartier , E. G., & Ziegler, P. A. (1984). Structure and development of the Mid-Norway continental shelf. In A. M. Spencer et al. (Ed.), *Petroleum Geology qf Northwest Europe* (pp. 407-425). London: Graham and Trotman.

Chen , B., Wang, F., Shi, J., Chen, F., & Shi, H. (2019). Origin and Sources of Minerals and Their Impact on the Hydrocarbon Reservoir Quality of the PaleogeneLulehe Formation in the Eboliang Area, Northern Qaidam Basin, China. *Minnerals, 9,* 436.

Chima , P., Baiyegunhi, C., Liu, K., & Gwavava, O. (2018). Diagenesis and rock properties of sandstones from the Stormberg Group, Karoo Supergroup in the Eastern Cape Province of South Africa. *Open Geosci., 10,* 740-771.

Chuhan, F. A., Kjeldstad, A., Bjørlykke, K., & Høeg, K. (2003). Experimental compression of loose sands simulating porosity reduction in petroleum reservoirs during burial. *Canadian Geotechnical Journal, 40,* 995-1011.

Chuhan, F. A., Kjeldstad, A., Bjørlykke, K., & Høeg, K. (2002). Porosity loss in sand by grain crushing. Experimental evidence and relevance to reservoir quality. *Marine and Petroleum Geology, 19,* 39-53.

Corfield, S., Sharp, I., Dreyer, T., Underhill, J., & Häger, K. O. (2001). An integrated study of the Garn and Melke formations (Middle to Upper Jurassic) of the Smørbukk area, Halten Terrace, mid-Norway. In O. J. Martinsen, & T. Dreyer (Eds.), *Sedimentary Environments Offshore Norway - Paleozoic to Recent* (pp. 199-210).

Dalland , A. G., Worsley, D., & Ofstad, K. (1988). A lithostratigraphic scheme for the Mesozoic and Cenozoic succession offshore mid-and northern Norway. *Norwegian Petroleum Directorate*.

Dore, A. G. (1991). The structural foundation and evolution of Mesozoic seaways between Europe and the Arctic. *Palaeogeography, Palaeoclimatology, Palaeoecology, 87*(1-4), 441-492.

Dott, R. H. (1964). Wacke, graywacke and matrix; what approach to immature sandstone classification? *Journal of Sedimentary Research, 34*(3), 625-632.

Dowey, P. J., Hodgson , D. M., & Worden, R. H. (2012.). Pre-requisites, processes, and prediction of chlorite grain coatings in petroleum reservoirs: A review of subsurface examples. *Marine and Petroleum Geology, 32*, 63-75.

Dowey, P. J., Hodgson, D. M., & Worden , R. H. (2012). Pre-requisites, processes, and prediction of chlorite grain coatings in petroleum reservoirs: A review of subsurface examples. *Marine and Petroleum Geology, 32*, 63-75.

Dutton, S. P. (2008). Calcite cement in Permian deep-water sandstones, Delaware Basin, west Texas: Origin distribution, and effect on reservoir properties. *Am. Assoc. Pet. Geol. Bull, 92*, 765-787.

Ehrenberg, S. (1990). Relationship Between Diagenesis and Reservoir Quality in Sandstones of the Garn Formation, Haltenbanken, Mid-Norwegian Continental Shelf. *AAPG Bulletin, 74* (1), 1538-1558.

Ehrenberg, S. (1993). Preservation of anomalously high porosity in deeply buried sandstones by grain-coating chlorite; examples from the Norwegian continental shelf. *AAPG Bulletin, 77*, 1260-1286.

Ehrenberg, S. N. (1990). Relationship between diagenesis and reservoir quality in sandstones of the Garn Formation, altenbanken, mid-Norwegian continental shelf. *AAPG Bulletin, 74*, 1538–1558.

Fagerland, N. (1990). Mid-Norway shelf - hydrocarbon habitat in relation to tectonic elements. *Norsk Geologisk Tidsskrift, 70*, 65-79.

Faleide, J. I., Bjørlykke, K., & Gabrielsen, R. H. (2010.). Geology of the Norwegian Continental Shelf. In *Petroleum Geoscience: From Sedimentary Environments to Rock Physics,* (pp. 467-499.).

Faleide, J. I., Vågnes, E., & Gudlaugsson, S. T. (1993). Late Mesozoic-Cenozoic evolution of the southwestern Barents Sea in a regional rift shear tectonic setting. *Marine and Petroleum Geology, 10*, 186-214.

Faleiden, J. I., Tsikalas, F., Breivk, A. J., Mjelde, R., Ritzmann, O., Engen, Ø., . . . Eldholm, O. (2008). Structure and evolution of the continental margin off Norway and the Barents Sea. *Episodes, 31*, 82-90.

Folk , R. L. (1951). Stages of textural maturity in sedimentary rocks. *Journal of Sedimentary Research, 21*, 127-130.

Folk, R. L. (1980). *Petrology of Sedimentary Rocks.* Austin, TX, USA: Hemphill Publishing Company.

Füchtbauer, H. (1967). Influences of different types of diagenesis on sandstone porosity. *: Proceedings of 7th World Petroleum Congress, 2*, pp. 353-369.

Fuchtbauer, H. (1983). Facies controls on sandstone diagenesis. In *Sediment Diagenesis.* Springer.

Gabrielsen, R. H., Odinsen, T., & Grunnaleite, I. (1999). Structuring of the Northern Viking Graben and the Møre Basin; the influence of basement structural grain, and the particular role of the Møre-Trøndelag Fault Complex. *Marine and Petroleum Geology, 16*(5), 443-465.

Geological Digressions. (n.d.). Retrieved from https://www.geological-digressions.com/classification-of-sandstones/

Gernigon, L., Ringenbach , J. C., Planke , S., Le Gall, B., & Jonquet-Kol-stø, H. (2003). Extension, crustal structure and magmatism at the outer Vøring Basin, Norwegian margin. *Journal of the Geological Society, 160*, 197-208.

Goldstein, J. I., Newbury , D. E., Michael , J. R., Ritchie, N. W., Scott, J. H., & Joy , D. C. (2018). X-Rays. In *Scanning Electron Microscopy and X-Ray Microanalysis* (pp. 39-63). New York: Springer.

Grunnaleite, I., & Gabrielsen, R. H. (1995). Structure of the Møre Basin, mid-Norway continental margin. *Tectonophysics, 252*(1), 221-251.

Hagevang, T., Eldholm, O., & Aalstad, I. (1983). Pre-23 magnetic anomalies between Jan Mayen and Greenland-Senja Fracture Zones in the Norwegian Sea. *Marine Geophysical Researches*, 345-363.

Hallam, A. (1988). A re-evaluation of Jurassic eustasy in the light of new data and the revised Exxon curve. In C. K. Wilgus, B. S. Hastings, C. G. Kendall, H. W. Posamentier, C. A. Ross, & J. C. Van Wagoner (Eds.), *Sea-level changes: an integrated approach. Soc. Econ. Paleontol. Mineral. Spec. Publ*, (Vol. 42, p. 26).

Hamar, G. P., & Hjelle, K. (1984). Tectonic framework of the Møre Basin and the northern North Sea. In Spencer et al. (Ed.), *Petroleum Geology of the North European Margin* (pp. 349-358). London: Graham & Trotman.

Hamar, G. P., Jacobsen, K., Ormaasen, D., & Skarpnes, O. (1980). Tectonic development of the Northern North Sea north of Central Highs. In *The Sedimentation of the North Sea Reservoir Rocks* (p. 11). Norsk Petroleumsforening.

Haq , B. U., Hardenbol,, J., & Vail, P. R. (1987). Chronology of fluctuating sea levels since the Triassic. *Science, 235*, 1156-1167.

Heald, M. T., & Renton, J. J. (1966). Experimental study of sandstone cementation. *Sediment. Petrol., 36*, 927-991.

Helsop, K., & Heslop, A. (2003). Interpretation of Shaly Sands. *LPS DiaLog, 15*.

Heum, O. R., & Larsen , R. M. (1990,). Haltenbanken hydrocarbon province (off-shore Mid-Norway). *Geological Society, London, Special Publications, 50* , 471.

Hillier, S. (1994). Hillier, S., Pore-lining chlorite in siliciclastic reservoir sandstones – electron microprobe, SEM and XRD data, implications for their origin. *Clay Miner., 29*(4), 665-679.

Hilliier, S. (1994). Pore-lining chlorites in siliciclastic reservoir sandstones: electron microprobe, SEM and XRD data, and implications for their origin. *Clay Minerals, 29*, 665-680.

Hinz, K. (1981). A hypothesis on terrestrial catastrophes. Wedges of very thick oceanward dipping layers beneath passive continental margins - their origin and paleoenvironmental significance. *Geologisches Jahrbuch, 22*, 3-28.

Houseknecht, D. W. (1987). Assessing the relative importance of compaction processes and cementation to reduction of porosity in sandstones. *AAPG bulletin, 71*, 633-642.

Islam, M. A. (2009). Diagenesis and reservoir quality of Bhuban sandstones (Neogene),Titas Gas Field, Bengal Basin, Bangladesh. *Journal of Asian Earth Sciences, 35*, 89-100.

Jackson, J. S., & Hastings, D. S. (1986). The role of salt movements in the Tectonic history of Haltenbanken and Traenabanken and its relationship to structural styles. In A. M. Spencer (Ed.), *Habitat of Hydrocarbons on the Norwegian Continental Shelf* (pp. 241-257). London: Graham & Trotman.

Karlsson, W. (1984). Sedimentology and diagenesis of Jurassic sediments offshore mid-Norway. In *Petroleum Geology of the North European Margin (Norwegian Petroleum Society)* (pp. 389-396). Graham & Trotman.

Lander, R. H., & Walderhaug, O. (1999). Predicting Porosity through Simulating Sandstone Compaction and Quartz Cementation. *AAPG Bulletin, 83*, 433-448.

Marcussen , Ø., Maast, T. E., Mondol, N. H., & Jahren, J. (2010). Changes in physical properties of a reservoir sandstone as a function of burial depth – The Etive Formation, northern North Sea. *Marine and Petroleum Geology, 27*(8), 1725-1735.

Marsh, N., Imber, J., Holdsworth, R. E., Brockbank, P., & Ringrose, P. (2009). The structural evolution of the Halten Terrace, offshore Mid-Norway: extensional fault growth and strain localisation in a multi-layer brittle-ductile system. *Basin Research*, 195-214.

Martinius, A. W., Kaas, I., Næss, A., Helgesen, G., Kjærefjord, J. M., & Leith, D. A. (2001). Sedimentology of the heterolithic and tide-dominated Tilje Formation (Early Jurassic, Halten Terrace, offshore mid-Norway). In O. J. Martinsen, & T. Dreyer (Eds.), *Sedimentary Environments OffshoreNorway – Paleozoic to Recent* (Vol. 10, pp. 103-144). Amsterdam: Elsevier.

Martinius, A. W., Ringrose, P. S., Brostrøm, C., Elfenbein, C., Næss, A., & Ringås, J. E. (2011). Reservoir challenges of heterolithic tidal sandstone reservoirs in theHalten Terrace, mid-Norway. *Petroluem Geosciences, 11*, 3-16.

McBride, E. F. (1989). Quartz cement in sandstones: a review. *Earth-Science Reviews, 26*, 69-112.

Molenaar, N., Cyziene, J., & Sliaupa, S. (2007). Quartz cementation mechanisms and porosity variation in Baltic Cambrian sandstones. *Sedimentary Geology, 195*(3-4), 135-159.

Morad, S., Al-Aasm, I. S., Ramseyer , K., Marfil, R., & Aldahan, A. A. (1990). Diagenesis of carbonate cements in Permo-Triassic sandstones from the Iberian Range, Spain: Evidence from chemical composition and stable isotopes. *Sediment. Geol., 67*, 281-295.

Nadeau, P. H. (2000). The Sleipner effect: a subtle relationship between the distribution of diagenetic clay reservoir porosity, permeability, and water saturation. *Clay Minerals, 35*(1), 185-200.

NPD FactMaps. (n.d.). Retrieved from Norwegian Petroleum Directorate: https://factmaps.npd.no/FactMaps/3_0/?run=WellboreExpByNPDID&NPDID=2644

npd.no. (n.d.). *Factpage Norwegian Petroleum Directorate*. Retrieved from factpages.npd.no: https://factpages.npd.no/nb-no/wellbore/PageView/Exploration/All/2644

Oelkers, E. H., Bjørkum, P. A., & Murphy, W. M. (1996). A petrographic and computational investigation of quartz cementation and porosity reduction in North Sea sandstones. *American Journal of Science, 296*, 420-452.

Osmundsen, P. T., Sommaruga, A., Skilbrei, J. R., & Olesen, O. (2002). Deep structure of the Mid Norway rifted margin. *Norwegian Journal of Geology/Norsk Geologisk Forening, 82*(4), 205-224.

Osmundsen, P., & Ebbing, J. (2008). Styles of extension offshore mid-Norway and implications for mechanisms of crustal thinning at passive margins. *Tectonics, 27*.

Palmer, S. N., & Barton, M. E. (1987). Porosity reduction, microfabric and resultant lithification in UK uncemented sands. In J. D. Marshall (Ed.), *Diagenesis of sedimentary sequences* (Vol. 36, pp. 29-40). Geological Society Special Publication.

Pascoe, R., Hooper, R., Storhaug, K., & Harper, H. (1999). Evolution of extensional styles at the southern termination of the Nordland Ridge, Mid-Norway: a response to variations in coupling above Triassic salt. In A. J. Fleet, & S. A. Boldy (Eds.), *Petroleum Geology of Northwest Europe* (pp. 83-90). Geological Society of London.

Paxton , S., Szabo, J., Ajdukiewicz, J., & Klimentidis, R. (2002). Construction of an intergranular volume compaction curve for evaluating and predicting compaction and. *AAPG bulletin, 86*, 2047-2067.

Paxton, S. T., Szabo, J. O., Calvert, C. S., & Adukiewicz, J. W. (1990). Preservation of primary porosity in deeply buried sandstones: A new play concept from the Cretaceous Tuscaloosa Sandstone of Louisiana. *AAPG Annual Convention. 74*, p. 737. San Francisco, California: AAPG Bulletin.

Pittman, E. D. (1992). Relationship of porosity and permeability to various parameters derived from mercury injection-capillary pressure curves for sandstone. *Am. Assoc. Pet. Geol. Bull, 76*(2), 191-198.

Pszonka, J., & Wendorff, M. (2017). Carbonate cements and grains in submarine fan sandstones—the Cergowa Beds (Oligocene, Carpathians of Poland) recorded by cathodoluminescence. *Int. J. Earth Sci, 106*, 269-282.

Ramm , M., & Bjørlykke, K. (1994). Porosity/depth trends in reservoir sandstones; assessing the quantitative effects of varying pore-pressure, temperature history and mineralogy, Norwegian Shelf data. *Clay Minerals, 29*, 475-490.

Ramm, M. (396-409). Porosity-depth trends in reservoir sandstones: Theoretical models related to Jurassic sandstones offshore Norway. *Marine and Petroleum Geology, 33*, 1992.

Ramm, M., & Ryseth, A. E. (1996). Reservoir quality and burial diagenesis in the Statfjord Formation, North Sea. *Petroleum Geosciences, 2*, 313-324.

Ren, S., Faleide, J. I., Eldholm, O., Skogseid, J., & Gradstein, F. (2003). Late Cretaceous-Paleocene tectonic development of the NW Vøring Basin. *Marine and Petroleum Geology, 20*, 177-206.

RESERVOIR QUALITY. (n.d.). Retrieved from AAPG WIKI: https://wiki.aapg.org/Reservoir_quality

Rittenhouse , G. (1971). Mechanical compaction of sands containing different percentages of ductile grains: a theoretical approach. *AAPG Bulletin, 55*, 92-96.

Rønnevik, H. C. (2000). The exploration experience from Midgard to Kristin—Norwegian Sea. *Norwegian Petroleum Society Special Publications , 9*, 113-129.

Shang, Y., & Li, X. (2018). Reservoir characteristics and physical property controlling factors of Kexia Formation in WEH Oilfield, Junggar Basin. *OP Conference Series: Earth and Environmental Science, 208*(1).

Siever, R., & Stone, W. N. (1994). Quantitative petrologic constraints on basin paleohydrologic models . *AAPG Annual Convention Program and Abstracts*, 258-259.

Stephan, H. J. (1970). Diagenesis of the Middle Buntsandstein in South Oldenburg, Lower Saxony Meyniana. 39-82.

Storvoll, V., Bjørlykke, K., Karlsen , D., & Saigal, G. (2002). Porosity preservation in reservoir sandstones due to grain coating illite: A study of the Jurassic Garn Formation from the Kristin and Lavrans Fields offshore Mid-Norway. *Marine and Petroleum Geology, 19*, 767-781.

Storvoll, V., Bjørlykke, K., Karlsen , D., & Saigal, G. (2002). Porosity preservation in reservoir sandstones due to grain-coating illite: a study of the Jurassic Garn Formation from the Kristin and Lavrans fields, offshore Mid-Norway. *Marine and Petroleum Geology and Petroleum Geology, 19*, 767-781.

Surlyk, F. (1990). Timing, style and sedimentary evolution of Late Paleozoic-Mesozoic extensional basins of East Greenland. In R. P. Hardman, & J. Brooks (Eds.), *Tectonic-Events Responsible.[or Britain's Oil and Gas Reserves* (Vol. 55, pp. 107-125). Geological Socie O, Special Publication.

Swiecicki, T., Gibbs, P., Farrow, G., & Coward, M. (1998). A tectonostratigraphic framework for the Mid-Norway region. *Marine and Petroleum Geology, 15*(3), 245-258.

Szabo, J. O., & Paxton , S. T. (1991). Intergranular volume (IGV) decline curves for evaluating and predicting compaction and porosity loss in sandstones. *AAPG Bulletin, 75*, 678.

Talwani, M., Mutter, J. C., & Hinz, K. (1983). Ocean continent boundary under the Norwegian Continental Margin. In *Structure and Development of the Greenland-Scotland Ridge* (pp. 121-131). New York: Plenum.

Thyne , G., Boudreau, B. P., Ramm, M., & Midtbø, R. E. (2001). Simulation of potassium feldspar dissolution and illitization in the Statfjord Formation, North Sea. *AAPG Bulletin, 85*, 621-635.

Tsikalas, F., Faleide , J. I., & Eldholm, O. (2001). Lateral variations in tectono-magmatic style along the Lofoten-Vesterålen volcanic margin off Norway. *Marine and Petroleum Geology, 18*, 807-832.

Walderhaug, O. (1990). fluid inclusion study of quartz cemented sandstones from offshore mid-Norway: Possible evidence for continued quartz cementation during oil emplacements. *Journal of Sedimentary Petrology, 60*, 203-210.

Walderhaug, O. (1994b). Precipitation rates for quartz cement in sandstones determined by fluid inclusion microthermometry and temperature history modelling. *Journal of Sedimentary Research, A64*, 324-333.

Walderhaug, O. (1996). Kinetic modeling of quartz cementation and porosity loss in deeply buried sandstone reservoirs. *AAPG Bulletin, 80*, 731-745.

Wentworth, C. K. (1992). A scale of grade and class terms for clastic sediments. *The Journal of Geology, 30*(5), 377-392.

Wilson, M. D. (1992). Inherited grain-rimming clays in sandstones from eolian and shelf environments: their origin and control on reservoir properties. In D. W. Houseknecht, & E. D. Pittman (Eds.), *Origin, diagenesis, and petrophysics of clay minerals in sandstones* (Vol. 47, pp. 209-225). SEPM Special Publication.

Worden , R. H., Oxtoby, N. H., & Smalley, P. C. (1998). Can oil emplacement prevent quartz cementation in sandstones? *Petroleum Geoscience, 4*, 129-137.

Xi, K., Cao, Y., Jahren , J., Zhu, R., Bjørlykke, K., Haile, B. G., . . . Hellevang, H. (2015). Diagenesis and reservoir quality of the Lower Cretaceous Quantou Formation tight sandstones in the southern Songliao Basin, China. *Sedimentary Geology, 330*, 90-107.

Yu, Y., Lin, L. B., & Gao, J. (2016). Formation mechanisms and sequence response of authigenic grain-coating chlorite: evidence from the Upper Triassic Xujiahe Formation in the southern Sichuan Basin, China. *Petroleum Science, 13*, 657-668.

Appendix

Appendix 1: Grain size analysis

6406/2-1

4884.75	Area
	153917.303
	208368.369
	295170.548
	131978.211
	66190.18
	236138.632
	59883.742
	128874.347
	180393.375
	151113.223
	143837.97
	238083.574
	190001.097
	115000.183
	99641.721
	159265.894
	101879.136
	267992.542
	243198.187
	208368.369
Mean	168964.8
Diameter (µm)	463.7939

4847.50	Area
	167624.9
	64372.23
	52124.13
	40889.76
	102267.9
	29604.71
	155742.4
	64915.3
	426525.8
	156966.1
	199130.3
	140836.9
	93328.87
	73278.63
	75990.37
	77402.36
	161013.8
	90675.06
	118809.8
	87738.84
	74592.86
	270873.9
	161097.1
	154978.5
	126326
	103520.5
	243970
Mean	130170.3
Diameter (µm)	407.0828

4850.25	Area
	93995.83
	38914.55
	78473.72
	54076.1
	71535.75
	55991.78
	30213.86
	36700.22
	101469.2
	137674.1
	42414.49
	105202.2
	85298.79
	74733.41
	84570.39
	39027.45
	46741.16
	42327.08
	213991.8
	95667.5
	188873
	206627.7
	107125.2
	73790.14
	31109.78
	160389.1
	77701.62
	67609.7
	211023.5
	101166.9
	101603.9
	254945.8
	324766.2
	68709.57
	53059.99
Mean	101643.5
Diameter (µm)	359.7217

5101.5	Area
	202530.4
	251791.9
	204202.1
	88412.68
	120957.4
	88948.05
	45058.56
	111546.5
	108833.3
	180307.1
	132007.2
	111874.3
	131606.6
	112682.8
	93649.85
	77399.34
	139618.9
	42032.08
	333321.2
	55725.92
	39744.92
	236058.5
	159529.6
	106130.9
	214326.8
	49672.95
	192307.4
	403258.1
	54072.46
	100336.5
	40145.53
Mean	136390
Diameter (µm)	416.6949

5104.00	Area
	53784.74
	37366.7
	72573.71
	124439.1
	68039.45
	84628.66
	187368.9
	23217.62
	84297.24
	103228.3
	156772.6
	48813.44
	148323.2
	178413.3
	132804.8
	114114.1
	126737.2
	53027.21
	268089.7
	88667.62
	92509.91
	119992.3
	64135.25
	72122.11
	38233.5
	220004.7
	105610.1
	128492.7
	148763.9
	98435.41
	80072.55
	170233.4
	76303.1
	64284.57
	48383.69
	54014.19
	273745.7
	265831.7
	19397.18
Mean	110135.2
Diameter (µm)	374.4467

6406/2-2

4706.25	Area
	238814
	202371.5
	120172.2
	160380.1
	224369.1
	52043.42
	31110.08
	25931.8
	64572.6
	18878.17
	166053.8
	117581.2
	56748.29
	151029.1
	83575.55
	285693.8
	47940.43
	166318
	85315.1
	389942.2
	248935.7
	186895.4
	83670.97
	109474.3
	137714.5
	54216.03
	37697.63
	12998.93
	34383.67
	30232.97
	17582.68
Mean	117504.6
Diameter (µm)	386.7714

4716.25	Area
	6821.722
	3189.169
	3741.974
	4441.813
	8197.465
	7062.221
	3134.459
	2009.473
	3938.02
	3193.729
	4333.532
	5081.243
	6215.347
	2573.676
	2873.444
	3302.01
	4603.665
	3632.553
	8595.256
	4002.989
	15151.4
	3306.569
	2631.806
	8974.81
	6948.24
	3364.699
	3528.831
	7340.333
	1822.545
	5011.715
	6944.821
	7294.74
	4031.484
	4862.4
	5787.921
	3830.879
	3161.814
	2911.057
	12173.1
	13095.2
	4658.376
Mean	5311.622
Diameter (µm)	82.23193

4716.25	Area
	119177.3
	109446.2
	72616.94
	114635.4
	135056.4
	86110.88
	41003.13
Mean	96863.75
Diameter (µm)	351.162

4726.25	Area
	420002.6
	288761.9
	64304.69
	288273.8
	122473.2
	621302.5
	95627.63
	304161
	253464.4
	321072.1
	171661.5
	151939.2
	126554.2
	47301.86
	62480.73
	42505.25
	29183.37
	34453.4
	21296.66
	110755.1
	112245.1
	34394.68
	83292.96
Mean	165543.8
Diameter (µm)	459.0747

4884.50	Area
	379787.9
	594132.4
	223831.3
	311636.8
	88936.45
	110060.8
	107290.4
	236364.4
	260564.9
	145166
	49344.06
	138302.6
	52468.12
	31605.4
	213831.3
	100060.8
	23468.12
	336464.4
	1240573
	161165
Mean	240252.7
Diameter (µm)	553.0457

4897.00	Area
	845961.6
	115617.8
	152038.3
	145931.5
	63137.65
	117155.5
	226090.3
	180851
	178392.1
	180590.4
	97293.79
	117269.3
	158882.7
	57724.49
	55838.14
	68407.69
	208392.1
	90590.42
	101293.8
	117269.3
Mean	3278728
Diameter (µm)	456.8405

4897.75	Area
	68968.95
	96993.45
	74192.92
	99874.37
	175367.8
	173242.1
	92627.86
	33974.23
	24627.82
	31082.26
	23879.96
	53215.98
	57622.1
	205337.4
	104015.2
	177909.7
	11413.16
	31178.05
	139496.2
	425359.5
	51933.94
	48894.6
	158811.7
	34674.2
	111552.8
	41073.38
	43876.94
	92358.93
	101418
	279290.9
	88744.88
	80253.17
	162396.2
	335196.2
Mean	109731
Diameter (µm)	373.759

4910.25	Area
	53927
	160904.2
	55238.52
	187565.6
	158108
	48157.8
	52895.47
	57010.55
	201402.9
	159467.4
	108119.3
	69226.83
	115391.6
	34099.49
	85285.57
	159611.1
	36600.96
	59950.41
	97932.88
	83484.07
	65233.33
	62978.7
	198761.4
	116706.8
	56015.86
	100968.5
	62547.66
	80382.11
	77932.22
	45354.24
	257488.7
	77405.4
	56704.77
	128403.6
	176366.1
	40303.42
	91997.89
Mean	99457.58
Diameter (µm)	355.8327

4919.75	Area
	43379.59
	276159.5
	144322.3
	41732.83
	88520.16
	142904
	68519.49
	105934.6
	55680.61
	34722.09
	144952.3
	150979.4
	30411.77
	22888.95
	112952.7
	90546.38
	28267.65
	31726.97
	106748.8
	31229.62
	14478.28
	46175.78
	29221.82
	53109.15
	69315.25
	81881.51
	114982.6
	120147.7
	14666.17
	40270.26
	21699.01
	22225.82
	40325.52
	31656.97
Mean	72139.28
Diameter (µm)	303.1455

4910.25	Area
	53927
	160904.2
	55238.52
	187565.6
	158108
	48157.8
	52895.47
	57010.55
	201402.9
	159467.4
	108119.3
	69226.83
	115391.6
	34099.49
	85285.57
	159611.1
	36600.96
	59950.41
	97932.88
	83484.07
	65233.33
	62978.7
	198761.4
	116706.8
	56015.86
	100968.5
	62547.66
	80382.11
	77932.22
	45354.24
	257488.7
	77405.4
	56704.77
	128403.6
	176366.1
	40303.42
	91997.89
Mean	99457.58
Diameter (µm)	355.8327

4919.75	Area
	43379.59
	276159.5
	144322.3
	41732.83
	88520.16
	142904
	68519.49
	105934.6
	55680.61
	34722.09
	144952.3
	150979.4
	30411.77
	22888.95
	112952.7
	90546.38
	28267.65
	31726.97
	106748.8
	31229.62
	14478.28
	46175.78
	29221.82
	53109.15
	69315.25
	81881.51
	114982.6
	120147.7
	14666.17
	40270.26
	21699.01
	22225.82
	40325.52
	31656.97
Mean	72139.28
Diameter (µm)	303.1455

4984.25	Area
	105511.4
	65380.57
	20551.61
	47025.06
	69736.36
	70730.62
	56097.2
	149761.3
	76138.93
	113002.9
	42753.04
	28472.89
	53165.41
	53453.13
	33134.6
	86099.71
	53850.1
	57885.4
	120782.1
	74791.41
	50266.41
	271636
	67518.4
	93529.32
	34500.34
	82268.36
	34871.82
	84438.97
	84996.19
	21997.47
	44238.96
Mean	72535.03
Diameter (µm)	303.8791

4986.75	Area
	56326.75
	19189.92
	7118.075
	10046.47
	8441.518
	19767.56
	24001.11
	177546.1
	19354.44
	68080.53
	25653.59
	10189.05
	8324.529
	5571.621
	7008.398
	10390.12
	7805.388
	7249.688
	9340.874
	13950.99
	363566.6
	40770.81
	14598.09
	5622.804
	7995.496
	47834.05
	37334.25
	13698.73
	340563.5
	15676.58
	9392.057
	24549.5
	10123.24
	10726.47
	12302.17
	7136.355
	222502.9
	48148.46
	10836.15
	13731.63
	11077.44
	9194.637
	22663.05
	17467.98
	6847.537

5124.5	Area
	15259.3
	67458.49
	28801.84
	67587.43
	25799.35
	10705.83
	14327.24
	25600.41
	41147.06
	15951.9
	16044
	18188.12
	21363.76
	6366.024
	13649.38
	19164.39
	49959.29
	48909.34
	27921.35
	21334.29
	23032.63
	18759.14
	45361.61
	23441.56
	65004.92
	26572.99
	134342.3
	148570
	66301.7
	44488.49
	20818.52
	14106.2
	9467.988
	67521.12
	80238.43
	63870.23
	28669.21
	20405.91
	21669.53
	27221.39
	13255.18
	12967.83
	27088.76
	34221.07
	16283.47

5126.50	Area
	37315.72
	27679.04
	64288.21
	67802.72
	50976.78
	13748.47
	49669.31
	66258.52
	19579.28
	37865.66
	81613.11
	23483.48
	27460.52
	93161.82
	92812.19
	53937.71
	33560.84
	30443.3
	43685.54
	39788.62
	43470.66
	13701.13
	14017.98
	42469.12
	38896.34
	110836.3
	14640.76
	71991
	70344.82
	37567.01
	16476.31
	19841.5
	35727.81
	27526.08
	83885.7
	13974.27
	17386.81
	10725.63
	230074.7
	89447
	65821.49
	23760.27
	7750.131
	26848.67
	17171.93

Mean	40882.6
Diameter (µm)	228.1372

	17591.3
	25272.53
	12765.21
	136283.8
	50397.69
	33005.33
	84250.35
	17897.08
	18449.68
Mean	37132.07
Diameter (µm)	217.421

	17386.81
	8726.181
	33101.95
	193731.4
	77563.23
	89494.35
	32104.04
	85022
	209446.6
	59204.01
	94753.37
	56060.98
	72471.74
	107434.7
	57962.09
	178773.8
	211395
	14032.55
	236506.5
	35312.63
	167487.3
	158517.1
	34704.42
	27912.13
Mean	63167.96
Diameter (µm)	283.5798

6506/11-5S

4554.54	Area
	420766.5
	242988.2
	290086.6
	225762.3
	347579.8
	136650.8
	119330.9
	141071.1
	49650.13
	27309.92
	425038.7
	237075.7
	49004.99
	319704.3
	290555.1
	149636.3
	345039.5
	244451.7
	250698
	152027.2
	143599.1
	260580
Mean	211678.6
Diameter (µm)	519.1171

4703.28	Area
	70980.05
	86316.55
	98540.59
	83149.21
	232993.2
	44121.54
	25552.83
	288925.5
	236455.5
	230176.7
	324764.7
	191112.8
	178016.3
	70597.34
	280037.6
	122661.9
	273365.5
	60992.22
	99517.07
	95201.33
Mean	154673.9
Diameter (µm)	443.747

6506/12-1

4255.00	Area
	40666.61
	18459.8
	13398.95
	24775.77
	64829.5
	18166.2
	6741.68
	20815.9
	24364.73
	66176.36
	69934.38
	20445.24
	36159.92
	29689.82
	75131.02
	35668.15
	129989.3
	108098.1
	56322.57
	37565.51
	57482.27
	34992.88
	62077.04
	54388.52
	44861.35
	25836.38
	25179.46
	41220.77
	26618.08
	27887.88
	9857.46
	13843.02
	6580.203
	24335.37
	6011.362
	13879.71
	14389.84
Mean	37482.19
Diameter (µm)	218.4436

4271.66	Area
	90342.93
	77570.51
	51399.25
	39945.23
	95084.79
	72486.31
	84748.85
	115676.5
	141902.4
	87411.14
	71787.05
	117024.1
	68858.9
	52714
	36121.15
	53569.87
	64816.3
	47498.69
	34926.58
	40535.23
	82516.32
	80596.99
	6952.538
	29842.38
	76430.57
	31860.03
	29274.23
Mean	65996.03
Diameter (µm)	289.8583

4273.66	Area
	34100.45
	23127.17
	29727.86
	63230.84
	124035.5
	46781.38
	62066.73
	37037.14
	20380.83
	56632.35
	48980.88
	60607.73
	50807.37
	17763.22
	37800.75
	16397.75
	50214.31
	15977.43
	17050.22
Mean	42774.73
Diameter (µm)	233.3569

6506/12-10

4943.25	Area
	59276.23
	31889.07
	63045.01
	52276.55
	116493.1
	55290.1
	48095.17
	74189.23
	71470.41
	90126.4
	70376.25
	283811.2
	41869.14
	154442.4
	42469.63
	46831.54
	69609.97
	57784.2
	145983.8
	312226.2
	112470.1
	125596.4
	40185.53
	80463.16
	469479.6
	97015.56
	98238.66
	150809.9
	213132.9
	568569.2
	154221.4
	46330.51
	210679.3
	51329.76
	56152.17
	93788.34
	30481.76
	29111.3
	84176.67
	52014.99
Mean	116295.1
Diameter (µm)	384.7756

4962.66	Area
	135248.5
	54899.19
	125000
	253703.9
	335659.3
	96913.06
	92746.64
	57714.44
	43805.72
	107289.1
	108683.9
	26477.19
	15150.63
	183523
	94909.97
	70989.45
	115570.9
	282271.6
	146495
	40473.31
	140879
	106775.5
	71156.98
	67886.49
	131653.9
	98034.79
	74387.42
	171555.4
	32417.25
	15846.25
	52717.65
Mean	108091.5
Diameter (µm)	370.9562

5012.85	Area
	117836.2
	42683.99
	84515.76
	15879.03
	55121.35
	54341.97
	108898.8
	38783.43
	152413.2
	35389.11
	88412.68
	66903.15
	45400.91
	27118.18
	13792.17
	107671.5
	75042.98
	33265.84
	48434.68
	101793.3
	58537.53
	53333.14
	106546.1
	51519.43
	54687.96
	43459.73
	26003.73
	55154.13
	48533.01
	118404.4
	123663.4
	83852.92
	68414.57
	106007.1
	43798.44
	87087
	33855.84
Mean	66933.96
Diameter (µm)	291.9108

6506/12-10A

5686.85	Area
	26819.83
	29400.9
	79125.07
	50532.12
	50221.37
	16528.41
	85062.28
	67597.95
	74445.49
	22772.72
	17928.63
	31239.83
	13442.82
	69053.01
	31722.41
	45029.96
	48616.42
	19431.21
	46989.53
	79677.11
	28157.89
	30519.62
	46389.96
	61002.67
	65356.87
	32534.03
	18023.68
	27474.24
	52392.98
	33736.83
	42836.41
	46649.53
	44262.22
	64658.59
	53815.14
Mean	44384.22
Diameter (µm)	237.7066

5694.5	Area
	13970.12
	14760.07
	10887.28
	18157.54
	13542.33
	13018.33
	32959.48
	6407.877
	8819.602
	13062.47
	38480.08
	12684.47
	10997.06
	8835.446
	4844.952
	17215.94
	23963.33
	8370.303
	6888.864
	6075.147
	3744.907
	15602.08
	10440.24
	16437.3
	3037.574
	5245.586
	12197.83
Mean	12986.9
Diameter (µm)	128.5818

5694.5	Area
	55564.45
	50701.67
	27293.35
	15769.07
	19082.34
	55365.96
	49760.01
	14324.44
	29728.12
	30736.32
	26959.54
	14556.76
	20128.88
	9021.85
	12569.69
	12491.88
	26763.32
	32972.61
	29313.12
	32408.74
	16503.22
	63343.54
	24564.24
	12121.98
	23362.08
Mean	28216.29
Diameter (µm)	189.5295

Appendix 2: Volume of shale log

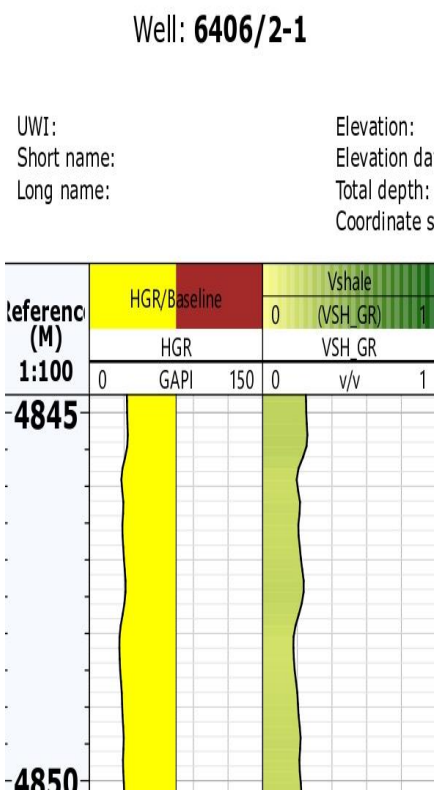

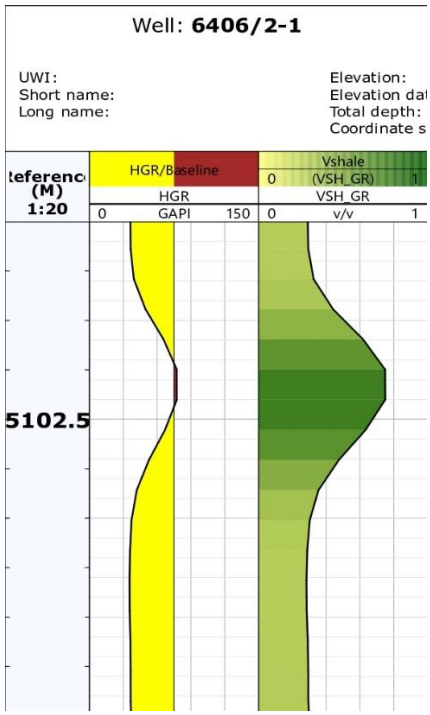

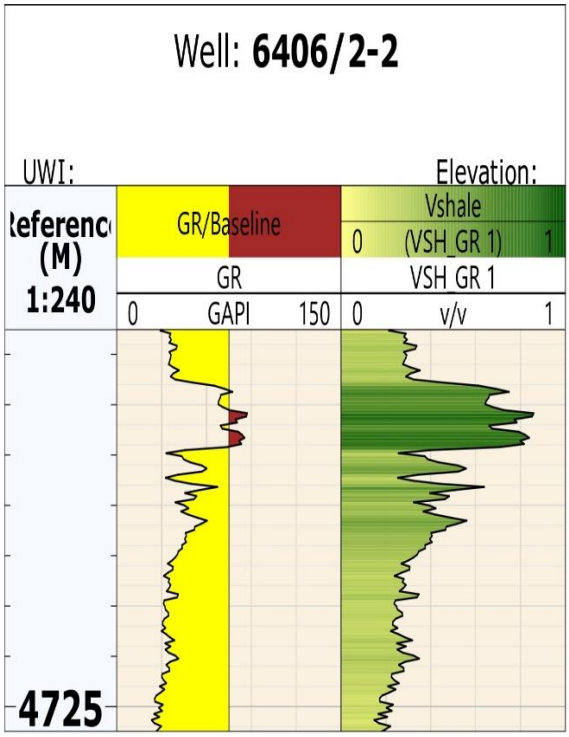

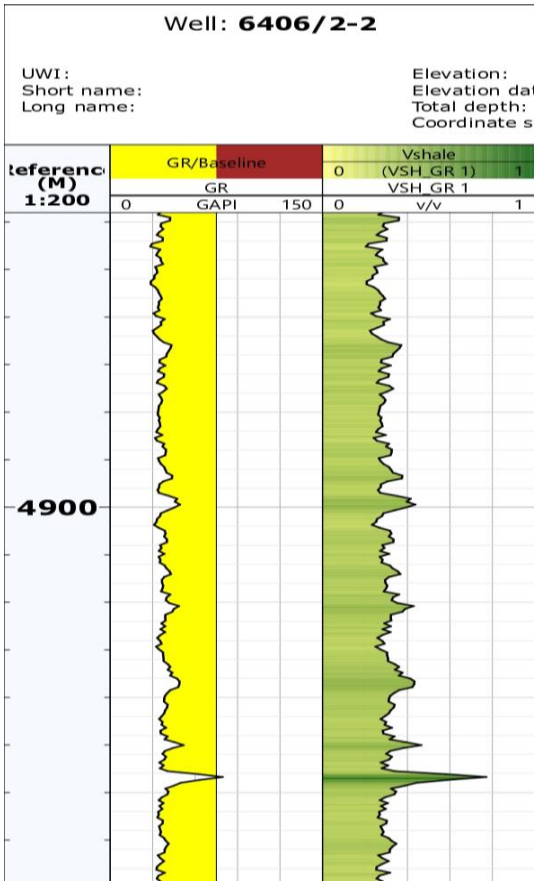

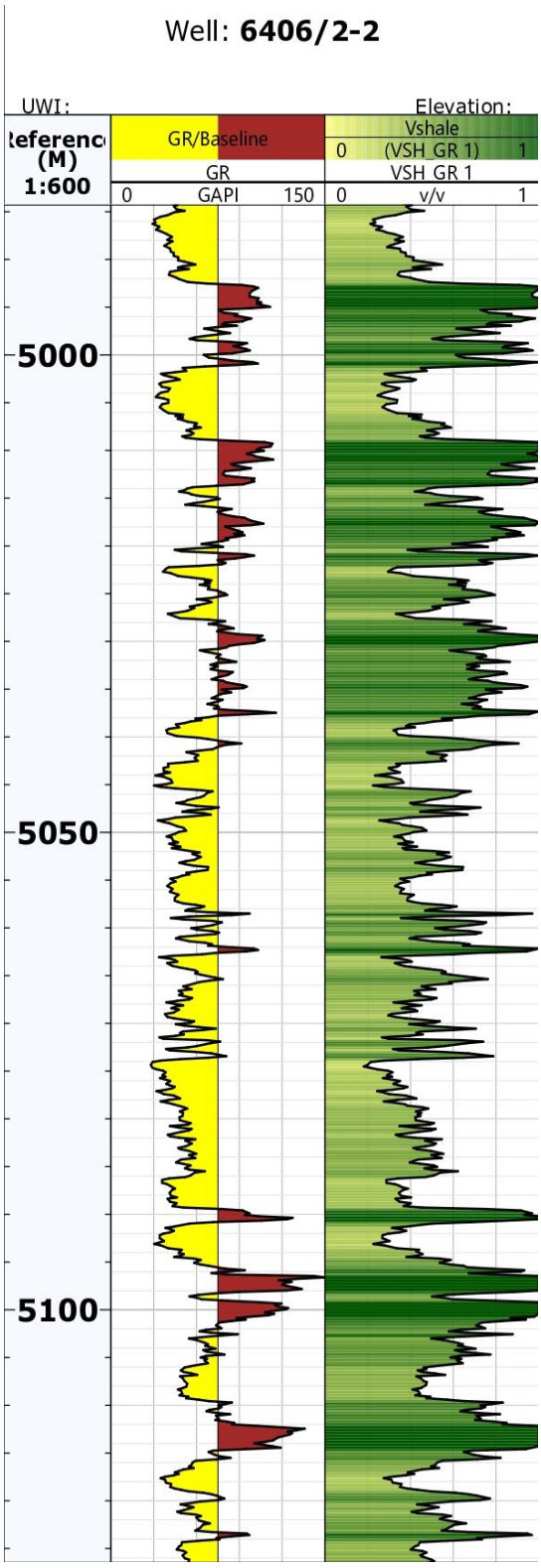
Well: 6406/2-2
UWI:
Elevation:
Reference (M) 1:600
GR/Baseline
GR
0 GAPI 150
Vshale
0 (VSH_GR 1) 1
VSH_GR 1
0 v/v 1
5000
5050
5100

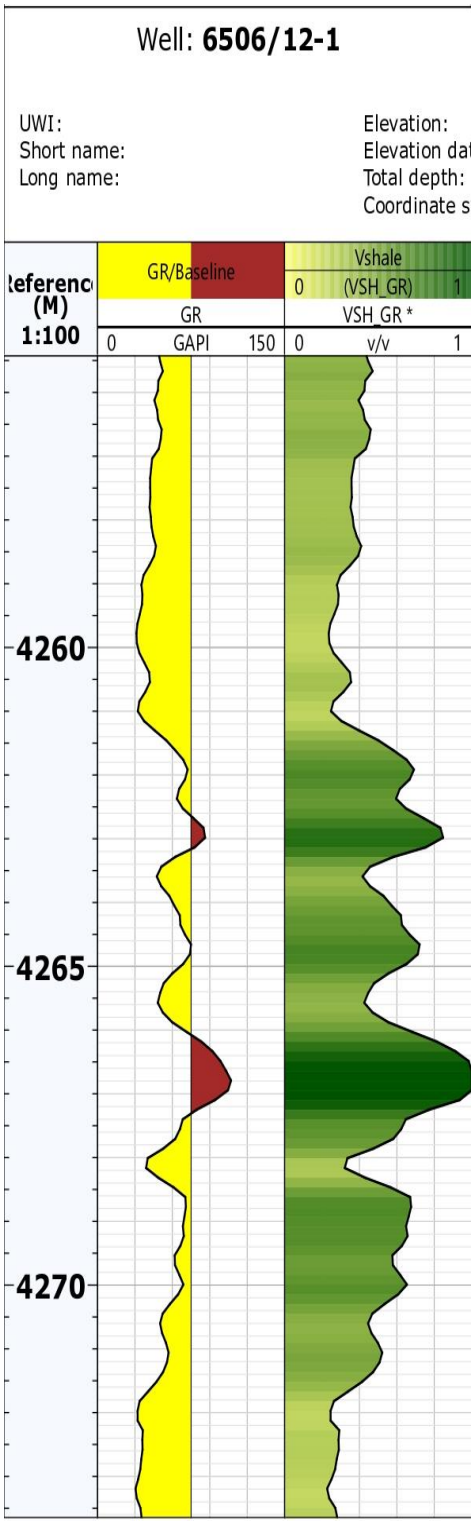
Well: 6506/12-1
UWI:
Short name:
Long name:
Elevation:
Elevation dat
Total depth:
Coordinate s
Reference (M) 1:100
GR/Baseline
GR
0 GAPI 150
Vshale
0 (VSH_GR) 1
VSH_GR *
0 v/v 1
4260
4265
4270

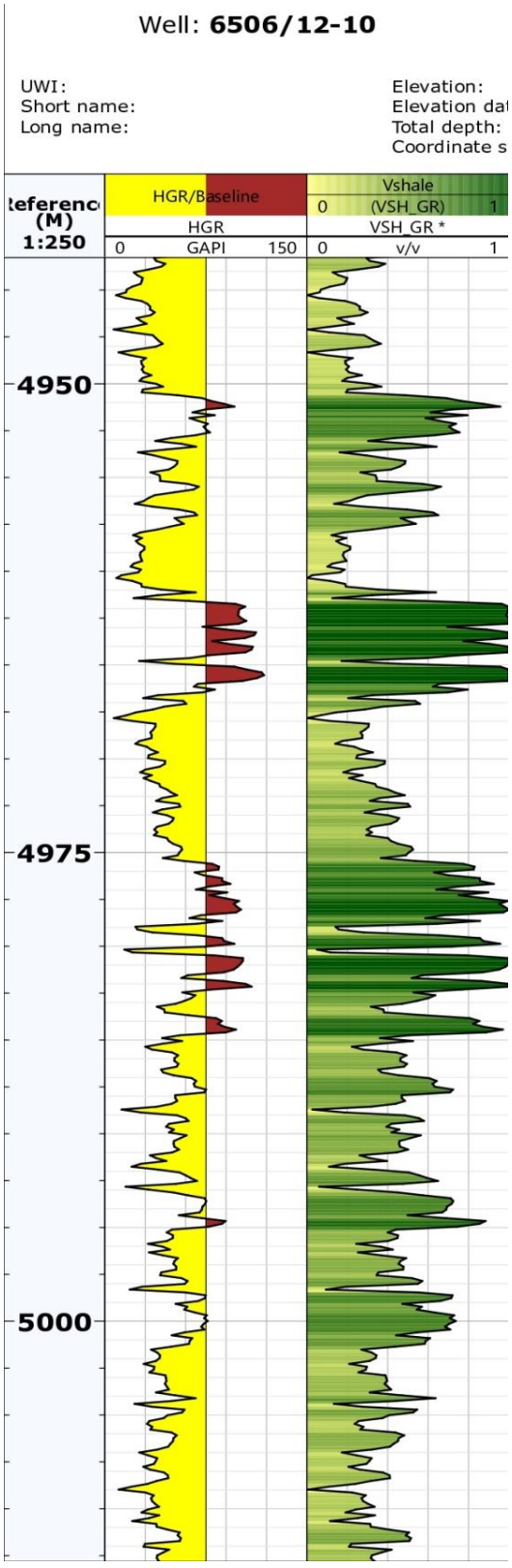
Well: 6506/12-10
UWI:
Short name:
Long name:
Elevation:
Elevation dat
Total depth:
Coordinate s
eferenc
(M)
1:250
HGR/Baseline
HGR
0 GAPI 150
Vshale
0 (VSH_GR) 1
VSH_GR *
0 v/v 1
4950
4975
5000

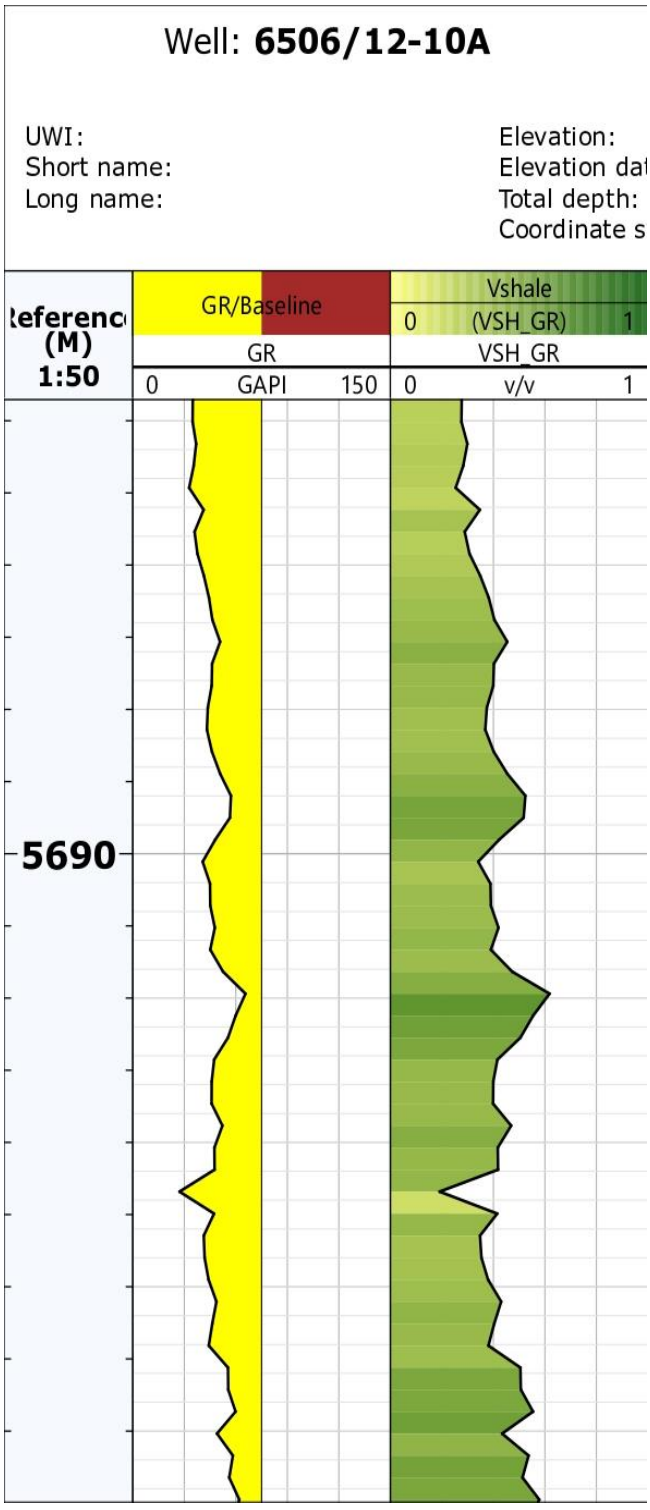
Well: 6506/12-10A
UWI:
Short name:
Long name:
Elevation:
Elevation dat
Total depth:
Coordinate s
eferenc
(M)
1:50
GR/Baseline
GR
0 GAPI 150
Vshale
0 (VSH_GR) 1
VSH_GR
0 v/v 1
5690

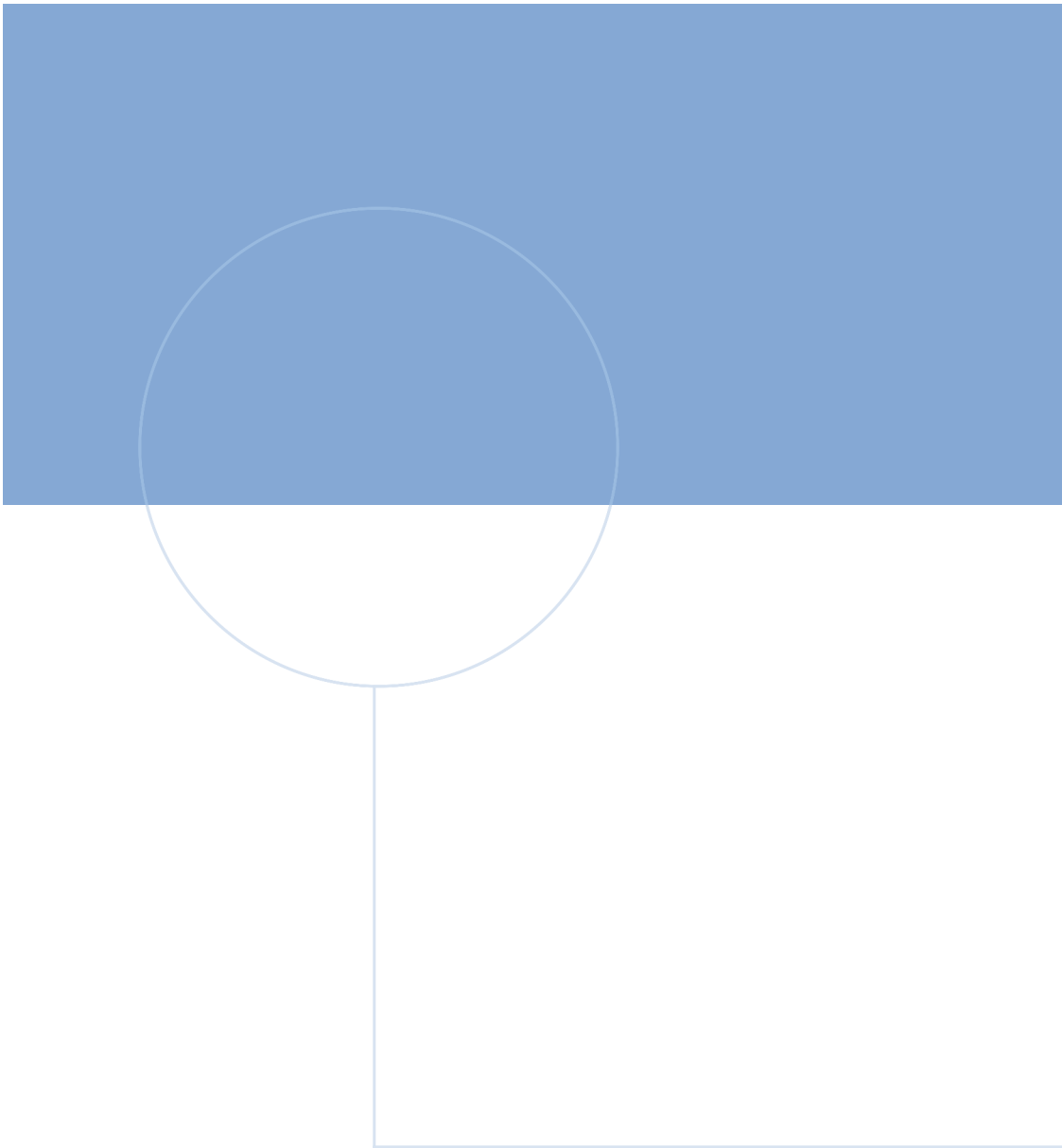

NTNU

Norwegian University of
Science and Technology